学位論文

Evolutionary biological studies on the initial stage of multicellularity based on comparative analyses of volvocine green algae

(緑藻ボルボックス系列を用いた多細胞化初期段階の進化生物学的研究)

平成 29 年 7 月博士 (理学) 申請

東京大学大学院理学系研究科
生物科学専攻
新垣　陽子

Contents

Abbreviations

BB	basal body
BLAST	basic local alignment search tool
CB	cytoplasmic bridge
CBB	Coomassie brilliant blue
cDNA	complementary DNA
CDS	coding sequence
CTAB	cetyltrimethylammonium bromide
CYCD1	cyclin D1
DIC	Nomarski differential interference optics
Dlp	dynamin-like protein
DP	dimerization partner
DRP	dynamin-related protein
ECM	extracellular matrix
EDTA	ethylenediaminetetraacetic acid
ETI	evolutionary transitions in individuality
E2F	E2 promoter binding factor
GED	GTPase effector domain
GTP	guanosine triphosphate
GTPase	guanosine triphospatease
L1	linker region in the binding pocket of RB/MAT3
MAT3	retinoblastoma related homologue, identified in *Chlamydomonas* maternal inheritance mutant *mat-3*
ML	maximum likelihood
mRNA	messenger RNA
MTR	microtubular rootlet
MYA	million years ago
NJ	neighbor joining

pBB	pro basal body
PBS	phosphate-buffered saline
PCR	polymerase chain reaction
PEI	polyethylenimine
RACE	rapid amplification of cDNA ends
RB	retinoblastoma
RT-PCR	reverse transcription polymerase chain reaction
SAS-6	spindle assembly abnormal 6
SDS-PAGE	sodium dodecyl sulfate poly acrylamide gel electrophoresis
SVM	standard *Volvox* medium
TAP	tris acetate phosphate
TEM	transmission electron microscopy
TGV-clade	colonial volvocalean clade consisting of Tetrabaenaceae, Goniaceae and Volvocaceae
TPBS	0.1% Tween 20 in PBS
WB	western blot

Abstract

Transitions to multicellularity occurred more than twenty-five times independently in various eukaryotic lineages such as land plants, metazoans, fungi, and brown algae (Grosberg & Strathmann 2007). There are few lineages that still retain ancestral multicellular species or transitional forms from unicellular to multicellular, because of extinction. However, volvocine lineage in green algae contains various extant organisms that exhibit successive incipient stages in evolution of multicellularity: unicellular, simple undifferentiated multicellular, and complex differentiated multicellular species (e.g. Kirk 2005; Sachs 2008).

Colonial and multicellular volvocine algae constitute a robust monophyletic group composed of Tetrabaenaceae, Goniaceae, and Volvocaceae (TGV-clade) (Nozaki et al. 2000; Nakada et al. 2010). The Tetrabaenaceae is significantly important to study the initial evolution of multicellularity because it is the most ancestral colonial group based on both morphological and molecular phylogenetic data (Nozaki and Ito 1994; Nozaki et al. 2000). Nevertheless, species of this family have not previously been studied at cell morphological and molecular level except for their light microscopy (Stein 1959; Nozaki 1986), vegetative ultrastructure (Nozaki 1990; Nozaki et al. 1996) and molecular phylogenetic analyses (Nozaki et al. 2000; Herron et al. 2009). Kirk (2005) proposed evolutionary twelve steps from a unicellular *Chlamydomonas reinhardtii*-like ancestor to the most complex, differentiated multicellular *Volvox carteri* based on the morphology and phylogeny of volvocine lineage, but he ignored the presence of the Tetrabaenaceae in this lineage. Herron et al. (2009) analyzed and discussed Kirk's twelve steps based on their Bayesian tree of the volvocine algae including the Tetrabaenaceae. According to their analysis, the Tetrabaenaceae has not experienced two of Kirk's twelve steps that are proposed to be important for integrated multicellular organisms: rotation of the basal bodies and incomplete cytokinesis (Herron et al. 2009). However, this situation seems to be possibly due to the lack of morphological information of Tetrabaenaceae in their analysis. Very recently, whole genome analyses of *Gonium pectorale* were performed

and the results suggested that alternation of cell cycle-related genes might contribute to the evolution of multicellularity in volvocine lineage (Hanschen et al. 2016). Although those precedence studies provided important findings described above, early evolutionary transition from a unicellular ancestor to a primitive multicellular remains obscure due to the lack of information of Tetrabaenaceae. In the present thesis, therefore, I undertook evolutionary biological analyses of the volvocine algae based on both morphological and genomic information of the Tetrabaenaceae to understand the initial evolutionary steps of multicellularity.

In Chapter 2, in order to examine the multicellularity of the four-celled tetrabaenacean species *Tetrabaena socialis*, I established synchronous culture and performed morphological analyses of this species. Immunofluorescence microscopy by using an anti-acetylated tubulin antibody (Piperno and Fuller 1985) and an anti-*Chlamydomonas reinhardtii* SAS-6 antibody (Nakazawa et al. 2007) revealed that the four cells of *T. socialis* had rotational asymmetry in arrangement of microtubular rootlets, presumably by resulting from rotation of the basal bodies during cell development. Ultrastructural observations clearly showed the presence of cytoplasmic bridges between protoplasts in developing embryos of *T. socialis* that denoted incomplete cytokinesis during embryogenesis. Those results suggested that *T. socialis* actually has the two of Kirk's twelve evolutionary steps (Kirk 2005): rotation of the basal bodies and incomplete cytokinesis, and these two morphological attributes might have evolved in the common ancestor of TGV-clade. Therefore, *T. socialis* is the simplest integrated multicellular organisms in volvocine lineage and a suitable material to elucidate the initial evolution of multicellularity in this lineage.

In Chapter 3, in order to reveal the evolution of cell cycle-related genes in the initial stage of multicellular evolution in the volvocine lineage, I used newly constructed draft genome and transcriptome assemblies of the simplest multicellular species *T. socialis* and performed the comparative genome analyses. According to the genome

analyses of *G. pectorale* (Hanschen et al. 2016), duplications of the cell cycle-related gene *cycin D1* (*CYCD1*) and modification of retinoblastoma homologue RB/MAT3 protein might contribute to the evolution of multicellularity. BLAST-based searches against the *T. socialis* genome and transcriptome data and Sanger sequencings revealed that *T. socialis* had three *CYCD1* genes and a RB/MAT3 protein with a short L1 region like multicellular species *G. pectorale* and *Volvox carteri*. Thus, these two features of cell cycle-related molecules were thought to have been acquired by the common ancestor of all of the multicellular volvocine members (TGV-clade), and might have contributed to the transition to multicellularity.

In Chapter 4, in order to compare the cytokinesis-related genes between unicellular *C. reinhardtii* and ancestral multicellular volvocine species in detail, I focused on dynamin-related protein 1 (DRP1) which is known to participate in cell plate formation in the flowering plant *Arabidopsis thaliana* (Dombrowski and Raikhel 1995; Kang et al. 2003; Konopka and Bednarek 2008). Immunofluorescence microscopy by using a newly prepared anti-*T. socialis* DRP1 antibody elucidated that the DRP1 protein was mainly localized to the last division plane of unicellular *C. reinhardtii* during multiple fission, whereas the DRP1 was observed in all division planes in multicellular *T. socialis* and *G. pectorale* during embryogenesis. These results indicated that DRP1 probably functions in cytokinesis of volvocine algae and localizes differently between unicellular and multicellular members.

The present comparative morphological and genomic analyses in unicellular *C. reinhardtii*, the most ancestral multicellular *T. socialis* and undifferentiated multicellular *G. pectorale* demonstrated that evolution of cell cycle and cytokinesis-related attributes at cellular and molecular levels might have occurred in the common ancestor of TGV-clade: incomplete cytokinesis, modification of cell cycle-related genes and change in subcellular localization of cytokinesis-related factor DRP1. The present study firstly clarified that the cytokinesis in multicellular species is different from that of unicellular

species at subcellular levels. Further detailed comparative studies using *T. socialis* would shed light on the evolution of multicellularity.

Chapter 1.

General introduction

Organisms on the Earth exhibit a wide array of morphological and genetic diversity (e.g. Adl et al. 2005). The diversity can be considered to originate from the evolution of organisms since the origin of life on the Earth, via evolutionary transitions in individuality (ETIs), in which individuals gathered to become different individuals of higher-level (Michod 2005). According to Michod (2005), the major landmarks of diversification and hierarchical organization of organisms passed through serial steps of ETIs: from genes to first cells, from prokaryotic cells to eukaryotic cells, from independent unicellular cells to controlled multicellular organisms, from asexual to sexual populations, and from solitary to social organisms.

Transition to multicellularity is one of the attractive ETIs that has occurred more than twenty-five times in distinct eukaryotic lineages (Grosberg & Strathmann 2007) (Figure 1.1). Multicellular or colonial organisms are widespread in eukaryotic supergroups (Adl et al. 2005): metazoans, choanoflagellates, Filasterea, Fungi, and *Fonticula* in Opistokonta (Brown et al. 2009; Suga and Ruiz-Trillo 2015), land plants and some green and red algae in Archaeplastida (Bowman et al. 2016), brown algae (Cock et al. 2015), colonial diatoms (Chamnansinp et al. 2013) and *Sorodiplophrys* (Tice et al. 2016) in Stramenopiles, Dictyostelia (Parfrey and Lahr 2013) and *Copromyxa* (Brown et al. 2011a) in Amoebozoa, *Acrasis* (Brown et al. 2011b) in Excavata, *Sorogena* (Olive and Blanton 1980; Lasek-Nesselquist and Katz 2001) in Alveolata, and *Guttulinopsis vulgaris* (Brown et al. 2012) in Rhizaria. Major complex multicellular groups such as metazoans and land plants emerged from unicellular ancestors that existed approximately 600 to 1000 million years ago (MYA) (Sharpe et al. 2015). Thus, there are few species that represent the initial features of multicellular ancestors or transitional forms from unicellular to multicellular within the lineages closely related to these groups. To overcome such situation, some researchers focus on the choanoflagellates which is the sister group of metazoans in Opisthokonta (Lang et al. 2002). Genomic analyses of two choanoflagellates, solitary *Monosiga brevicollis* (King

et al. 2003; 2008) and colonial *Salpingoeca rosetta* (Fairclough et al. 2013) demonstrated that both of the two species contain homologues of a cell adhesion molecule cadherin and some signaling pathway components for metazoan development. The results suggested that ancestral molecular mechanisms related to metazoan multicellularity might have been present in the common ancestor of choanoflagellates and metazoans (King et al. 2003; 2008; Fairclough et al. 2013). However, it is difficult to predict the initial steps of transition to multicellularity of metazoans, because the evolution of multicellularity of choanoflagellates and metazoans occurred independently. On the other hand, the volvocine lineage (Figure 1.2) contains unicellular *Chlamydomonas reinhardtii* and colonial/multicellular species with various steps of transitional forms of multicellularity such as non-differentiated multicellular species *Gonium pectorale* and differentiated multicellular species *Volvox carteri* (Kirk 2005; Sachs 2008). Moreover, the whole genome data of *C. reinhardtii* (Merchant et al. 2007), *G. pectorale* (Hanschen et al. 2016) and *V. carteri* (Prochnik et al. 2010) are available, the phylogeny within this lineage is well resolved (e.g. Nozaki et al. 2000; Nozaki 2003; Herron et al. 2009), and culturing and molecular genetic methods have been established (Kirk 1998; Nishii et al. 2003; Harris 2009), therefore the volvocine lineage is a powerful model for comparative studies of multicellularity.

Colonial/multicellular volvocine algae constitute a robust monophyletic group composed of three families, the Tetrabaenaceae, Goniaceae, and Volvocaceae (TGV-clade) (Nozaki and Ito 1994; Nakada and Nozaki 2015). Both cladistic analyses of morphological data and molecular phylogenetic analyses demonstrated that Tetrabaenaceae is the most ancestral group within the colonial volvocine algae (Nozaki and Ito 1994; Nozaki et al. 2000; Nozaki 2003; Herron et al. 2009) (Figure 1.2). Tetrabaenaceae was established by Nozaki and Ito (1994) and includes two four-celled species *Tetrabaena socialis* and *Basichlamys sacculifera* (Nozaki et al. 1996; Nozaki et al. 2000). The colony of the Tetrabaenaceae consists of four *Chlamydomonas*-like cells

that are arranged like a four-leaf clover (Figure 1.3) by their extracellular matrices (ECM) (Stein 1959; Nozaki 1990; Nozaki et al. 1996). Thus, each tetrabaenacean alga may represent a simple and ancestral organism that is suitable for the studies of the initial steps of transition to multicellularity. Vegetative ultrastructure (Nozaki 1990; Nozaki et al. 1996), molecular phylogenetic analyses (Nozaki et al. 2000; Nakada et al. 2010) and cladistics analyses of morphological data (Nozaki and Ito 1994; Nozaki et al. 1995) using Tetrabaenaceae have been reported. However, molecular, cell biological and developmental studies of Tetrabaenaceae have not been performed previously.
The transition to multicellularity in the volvocine algae occurred approximately 200 MYA in the *Chlamydomonas*-like ancestor (Herron et al. 2009). Kirk (2005) proposed twelve evolutionary steps for differentiated *Volvox*, and subsequently, Herron et al. (2009) deduced the occurrence of the twelve steps based on the phylogenetic relationships of the volvocine algae including Tetrabaenaceae. However, their studies are not sufficient, because of less morphological studies of Tetrabaenaceae.

In asexual life cycles of unicellular and colonial volvocine algae, reproductive cells perform successive divisions (rapid S/M phase alternating without G2 phase) known as multiple fission (Kirk 1998; Harris 2009). *C. reinhardtii* forms 2^n daughter unicellular cells depending on the size of the mother cell (Umen & Goodenough 2001), while tetrabaenaceaean, goniaceaean, and volvocaceaean members form species-specific numbers of daughter cells depending on the mother cell size and genetic control (Herron et al. 2009). After the multiple fission in multicellular volvocine species, the daughter cells are arranged to shape daughter colonies by the connections known as cytoplasmic bridges (CBs) (e.g. Kirk 2005). The CBs are observed in various multicellular volvocine species such as *G. pectorale* (Iida et al. 2013), *Astrephomene gubernaculifera* (Hoops and Floyd 1982), *Pandorina morum* (Fulton 1978), *Eudorina elegans* (Marchant 1977), *Platydorina caudata* (Iida et al. 2011), and *V. carteri* (Green et al. 1981). It is considered that the bridges are formed by incomplete cytokinesis (Kirk

2005); therefore the change in cytokinesis from a unicellular ancestor to multicellular progenies is one of the essential evolutionary events in this lineage. Recently, whole genome analyses of *G. pectorale* demonstrated that modifications in cell cycle-related genes have occurred in a common ancestor of Goniaceae and Volvocaceae and it might attribute to the evolution of multicellularity (Hanschen et al. 2016). The cell cycle-related genes would control the cytokinesis-related genes directly/indirectly. However, evolutionary analyses of cytokinesis-related genes have not been carried out for the purpose of elucidating the evolution of multicellularity. No nuclear genome data have been constructed in the Tetrabaenaceae.

FIGURES

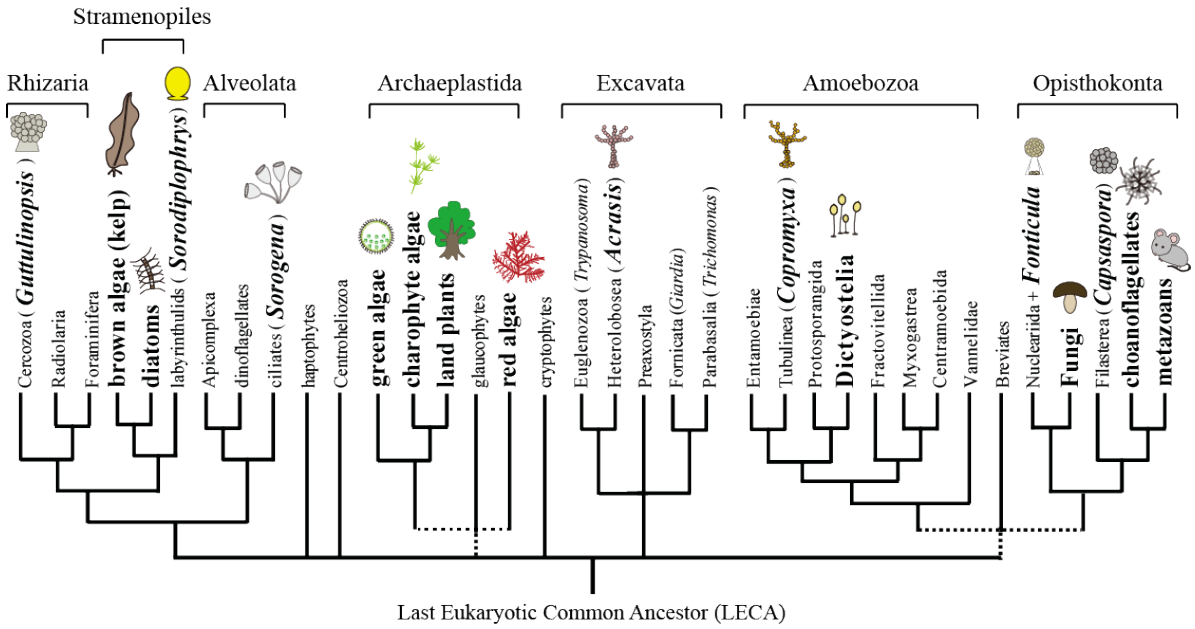

Figure 1.1. Diverse origins of multicellular organisms in eukaryotes.

Lineages shown in bold characters with illustration contain multicellular or colonial species. Based on Adl et al. (2005), Grosberg and Strathmann (2007) and Parfrey and Lahr (2013).

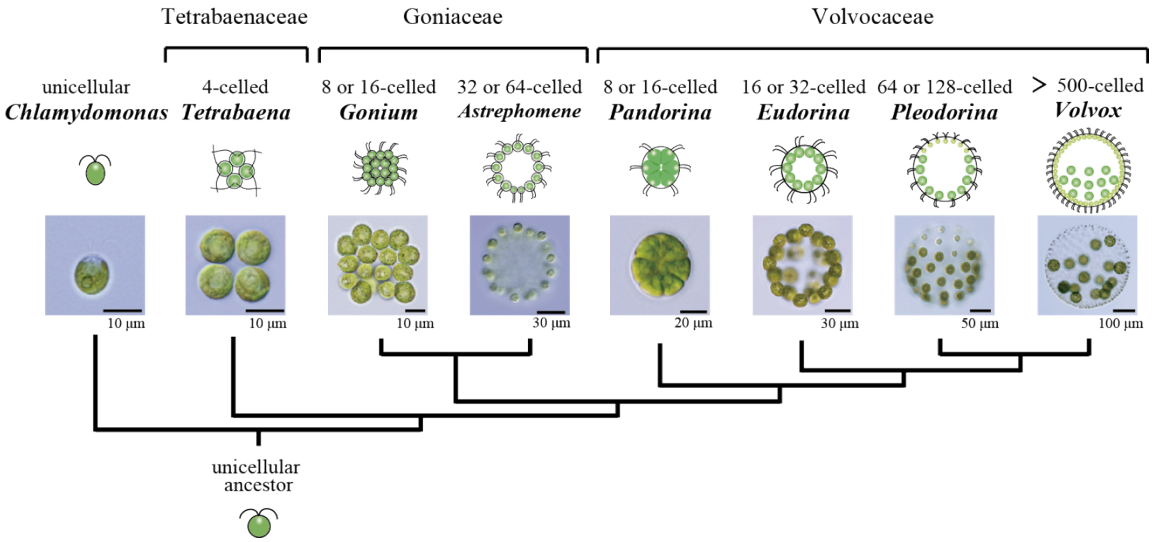

Figure 1.2. Schematic representation of volvocine lineage.

Based on Nozaki and Ito (1994), Nozaki et al. (2000) and Nozaki (2003).

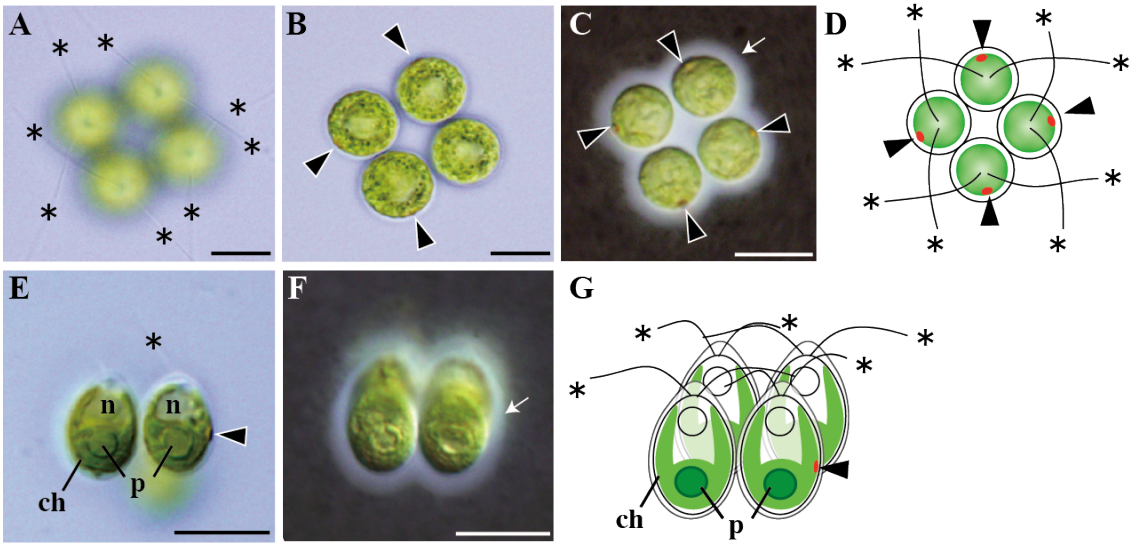

Figure 1.3. Vegetative colonies of the four-celled volvocine alga *Tetrabaena socialis* strain NIES-571.

A-C, E, F: Differential interference contrast microscopic images. D, G: Diagrams of light microscopy. C, F: Indian ink preparations showing extracellular matrices (arrows) surrounding the colonies. A-D: Top views showing flagella (asterisk) and eyespots (arrow heads). E-G: Lateral views. Each cell contains a nucleus (n), and a cup-shaped chloroplast (ch) with a single basal pyrenoid (p). Scale bars: 10 µm.

Chapter 2.

Morphological analyses of the four-celled volvocine species *Tetrabaena socialis*

2.1 INTRODUCTION

Volvocine lineage is a model to study the evolution of multicellularity, because it contains various evolutionary forms such as unicellular *Chlamydomonas reinhardtii,* undifferentiated multicellular *Gonium pectorale,* and differentiated multicellular *Volvox carteri* (Kirk 2005; Sachs 2008). Kirk (2005) proposed that there are twelve evolutionary steps for multicellularity leading to *Volvox* (Figure 2.1) where six of the steps (incomplete cytokinesis, partial inversion of embryo, rotation of BBs, establishment of organismic polarity, transformation of cell walls into ECM, and genetic modulation of cell number) are required for the divergence of the undifferentiated *G. pectorale* in the colonial volvocine algae. However, Kirk did not discuss the four-celled Tetrabaenaceae in his twelve-step model. Subsequently, Herron et al. (2009) deduced the character evolution of the twelve steps based on the phylogenetic relationships of the volvocine algae including the Tetrabaenaceae. According to the results in Herron et al. (2009), the unicellular ancestor at first embedded their cells in a common ECM and obtained a genetic control of cell number to become a common ancestor of three families of the colonial and multicellular volvocine algae (Tetrabaenaceae, Goniaceae and Volvocaceae: TGV-clade). After the divergence of the Tetrabaenaceae, incomplete cytokinesis, rotational asymmetry of cells (rotation of BBs), organismal polarity, and partial inversion (movements of daughter cells for colony formation) might have evolved in the common ancestor of the Goniaceae and Volvocaceae (Herron et al. 2009). As described in Chapter 1, in the multicellular members of volvocine algae such as *G. pectorale* (Iida et al. 2013), *Pandorina morum* (Fulton 1978) and *V. carteri* (Green et al. 1981), newly formed embryos have species-specific shapes due to connections or cytoplasmic bridges (CBs) between the protoplasts of the developing embryos before secretion of a new ECM. Furthermore, because the flagellar motion of the constitutive cells of the colonial or

multicellular forms is essentially different from that of the unicellular organization in the volvocine algae, rotational asymmetry of cells might have been acquired for effective swimming of the organized cells or multicellular organism (Hoops 1997) (Figure 2.2). Thus, character state changes deduced by Herron et al. (2009) indicates that the Tetrabaenaceae does not have these multicellular traits and may not be considered as integrated multicellular organisms. However, there have been no cell biological or ultrastructural studies of the Tetrabaenaceae except for transmission electron microscopic (TEM) observation of *Tetrabaena socialis* (Nozaki 1990) and *Basichlamys sacculifera* (Nozaki et al. 1996) in vegetative phase. In this chapter, I undertook to evaluate the multicellular morphological traits of the most primitive colonial volvocine alga *T. socialis*, with particular regard to the CBs between embryonic protoplasts and rotational asymmetry of the vegetative cells.

2.2 MATERIALS AND METHODS

2.2.1 Cultures

Three algal strains were used in this chapter. *C. reinhardtii* strain C-239, were cultured synchronously in 300 mL tris-acetate-phosphate (TAP) medium (Gorman and Levine 1965) in a silicon-capped 500 mL flask with aeration at 25°C, on a light: dark cycle 12 h: 12 h under cool-white fluorescent lamps at an intensity of 110–150 $\mu mol \cdot m^{-2} \cdot s^{-1}$. *T. socialis* strain NIES-571 were cultured in 300 mL standard *Volvox* medium (SVM) (Kirk and Kirk 1983) in a silicon-capped 500 mL flask with aeration at 20°C, on a light: dark cycle 12 h: 12 h under cool-white fluorescent lamps at an intensity of 110–150 $\mu mol \cdot m^{-2} \cdot s^{-1}$. Percentages of dividing cells and cell density of the culture were counted 24 h after the inoculation under the light microscope, for every one hour during dark period and every two hours during light period. Experiments were repeated three times (Figure 2.3). Daughter colonies before hatching from parental ECM were considered ‘‘one cell’’ in counting cell densities. *G. pectorale* strain K4-F3-4 were cultured in SVM as described above for *T. socialis*.

2.2.2 Indirect immunofluorescence microscopy

In order to examine the rotation of BBs, arrangements of microtubular rootlet (MTR) and distances between a pair of BBs were observed by immunostaining with some modifications from Nishii et al. (2003). Mature cells of *C. reinhardtii*, *T. socialis* and *G. pectorale* were attached to polyethylenimine (PEI) coated coverslips and fixed with 3.7% formaldehyde (Sigma Aldrich, St. Louis, MO, USA), 0.1% TritonX-100 (Sigma Aldrich), 1mM dithiothreitol (Nacalai Tedqce Inc., Kyoto, Japan) in phosphate-buffered saline (PBS). After fixation, chlorophyll was extracted in extracting solution [1% IGEPAL CA-630 (Sigma Aldrich), 1% bovine serum albumin powder (Sigma Aldrich), 1mM dithiothreitol in PBS]. Then, the fixed cells were incubated with two primary

antibodies, a monoclonal anti-acetylated tubulin antibody (# T6793, Sigma Aldrich) for MTR (e.g. Preble et al. 2001) and a rabbit anti-CrSAS-6 antibody (*C. reinhardtii* SAS-6 provided by Dr. M. Hirono; Nakazawa et al. 2007) for BBs that were diluted 1:500 and 1:300, respectively, with blocking buffer (0.44% Gelatin [Sigma Aldrich], 0.05% NaN_3, 1% bovine serum albumin [Sigma Aldrich], 0.1% Tween 20 (Sigma Aldrich) in PBS]. The cells were subsequently subjected to two secondary antibodies, Alexa Fluor 568 goat anti-mouse IgG (H＋L) (# A11004, Invitrogen, Carlsbad, CA, USA) and Alexa Fluor 488 goat anti-rabbit IgG (H＋L) (# A11008, Invitrogen) that were diluted 1:500 with the blocking buffer. Confocal images were obtained with a LSM 780 (Carl Zeiss, Jena, Germany). Distances between a pair of BBs and between a pair of pro basal bodies (pBBs) were measured using ImageJ 1.45s (National Institutes of Health, Bethesda, MD, USA). Evaluation of the specificity of the anti-CrSAS-6 antibody was analyzed by the SDS-PAGE and western blot (WB) with some modifications from Nakazawa et al. (2007). Cells were harvested, suspended in 1× SDS-sample buffer (100 mM dithiothreitol, 2% SDS, 10% glycerol, 0.005% Bromophenol blue in 62.5 mM Tris-HCl) and boiled for three minutes. The prepared samples were separated on an Any kD Mini-PROTEAN TGX precast gel (Bio-Rad, Hercules, CA, USA) and transferred onto a Hybond-P membrane (GE Healthcare, Uppsala, Sweden). The blotted membrane was blocked with 3% skim milk in TPBS at 4°C, overnight. The blot was incubated in anti-CrSAS-6, diluted 1: 500 with 3% skim milk in TPBS for 1 hour at room temperature and washed in 3% skim milk in TPBS. The membrane was incubated in an anti-IgG antibody conjugated to horseradish peroxidase (Jackson ImmunoReserch, WestGrove, PA, USA), diluted 1:1,000 with 3% skim milk in TPBS for 1 hour at room temperature and washed with TPBS. The protein signals were detected with Amersham ECL prime Western blotting detection reagent (GE Healthcare). Images were obtained by ChemiDoc XRS system (Bio-Rad) with Quantity One software (Bio-Rad).

2.2.3 Time-lapse analysis

T. socialis colonies in synchronous culture were attached to PEI-coated coverslips, put on slides and sealed with vaseline to avoid water evaporation. The preparations were observed under light microscopy BX-60 microscope (Olympus, Tokyo, Japan) with DP Controller 1. 2. 1108 (Olympus) for time-lapse images. Stage light was turned on manually only during image capturing, because cytokinesis often stopped under continuous light.

2.2.4 Transmission Electron microscopy

To observe the cytokinesis of *T. socialis*, synchronous cultured *T. socialis* cells were fixed for 1h at room temperature (20°C) with a final concentration of 2% glutaraldehyde obtained by mixing the culture with an equal volume of 4% glutaraldehyde in 0.025M sodium cacodylate buffer (pH 7.3). Cells were then rinsed with 0.05M sodium cacodylate buffer for 30min at room temperature and then added 2% osmium tetroxide in 0.025M sodium cacodylate buffer (pH 7.3) for 2h at room temperature. The fixed cells were dehydrated through an ethanol series, replaced by propylene oxide, and embedded in Spurr's resin (Spurr 1969). Sections were cut with a diamond knife on an Ultracut UCT (Leica, Vienna, Austria) and stained with uranyl acetate and lead citrate. These sections were observed under a JEM-1010 electron microscope (JEOL, Tokyo, Japan).

2.3 RESULTS

2.3.1 Synchronous culture and time-lapse analysis

Volvocine cells are able to grow to many times their original cell size, and they must divide multiple times (S/M phase), a process known as multiple fission (e.g. Harris 2009). The cell cycle of *C. reinhardtii* through an extended G1 phase correlates with the availability of light (Jones 1970). Entry into multiple fission of *C. reinhardtii* occurs during darkness, thus the *C. reinhardtii* cell cycle can be highly synchronized to light-dark cycles (Kates and Jones 1964; Jones 1970). The life cycles of the Volvocaceae, particularly *V. carteri* can also be synchronized to light-dark cycles even though its life cycle is 48 h compared to a 24 h cycle for *C. reinhardtii* (Kirk and Kirk1983). To determine if *T. socialis* can be synchronized to light-dark cycles, *T. socialis* were cultured in a light: dark cycle 12 h: 12 h for 50 h in photoautotrophic SVM. Fractions of the culture were harvested every hour, each cell concentration was calculated and the cells were observed by light microscopy to determine their cell phase. During the light period, most of the cells were considered to be in G1 phase because the cells were flagellated and cell densities were nearly constant (Figure 2.3A). At 5–6 h of the dark period, approximately 70% of cells were de-flagellated and undergoing either a first or second round of multiple fission (Figure 2.3A, Figure 2.4A-D, H.1-4). In the following light period, lots of small daughter colonies within their parental ECM were observed in the culture (Figure 2.3C, Figure 2.4E-G, H.5).

2.3.2 Comparative indirect immunofluorescence of rootlets and basal bodies

To examine rotation of BBs in *T. socialis*, indirect immunofluorescence microscopic observations of MTRs arrangements were performed in comparison with unicellular *C. reinhardtii* and 16-celled *G. pectorale.* MTRs were immunostained with an anti-acetylated tubulin α antibody (Figure 2.5A-F), and BBs and pro-basal bodies

(pBBs; basal bodies without flagella) were immunostained with an anti-CrSAS-6 antibody (Figure 2.5A-F, Figure 2.6B-D).

In *C. reinhardtii*, cells had X-shaped MTRs exhibiting 180º rotational symmetry (Figure 2.5D) as described by Ringo (1967). In four-celled *T socialis* colony, the four cells were identical to each other (Figure 2.5B), whereas each cell exhibited rotational asymmetry (Figure 2.5B, E). Two MTRs extending toward the center of the *T. socialis* colony were arranged nearly in parallel, while the other two MTRs extended toward the periphery were arranged 90º between them (Figure 2.5B, E). In *G. pectorale*, the peripheral cells of the 16-celled colony also exhibited rotational asymmetry (Figure 2.5C, F). Two MTRs extending toward the center of the *G. pectorale* colony showed a wider angle than those extending toward the periphery (Figure 2.5C, F) as reported by Greuel and Floyd (1985). Central four cells in 16-celled colony of *G. pectorale* exhibited rotational symmetrical MTR arrangements similar to *C. reinhardtii* cells, as reported by Greuel and Floyd (1985).

CrSAS-6 is a protein localized at central part of cartwheel of BBs (Nakazawa et al. 2007) and also attached to pBBs. WB showed that CrSAS-6 antibody cross-reacted with SAS from the three species specifically (Figure 2.7). Four dots immunostained with an anti-CrSAS-6 antibody were observed in each of the volvocine vegetative cells, represented a pair of BBs and a pair of pBBs. In all of the three volvocine species examined here, two flagella extended from two dots (BBs) that were closer to each other than another pair of dots (pBBs) (Figure 2.5D-F, Figure 2.6B-D). Thus, the closer pair can be considered as BBs, and another pair as pBBs. Based on our indirect immunofluorescence microscopic observations, pairs of BB of *C. reinhardtii* were very close to each other to appear to be almost one dumbbell-shaped dot (Figure 2.6B) and their distance was 280 ± 40 nm (n = 20) (Figure 2.6A). In contrast, two dots representing a pair of BBs in *T. socialis* cells and peripheral cells of the 16-celled *G. pectorale* colonies were apparently separated from each other (Figure 2.6A, C, D).

Distances between BBs in *T. socialis* and *G. pectorale* cells were 360 ± 40 nm (n = 20) and 470 ± 50 nm (n = 20), respectively. Distances between pBBs in the three species fell within a small range (Figure 2.6.A).

Additionally, the separation of proximal ends of BBs of *T. socialis* was confirmed by TEM (Figure 2.6E, F). The two BBs in the mature cell of *T. socialis* were inserted in the anterior region of the protoplast with an about 120º to each other and their proximal ends were separated, showing a striated distal fiber and an electron-dense proximal fiber (Figure 2.6E, F). In *C. reinhardtii*, two BBs are almost attached to each other at the proximal ends and show a 90º between them (Ringo 1967).

2.3.3 Observations of cytoplasmic bridges during the embryogenesis of *T. socialis*

CBs in the volvocine algae are thought to be important for embryogenesis of multicellular members, though it is not certain if they are structural, and/or for communication (Green et al. 1981). The simplest hypothesis is that CBs between daughter protoplasts form four-celled square daughter colonies during the multiple fission cell cycle of mother cells in *T. socialis*. To determine if and when CBs form in *T. socialis* daughter colonies, cultures were synchronized to a light-dark cycle and observed by light microscopy and TEM as they progressed through embryogenesis. Also, multiple fission has been hypothesized to be modified such that incomplete cytokinesis keeps daughter cells attached as a colony. To our knowledge, this hypothesis has not been examined directly in the most basal colonial multicellular *T. socialis,* relative to unicellular *C. reinhardtii*.

In *T. socialis*, each parental cell lost its flagella by absorption like in *C. reinhardtii* (Cavalier-Smith 1974). The cell then divided into four daughter protoplasts by two successive longitudinal divisions (Figure 2.4H.1-5). The second division was perpendicular to the first to form four daughter protoplasts arranged like a four-leaf clover (Figure 2.4H.2, 3). Each daughter cell formed two new flagella within the

parental ECM (Figure 2.4H.5). During these processes, the four daughter protoplasts maintained the four-leaf clover-like form without significant movement from one another, based on time-lapse analysis (Figure 2.4H.1-5). This result suggests that *T. socialis* daughter protoplasts are possibly connected via CBs until the daughter colony matures by the formation of new ECM.

To determine if CBs were present in daughter *T. socialis* colonies, cells during embryogenesis in synchronous culture were observed by TEM (Figure 2.8). In the four-celled embryo, CBs were observed in both sides facing the adjoining protoplasts (Figure 2.8A). One side was formed by first cleavage and another was formed by second cleavage, because the second cleavage of *T. socialis* was inserted perpendicularly to the first cleavage based on light microscopy (Figure 2.4). Moreover, the CBs remained even after the formation of new flagella within the parental ECM (Figure 2.8B-D). These results suggest that CBs may play an important role in conjunction with ECM deposition in keeping *T. socialis* daughter colonies multicellular.

2.4 DISCUSSION

The present immunofluorescence microscopic observations clearly demonstrated that the four-celled colony of *T. socialis* had cells with rotationally asymmetrical MTRs and separated BBs (Figures 2.5, 2.6). These two situations are essentially the same as those of other multicellular volvocalean species of the Goniaceae and Volvocaceae, such as *G. pectorale* (Greuel & Floyd 1985)*, Astrephomene gubernaculifera* (Hoops & Floyd 1983), *P. caudata* (Taylor et al. 1985), and *V. carteri* (Hoops 1984). In contrast, cells of *C. reinhardtii* exhibit rotational symmetry in arrangement of MTRs and have adjacent BBs (Figures 2.5D, 2.6B) as previously described by Ringo (1967). Previous studies demonstrated that peripheral cells of *G. pectorale* (Greuel & Floyd 1985) and cells of *V. carteri* (Hoops 1984) beat two flagella in nearly the same direction so that they can swim effectively as cooperative multicellular organisms (Gerisch 1959; Hoops 1997), whereas, in the unicellular species *C. reinhardtii*, cells beat their flagella like breast stroke so that the cells can swim effectively (Ringo 1967). Rotational asymmetry of MTRs in cells might be important for multicellularity in volvocine algae (Kirk 2005) and arrangements of MTRs are related to flagellar beating pattern (Hoops 1997). Therefore, the asymmetrical arrangement of MTRs and separated BBs in *T. socialis* may indicate that each cell has a role for colonial motility as the component of the multicellular individual. However, the mode of MTRs asymmetry in the *T. socialis* colony is different from that of other multicellular volvocine algae (Goniaceae and Volvocaceae). In peripheral cells of the flattened 16-celled colony of *G. pectorale*, the angle of two MTRs extending to the center of the colony are wider than that of the other two MTRs extending exteriorly (Figure 2.5C) as described by Greuel & Floyd (1985). MTR arrangements of mature cells of complex spheroidal colonies of *A. gubernaculifera* (Hoops & Floyd 1983) and *V. carteri* (Hoops 1993) are fundamentally the same as those of *G. pectorale* in having almost parallel MTRs positioned in eyespot

side (exterior side of the *G. pectorale* flattened colony) and their MTRs are significantly asymmetrical. In contrast, two MTRs extending to the center of *T. socialis* colony were nearly parallel whereas the other two MTRs extending to the colonial periphery were arranged with a 90º angle each other (Figure 2.5B). In addition, two BBs in mature vegetative cells of *T. socialis* were different from those of other multicellular volvocalean members. The two BBs of *T. socialis* were arranged each other with a 120º angle (Figure 2.6E) and bear an electron-dense proximal fiber (Figure 2.6F), while those of *G. pectorale* (Greuel & Floyd 1985)*, A. gubernaculifera* (Hoops & Floyd 1983), *P. caudata* (Taylor et al. 1985), and *V. carteri* (Hoops 1984) are nearly parallel without a proximal fiber. This suggested the possibility that rotation of BBs of *T. socialis* may evolve independently of Goniaceae and Volvocaceae.

The present TEM observations clearly demonstrate the presence of CBs between daughter protoplasts during multiple fission and they persisted after the formation of new flagella (Figure 2.8). Thus *T. socialis*-specific cell arrangement in a colony should be determined by means of the CBs before the formation of new ECM as observed in *G. pectorale* (Iida et al. 2013), *A. gubernaculifera* (Hoops and Floyd 1982), *P. morum* (Fulton 1978), *Eudorina elegans* (Marchant 1977), *Platydorina caudata* (Iida et al. 2011), and *V. carteri* (Green et al. 1981). These results suggest that the evolution of CBs may be a key structural innovation required to keep colonies together and thus multicellular.

Two morphological characteristics observed in *T. socialis* (rotational asymmetry of cells with separated BBs and CBs between daughter protoplasts) are considered to be important for multicellularity in volvocine lineage, and they are common to goniacean and volvocacean species such as *G. pectorale* and *V. carteri* (Kirk 2005). Based on the morphological and multi-gene sequence data (Nozaki and Ito 1994; Nozaki et al. 2000; Nozaki 2003; Herron et al. 2009), the Tetrabaenaceae (including *T. socialis*) is basal or sister to the clade composed of other members of the

colonial Volvocales (Goniaceae and Volvocaceae). Therefore, the two key characteristics, rotational asymmetry of cells with separated BBs and CBs during embryogenesis, might have been acquired in the common ancestors of the extant colonial or multicellular volvocine green algae.

2.5 FIGURES

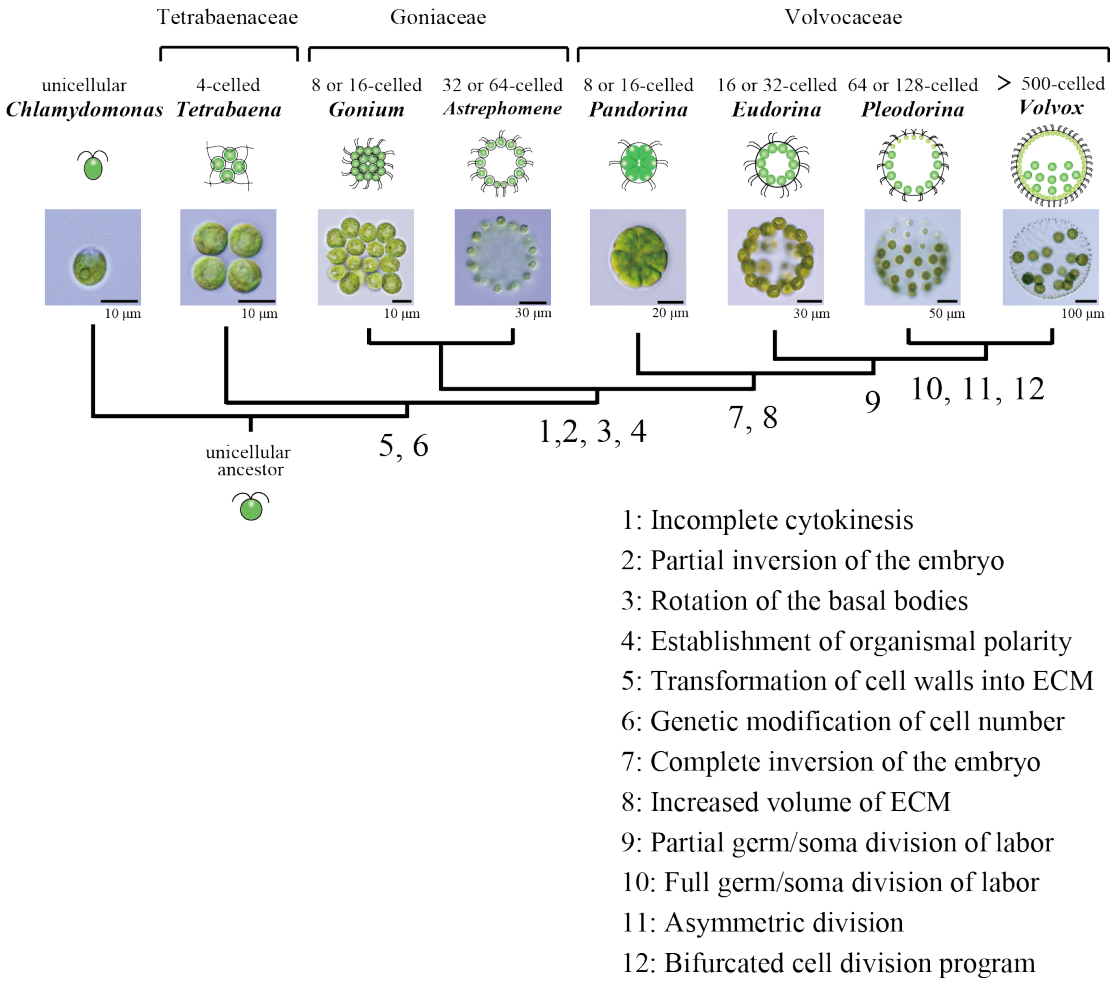

Figure 2.1. Twelve evolutionary steps from unicellular ancestor to differentiated *Volvox*, proposed by Kirk (2005).

Each number indicates the deduced acquisition time of the twelve steps. Based on Kirk (2005) and Herron et al. (2009).

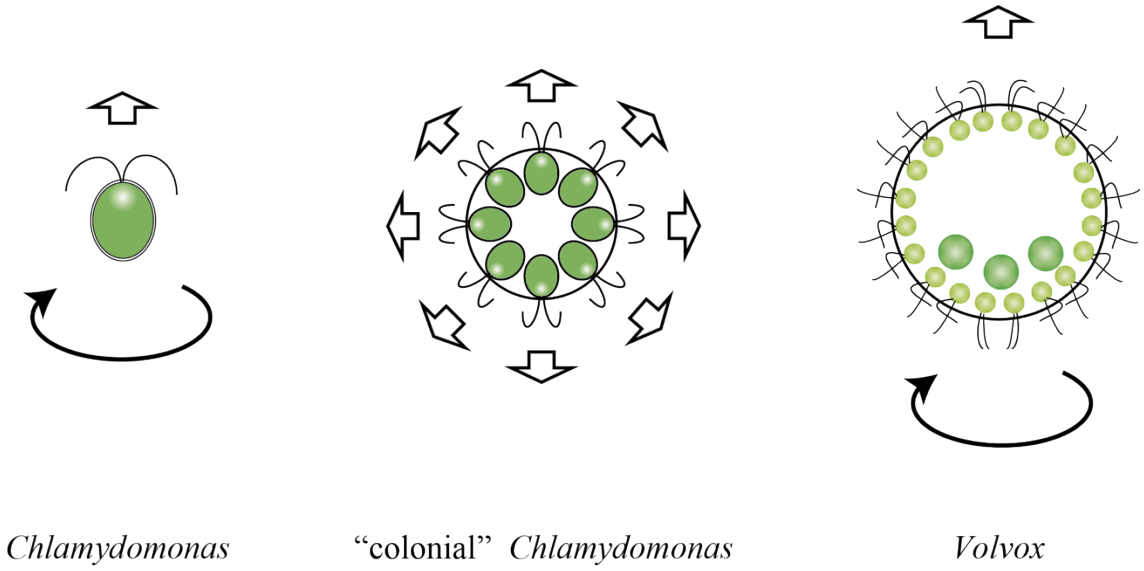

Figure 2.2. Breast-stroke type flagellar motion of unicellular *Chlamydomonas* and crawl type flagellar motion of multicellular *Volvox*.

White block arrows indicate the direction of progression and curvilinear arrows indicate the direction of rotation. Hypothetical "colonial" *Chlamydomonas* without rotation of basal bodies would not swim toward one direction because each cell beats flagella like *Chlamydomonas* cell. Based on Hoops (1997).

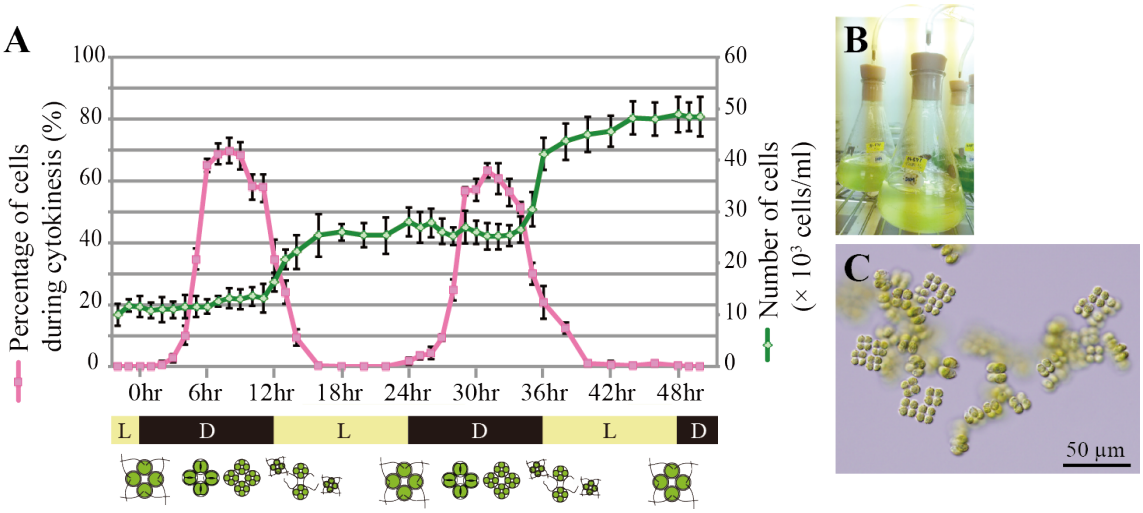

Figure 2.3. Newly established synchronous culture of *Tetrabaena socialis*.

A: Time course of synchronous culture of *T. socialis* strain NIES-571. Light (L): dark (D) cycle 12 h: 12 h is indicated on the horizontal axis. Percentages of cells during cytokinesis of cells (pink line) and number of cells (green line) are indicated on vertical axis of left and right side, respectively. Each error bar denotes standard deviation (n= 3).

B: *T. socialis* cultures growing synchronously in flasks with aeration.

C: *T. socialis* cells, just after cytokinesis, in the synchronous culture.

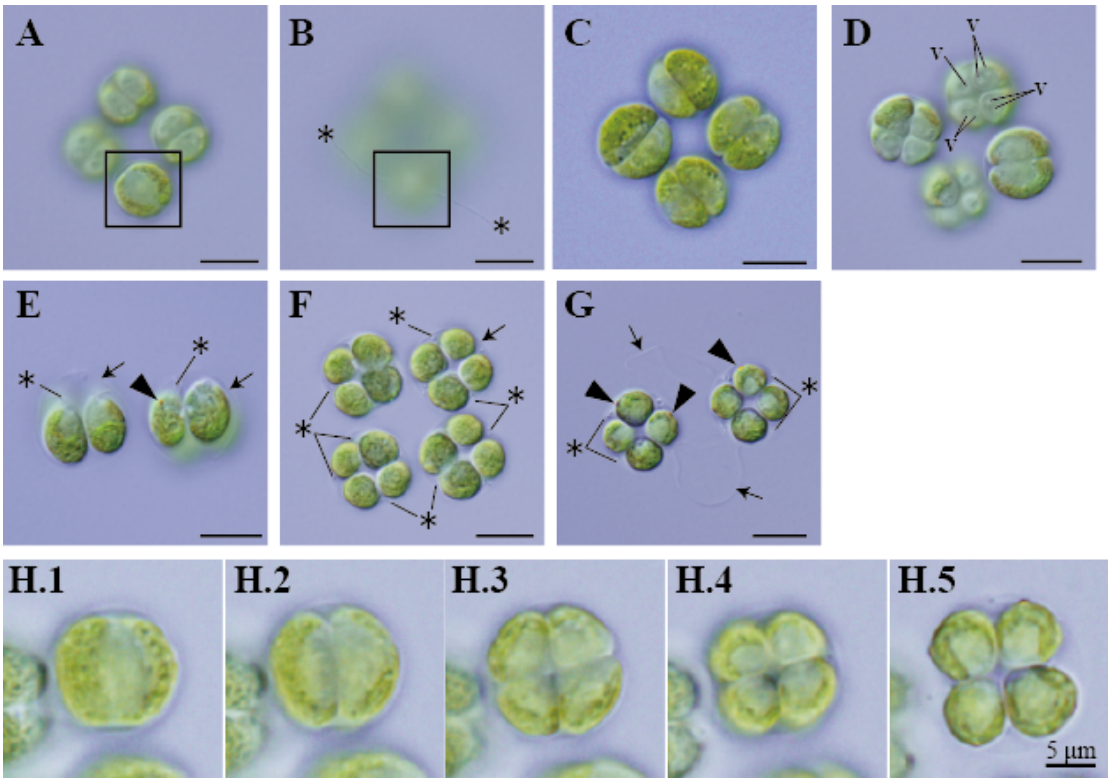

Figure 2.4. Light microscopic (A-H) and time-lapse (H.1-5) images of *Tetrabaena socialis* during asexual reproduction.

A, B: Two different views of a colony. Black square shows one of the four parental cells before cytokinesis with two parental flagella (asterisks).

C: Anterior view of a parental colony in a two-celled stage.

D: Anterior view of a parental colony. Note two contractile vacuoles (v) in each daughter protoplast.

E-G: Daughter colonies with newly formed flagella (asterisks) and eyespots (arrowheads) in parental ECM (arrows).

H: Time-lapse images. Each cell divided into four daughter protoplasts by two successive longitudinal divisions and formed daughter colonies of the same shape to parental colonies.

Scale bars (A-G): 10 µm.

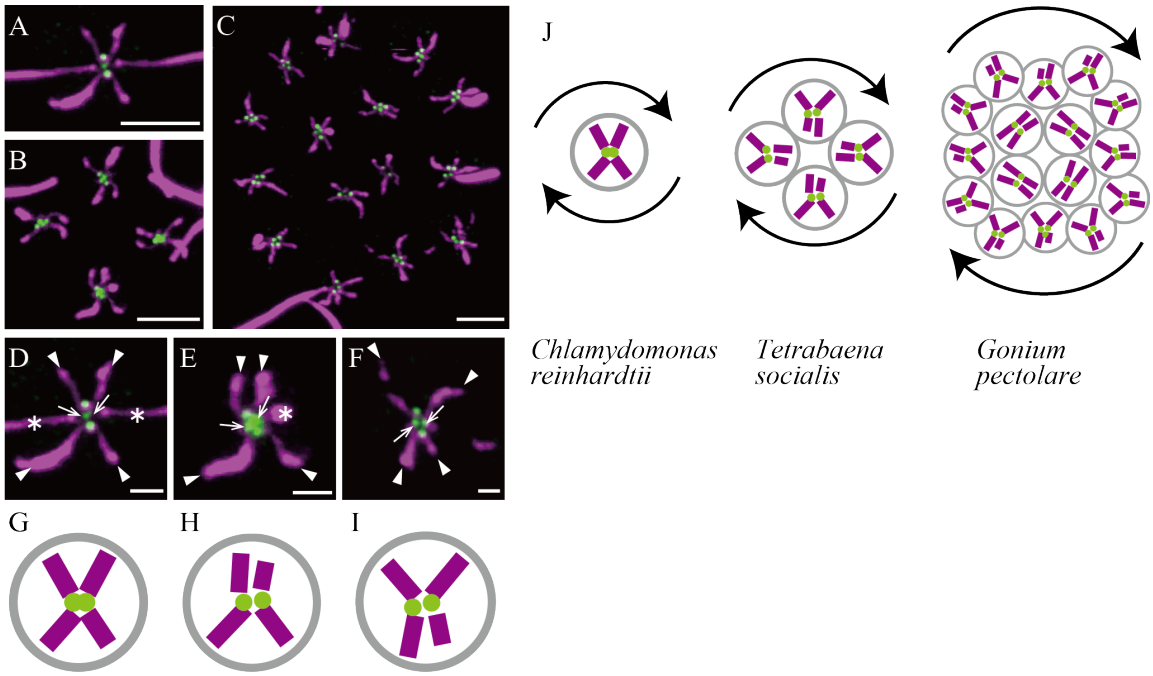

Figure 2.5. Confocal images and diagrams of microtubular rootlet (MTR) and basal bodies (BBs)/pro-basal bodies (pBBs).

A-F: Double stained immunofluorescence with an anti-acetylated tubulin α antibody (magenta; arrowheads) and an anti-*Chlamydomonas* SAS-6 antibody (green; arrows), showing MTRs and BBs/pBBs, respectively. Scale bars (A-C): 5 µm, (D-F): 1 µm. Asterisks: flagella. Arrangements of MTR in *Chlamydomonas reinhardtii* were 180º rotational symmetry (A, D). Arrangements of MTRs in *Tetrabaena socialis* were rotational asymmetry (B: whole colony, E: a cell in four-celled colony). Arrangements of MTRs in *Gonium pectorale* were rotational asymmetry (C: whole colony, F: a cell in 16-celled colony). Upper sides of E and F represent the direction to the center in the flattened colonies.

G-I: Diagrams of MTRs and BBs arrangements in *C. reinhardtii* (G), *T. socialis* (H), and *G. pectorale* (I) based on the immunofluorescence microscopy. Upper sides of H and I represent the direction to the center in the flattened colonies.

J: Diagrams showing MTRs and BBs in *C. reinhardtii*, *T. socialis* and *G. pectorale*. Curvilinear arrows indicate the direction of rotation.

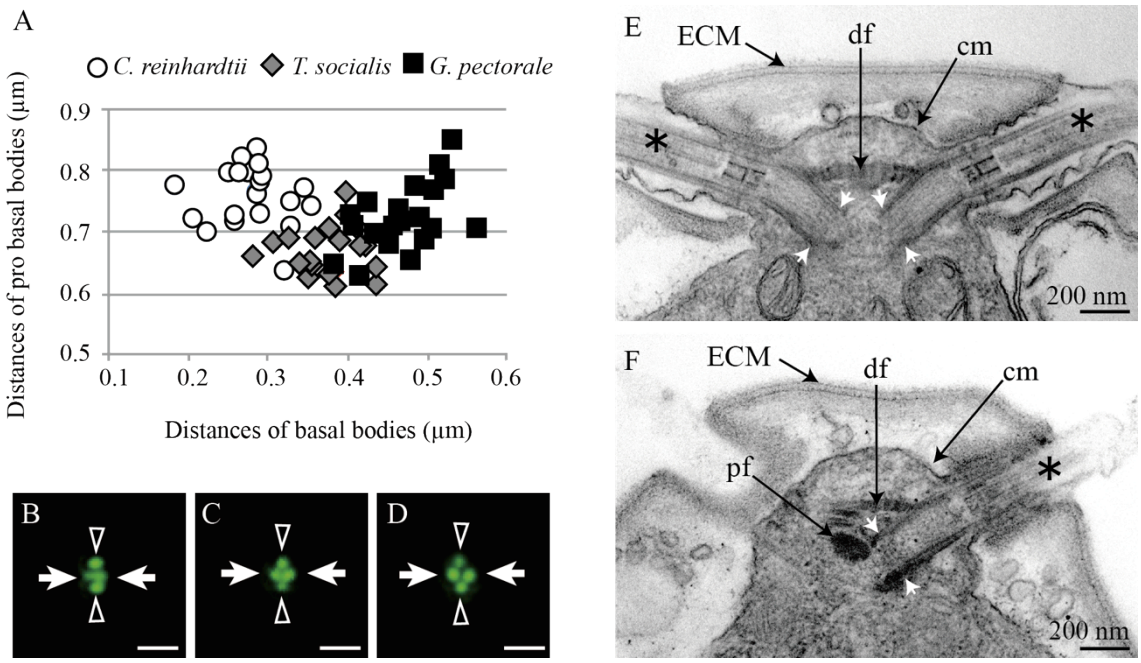

Figure 2.6. Distances of basal bodies (BBs) and pro-basal bodies (pBBs).

A: Scatter plot of distances between each pair of BBs and pBBs of mature cells. Distances between BBs and pBBs are indicated on the horizontal and vertical axes, respectively. White circles indicate *Chlamydomonas reinhardtii*, gray lozenges indicate *Tetrabaena socilais*, and black squares indicate *Gonium pectorale*.

B-C: Confocal images of BBs (arrows) and pBBs (arrowheads) of *C. reinhardtii* (B), *T. socialis* (C), and *G. pectorale* (D) stained with the anti-*Chlamydomonas* SAS-6 antibody. BBs of *C. reinhardtii* were very close to each other to represent a large dot (B). BBs of *T. socialis* (C) and *G. pectorale* (D) were separated each other. Scale bars: 1 μm.

E, F: Transmission electron microscopy of flagella apparatus of *T. socialis*. Proximal ends of BBs (white arrows) were separated from each other as well as the immunofluorescence microscopy. Asterisks: flagella, ECM; extracellular matrices, df: distal fiber, cm: cell membrane, pf: proximal fiber.

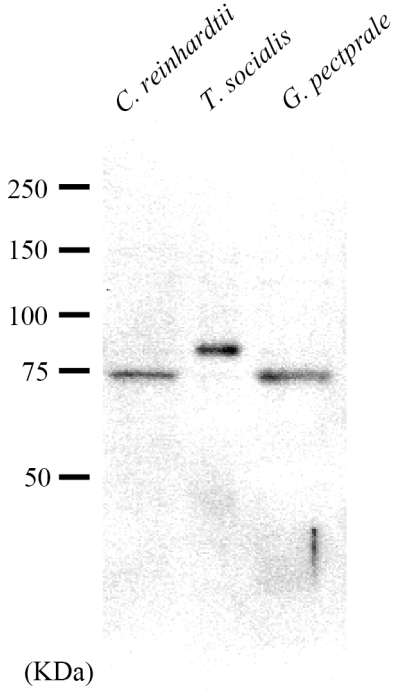

Figure 2.7. Western blot analysis of *Chlamydomonas reinhardtii*, *Tetrabaena socialis* and *Gonium pectorale* with an antibody against *Chlamydomonas* SAS-6 (anti-CrSAS-6 antibody).

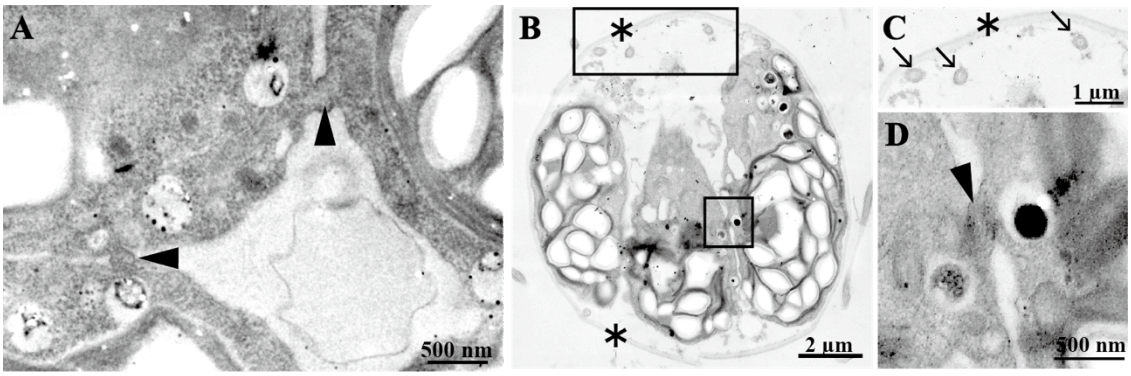

Figure 2.8. Transmission electron microscopy of four-celled embryos of *Tetrabaena socialis.*

A: Transverse section of central part of four-celled embryo of *T. socialis.* Note the cytoplasmic bridges (CBs) between daughter protoplasts (arrowheads).

B-D: Longitudinal section of four-celled embryo of *T. socialis* after formation of new flagella (arrows in C) within parental extracellular matrices (asterisks). Daughter protoplasts were connected by CB (arrowhead in D) even after new flagella were formed. C and D were enlarged images of upper and lower frame in B, respectively.

Chapter 3.

Comparative analyses of cell cycle-related genes in the initial stage of multicellularity based on *de novo* genome/transcriptome assembly of *Tetrabaena socialis*

3.1 INTRODUCTION

As discussed in Chapter 2, the simplest multicellular volvocine species *Tetrabaena socialis* belongs to the most ancestral multicellular volvocine family Tetrabaenaceae and this alga represents four common morphological features with more advanced multicellular volvocine members: incomplete cytokinesis, rotation of basal bodies, transformation of cell wall to extracellular matrix, and modulation of cell number. Recently, Hanschen et al. (2016) analyzed the whole genome of *Gonium pectorale*, and proposed the candidate molecules that might have been key factors for the evolution of volvocine multicellularity. According to Hanschen et al. (2016), modifications of cell cycle regulation molecules, multiplication of *cyclin D1* (*CYCD1*) gene and alternations in retinoblastoma (RB) /MAT3 protein might have occurred in the common ancestor of *G. pectorale* and *Volvox carteri.* However, such molecular characteristics have not been studied in the Tetrabaenaceae possibly because of the lack of nuclear genome data.

In this chapter, in order to reveal the cell cycle-related genes of the Tetrabaenaceae, I analyzed our *de novo* genome and transcriptome sequences of *T. socialis*. Evolution of *CYCD1* genes and RB/MAT3 proteins is discussed during the initial stage of the volvocine lineage.

3.2 MATERIALS AND METHODS

3.2.1 Preparation of genome/transcriptome assembly

For construction of *T. socialis* draft genome and transcriptome assemblies, *T. socialis* strain NIES-571 was used. Cells were grown as described in Chapter 2 (2.2.1 Cultures). No contaminated bacteria were observed in the *T. socialis* cultures by 4',6-diamidino-2-phenylindole (DAPI) staining based on Kawafune et al. (2014).

Genomic DNA extraction was performed by modified methods from Miller et al. (1993). Approximately 1.8 liters of an active growing, four-days-old *T. socialis* culture were harvested by centrifuge and washed by fresh SVM (Kirk and Kirk 1983). Resuspension buffer (50mM Tris pH 8.0, 10mM EDTA), 20% sarcosyl, and glass beads (Sigma Aldrich) were added to the concentrated cells in 1/10, 1/5 and 1/3 volumes of the pellet, respectively. The cells were disrupted by five freeze/thaw cycles. Each cycle consisted of vortexing 3 minutes at room temperature, and freezing for 30 minutes at –80ºC, and then thawing for six minutes at 37ºC (freeze/thaw cycle). The disrupted sample was put in –80ºC freezer overnight. The supernatant of thawed sample was transferred to a new tube and glass beads were removed by centrifuge. Pre-warmed 65ºC 2x CTAB buffer (2% CTAB, 100 mM Tris pH 8.0, 20 mM EDTA, 1.4 M NaCl, 1% polyvinyl pyrrolidone) was added to the sample in equal volume of the sample, and the tube was incubated for 15 minutes at 65ºC. Then the sample was purified by chloroform extraction, and pre-warmed 65ºC 10% CTAB buffer (10% CTAB, 0.7M NaCl) was added to the sample in 1/10 volume, vortexed for 30 seconds at room temperature, and incubated for 20 minutes at 65ºC. Subsequently, the sample was purified by chloroform extraction again. The purified sample was added by the equal volume of CTAB precipitation buffer (1% CTAB, 50 mM Tris pH8.0, 10 mM EDTA), mixed briefly, and incubated for 30 minutes at 65ºC. The supernatant of the sample was removed by centrifuge, and 400 μL high salt TE buffer (1M NaCl in TE buffer) was added to the pellet to dissolve the sample. Then the sample was purified by ethanol precipitation and dissolved in TE buffer. Sodium acetate solution (3M) was added to the

sample in 1/10 volume, and DNA was precipitated with ethanol at –20ºC for one hour. The supernatant was removed by centrifuge, the pellet was purified by ethanol precipitation again, and dissolved in TE buffer. Spermin-4HCl solution (200 mM) was added to the sample in 1/10 volume, the mixture was mixed gently. The supernatant was removed by centrifuge, 75 µL 100 mM EDTA and 65 µL 4 M ammonium acetate were added to the sample, the sample was mixed by vortex briefly, and incubated at 4ºC overnight. EDTA (100 mM, 500 µL) was subsequently added to the sample, the pellet was dissolved in the solution by pipetting, and incubated for one hour at 4ºC. Pre-chilled –20ºC 520 µL isopropanol was added to the tube, and the sample was mixed and incubated for 15 minutes at –20ºC. After the supernatant was removed by centrifuge, the pellet was dried well, and then dissolved in TE buffer. The sample was purified by phenol/chloroform extraction. Then, sodium acetate solution (3M) and ethanol were added to the purified sample in 1/10 and 2.5 times volume, respectively, and the mixture was incubated for 3.5 hours at –20ºC. The supernatant was removed by centrifuge, the pellet was washed by 70% ethanol, dried well and dissolved in TE buffer. RNase (Nippon Gene, Toyama, Japan) treatment was performed to the sample, according to the manufacture's protocol. The sample was purified by chloroform extraction and following ethanol precipitation was performed overnight. The supernatant was removed by centrifuge, the pellet was washed by 70% ethanol, dried well and resolved in TE buffer. The quality of purified DNA was checked by agarose gel electrophoresis and values of a spectrometer NanoDrop 2000 (Thermo Fisher Scientific, Waltham, MA, USA) and a Qubit 2.0 fluorometer (Thermo Fisher Scientific). The purified DNA was shipped to Witwatersrand University for generating *de novo* nuclear genome data (size: 133 Mb, GC content: 66%) based on sequencing by Hiseq (illumina, San Diego, CA, USA) and Miseq (illumina) and assembling by Allpaths-LG software (Gnerre et al. 2011) and SPAdes software (Bankevich et al. 2012).

Total RNA was extracted by using TRI reagent (Molecular Research Center Inc, Cincinnati, OH, USA). Approximately 1.2 liters of an active growing, four-days-old *T. socialis* culture was harvested by centrifuge. The concentrated culture

was transferred to a mortar cooled with liquid nitrogen, and TRI reagent was added there in 10 times volume of the sample. The cells were disrupted by homogenize in the cooled mortar sufficiently, and purified by chloroform extraction. Isopropanol was added to the upper aqueous layer after chloroform extraction in equal volume of the sample and the mixture was mixed gently and incubated for 10 minutes at room temperature. The supernatant was removed by centrifuge, 75% ethanol was added to the precipitation, and the sample was vortexed. The sample was treated with 75% ethanol washing again, the precipitation was resolved in RNase-free water and incubated for 15 minutes at 68ºC. The quality of purified RNA was checked by agarose gel electrophoresis and values of a spectrometer NanoDrop 2000 and a Qubit 2.0 fluorometer. The purified RNA was dried by GenTegra RNA (GenTegra LLC, Pleasanton, CA) to stabilize RNA according to the manufacture's protocol. The stabilized RNA was shipped to Witwatersrand University, where *de novo* transcriptome assembly data were generated by sequencing with Hiseq 2500 system (illumina) and mapping with Bridger *De Novo* software (Chang et al. 2015) using the whole genome assembly.

3.2.2 BLAST-based search of the homologues

To examine the copy number of *T. socialis CYCD1* (*TsCYCD1*) gene, TBLASTN (Altschul et al. 1997) search was performed against the newly constructed *T. socialis* nuclear genome and transcriptome assemblies by using CYCD1 of *C. reinhardtii* (CrCYCD1), *G pectorale* (GpCYCD1.1-4), and *V. carteri* (VcCYCD1.1-4) (Table 3.1) as queries. Partial sequences of *CYCD1* and three other *cyclin D* (*CYCD*) of *T. socialis* (*TsCYCD*2, *TsCYCD3*, and *TsCYCD*4) were obtained.

To examine the copy number of *CYCD1* gene in other species of *Chlamydomonas* that are closely related to volvocine algae (Yumoto et al. 2013), I explored *CYCD1* homologues from *C. debaryana* and *C. sphaeroides* nuclear genome (Hirashima et al. 2016). AUGUSTUS (Keller et al. 2011) server (http://bioinf.uni-greifswald.de/augustus/) was used for automated gene calling on

nuclear genome of the two *Chlamydomonas* spp. TBLASTN searches were performed against AUGUSTUS treated assemblies of *Chlamydomonas* spp. using CrCYCD1 as a query (Table 3.3).

To compare the RB/MAT3 domain structure of *T. socialis* (TsRB/MAT3), partial sequence of *RB/MAT3* was obtained from *T. socialis* genome and transcriptome assemblies by TBLASTN search with RB/MAT3 of *C. reinhardtii* mating type plus (CrRB/MAT3) (Table 3.4) as a query.

3.2.3 Sequencing

To determine the complete CDS of *cyclin D* genes and *RB/MAT3* gene of *T. socialis*, sequence analyses were performed with newly designed primers (Tables 3.2, 3.5). Polyadenylated mRNA of *T. socialis* was isolated with Dynabeads oligo $(dT)_{25}$ (Life Technologies, Carlsbad, CA, USA) and reverse transcribed with Superscript III reverse transcriptase (Life Technologies) (Kawai-Toyooka et al. 2014). PCR was carried out using the synthesized cDNA as follows: 94°C for 1 minute, 35 cycles of 94°C for 30 seconds, 60°C for 30 seconds, and 72°C for 2 minutes, followed by 72°C for 5 minutes with *TaKaRa LA-Taq* with GC Buffer (Takara Bio Inc., Otsu, Japan) by using a thermal cycler GeneAmp PCR System 9700 (Life Technologies). Amplified DNA were purified with illustra GFX PCR DNA and Gel Band Purification Kits (GE Healthcare, Buckinghamshire, UK), and some samples were TA subcloned with TOPO TA Cloning Kit for Sequencing (Life Technologies) according to the manufacture's protocol, additionally. The purified PCR products were sequenced by an ABI PRISM 3100 Genetic Analyzer (Life Technologies) with a BigDye Terminator cycle sequencing ready reaction kit, v.3.1 (Life Technologies) directly or after TA cloning. The 5' and 3' ends of *cyclin D* genes and *RB/MAT3* of *T. socialis* were determined by RACE using the GeneRacer kit (Life Technologies) according to the manufacture's protocol. Each synthesized RACE product was amplified with KOD FX Neo DNA polymerase (TOYOBO, Osaka, Japan). PCR was carried out as follows: 94°C for 2 minutes, 5 cycles of 98°C for 10 seconds and 74°C for 1.5 minutes, 5 cycles of 98°C for 10

seconds and 72°C for 1.5 minutes, 5 cycles of 98°C for 10 seconds and 70°C for 1.5 minutes, 15 cycles of 98°C for 10 seconds and 68°C for 1.5 minutes, and followed by 68°C for 7 minutes. Amplified DNA was purified and sequenced as described above.

3.2.4 Phylogenetic analyses

The amino acid sequences of CYC family from three volvocine algae (Table 3.1) were obtained from Phytozome version 10 (http://www.phytozome.net/) and National Center for Biotechnology Information (NCBI; https://www.ncbi.nlm.nih.gov). Volvocine CYC sequences were aligned with the newly determined CYC proteins of *T. socialis* by MAFFT version 7 (Katoh and Standley 2013) server (http://mafft.cbrc.jp/alignment/server/), and trimmed the low-alignment regions manually. Phylogenetic analyses of CYC family were performed based on the alignment (Figure 3.1) using the maximum-likelihood (ML) and the neighbor joining (NJ) methods with PhyML program (Guindon et al. 2010) and MEGA 5.2.2 program (Tamura et al. 2011), respectively. The WAG+I+G+F model, selected by ProtTest3 (Darriba et al. 2011) optimized using Akaike information criteria. The bootstrap analyses were performed with 1000 replicates. The sequences of CYCA1, CYCB1, and CYCAB1 were used as outgroup (Figure 3.4) based on the phylogenetic results of these proteins by Prochnik et al. 2010.

The amino acid sequences of RB/MAT3 from nine volvocalean algae (Table 3.4) were obtained from Phytozome version 10 and NCBI. The RB/MAT3 sequences were aligned with the newly determined TsRB/MAT3, based on the alignment of Hanschen et al. (2016). Phylogenetic analyses of RB/MAT3 were performed using the ML and the NJ methods with PhyML program and MEGA 5.2.2 program, respectively. The JTT+G+F model, selected by ProtTest3 optimized using Akaike information criteria. The bootstrap analyses were performed with 1000 replicates. The sequences of *C. globosa* and *C. reinhardtii* were used as outgroup (Figure 3.6) according to Hiraide et al. (2013).

3.2.5 Prediction of cyclin dependent kinase phosphorylation sites of RB/MAT3

Phosphorylation sites between RB-B domain and C domain were predicted by using PlantPhos (Lee et al. 2011) server (http://csb.cse.yzu.edu.tw/PlantPhos/). I extracted the serine-prolin (SP) motifs that have a positively charged amino acid (arginine or lysine) after the SP motif from all predicted phosphorylation site, based on Hanschen et al. (2016) (Figures 3.5, 3.7).

3.3 RESULTS

3.3.1 Duplication of *CYCD1* genes of *T. socialis*

Three full-length CDSs of *TsCYCD1* genes, *TsCYCD1.1* (1782 bp), *TsCYCD1.2* (1098 bp), and *TsCYCD1.3* (1137 bp), were determined. The CYC proteins were highly diverse each other, except for cyclin domain region (Appendix 1). Within the nuclear genome assembly, *TsCYCD1.1* and *TsCYCD1.2* were located on the same scaffold (scaffold_357), and the distance between them was approximately15.6 kbp (Table 3.1, Figure 3.1) whereas *TsCYCD1.3* was found in another scaffold (scaffold_221). TsCYCD1.1 and TsCYCD1.2 possessed the LXCXE motif (X represents any amino acid) that is conserved in CYCD proteins from land plants and metazoans (Xie et al. 1996; Dahiya et al. 2000). However, TsCYCD1.3 lacked the motif (Table 3.1, Figure 3.2).

TBLASTN searches against the predicted CDS demonstrated that *Chlamydomonas debaryana* and *C. sphaeroides* had a single *CYCD1* candidate (Table 3.3). The CYCD1 candidates of these two unicellular species possessed the LXCXE motif (Table 3.3, Figure 3.2).

Based on the present phylogenetic analyses, volvocine CYCD proteins (CYCD1-4) formed a robust monophyletic group with 99% and 89% bootstrap values in ML and NJ analysis, respectively (Figure 3.3). Within CYCD clade, CYCD1 of *C. reinhardtii*, *T. socialis*, *G. pectorale*, and *V. carteri* formed a monophyletic group though it was supported with low bootstrap values (49% and 18% bootstrap values in ML and NJ analysis, respectively). Although supported with low bootstrap values, expanded CYCD1s in each volvocine species formed a clade (Figure 3.3). These results were consistent with those of Hanschen et al. (2016).

3.3.2 Comparative examination of RB/MAT3 primary structures

Full-length CDS of *TsRB/MAT3* (3510 bp) was determined and the length of L1 region and phosphorylation sites were examined because Hanschen et al. (2016) discuss that

these features are important in the evolution of multicellularity. Figure 3.4 shows the alignment of the deduced amino acid sequence of TsRB/MAT3 (1169 amino acids) and nine volvocalean RB/MAT3 homologues (Prochnik et al. 2010; Hiraide et al. 2013) (Table 3.4), based on Hanschen et al. (2016). RB-A domain, RB-B domain, and conserved N-terminal (N1-3) and C-terminal (C1 and C4) regions were indicated in Figure 3.4. These domains and conserved regions were observed in newly determined TsRB/MAT3 as in other volvocalean RB/MAT3 proteins (Figure 3.4). The results of phylogenetic analyses (Figure 3.5) were consistent with those of the previous study (Hiraide et al. 2013).

The L1 regions between RB-A domain and RB-B domain were highly diverse (Figure 3.4), and the lengths of multicellular members (197-201 amino acids) were shorter than those of unicellular *C. reinhardtii* and *C. globosa* (106-174 amino acids) (Table 3.6, Figures 3.4, 3.6).

Two unicellular species *C. reinhardtii* and *C. globosa* had two phosphorylation sites between RB-B domain and C-terminal conserved region (indicated with orange background color in Figure 3.4, arrowheads in Figure 3.6). Multicellular *T. socialis* had three phosphorylation sites, and *Yamagishiella unicocca* and *Eudorina* sp. had one phosphorylation site (indicated with blue background color in Figure 3.4, arrowheads in Figure 3.6) within the region. Thus, there was no clear difference in the number of phosphorylation sites between unicellular and multicellular members.

3.4 DISCUSSION

According to the whole genome analysis of differentiated multicellular *V. carteri* (Prochnik et al. 2010), *V. carteri* has four *CYCD1* genes in genome, unlike unicellular *C. reinhardtii* that has a single *CYCD1* gene. The *CYCD1* expansion in *V. carteri* is thought to be important for development of the tissues as well as highly differentiated metazoans and land plants (Beumer et al. 2000; Dewitte et al. 2002; Hanschen et al. 2016). Hanschen et al. (2016) demonstrated the *CYCD1* expansion in non-differentiated *G. pectorale* genome and they proposed that the duplication of *CYCD1* genes may be important for the transition from unicellular to simple multicellular, rather than tissue differentiation observed in *V. carteri*. In this chapter, I demonstrated that *CYCD1* genes of four-celled *T. socialis* were expanded to three copies and two of the three *TsCYCD1* genes, *TsCYCD1.1* and *TsCYCD1.2*, were located in the vicinity of the genome (Table 3.1, Figure 3.1-3). This situation was also similar to those of the multicellular species *G. pectorale* and *V. carteri*, which have four *CYCD1* genes arrayed in tandem; in contrast, unicellular *C. reinhardtii* has a single *CYCD1* gene (Prochnik et al. 2010; Hanschen et al. 2016). In addition, TBLASTN searches against other species of *Chlamydomonas* spp. demonstrated that *C. debaryana* and *C. sphaeroides* had a single *CYCD1* gene in the nuclear genome (Table 3.3). These results suggested that the expansion of *CYCD1* genes may be specific to the multicellular species within the Volvocales.

In CYCD proteins, LXCXE motifs are important for interacting with RB protein (Xie et al. 1996; Dahiya et al. 2000), and they are detected in land plant CYCD proteins as in metazoans (Dahl et al. 1995; Soni et al. 1995). The LXCXE motif is found in N-terminal conserved regions of CYCD1 of unicellular *C. reinhardtii* (Hanschen et al. 2016), *C. debaryana* and *C. sphaeroides* (Table 3.3, Figure 3.2), whereas presence and absence of this motif are found within the CYCD1 paralogues of *T. socialis*, *G. pectorale* (Hanschen et al. 2016) and *V. carteri* (Hanschen et al. 2016) (Table 3.1, Figure 3.2). The three multicellular volvocine algae had two CYCD1 paralogues with LXCXE motif (Table 3.1, Figure 3.2). Each of those paralogues with

the LXCXE motif has a potential to bind and interact with RB and the RB pathway of the multicellular volvocine members might be regulated by at least two CYCD1 paralogues. Thus, the duplicated *CYCD1* genes, which exist in multicellular volvocine species, may be involved in different RB regulation from unicellular volvocine alga *C. reinhardtii*.

CYCD proteins are involved in eukaryotic cell cycles through the RB cascade: dimers of CYCD proteins and cyclin-dependent kinases phosphorylate RB proteins, the phosphorylated RB stops inhibiting transcription by E2F/DP transcription factors, then transcriptions of genes for mitosis start, and cell cycles progress (Hanschen et al. 2016; Olson and Nedelcu 2016). Hanschen et al. (2016) found out two structural differences in RB/MAT3 protein between unicellular *C. reinhardtii* and multicellular *G. pectorale* and *V. carteri*. One of the two is the shortening of L1 regions, which are thought to act as binding pocket for interaction with E2F/DP complexes (Knudsen and Wang 1997; Hanschen et al. 2016). The second difference is lacking of the phosphorylation sites between RB-B domain and C-terminal conserved region of multicellular *G. pectorale* and *V. carteri* (Hanschen et al. 2016). Hanschen et al. (2016) discussed that the two differences might reflect the different approach of RB to bind chromatin via E2F/DP and contribute to the stage or locus-specific gene expressions in multicellular species (Hanschen et al. 2016). In this chapter, I added RB/MAT3 sequences of unicellular *C. globosa*, multicellular *T. socialis*, *Y. unicocca*, *Eudorina* sp., and *Pleodorina starrii* (Table 3.4) to the data set of Hanschen et al. (2016) and compared those characteristics. Each multicellular member has a shorter L1 region than that of unicellular members (Table 3.6, Figures 3.4, 3.6), as discussed in Hanschen et al. (2016). Therefore, the ancestor of TGV-clade might have shortened its L1 region during evolution to multicellularity.

Hanschen et al. (2016) discussed the importance of phosphorylation sites between RB-B domain and conserved C-terminal region in transition to multicellularity in volvocine green algae. According to their results, unicellular *C. reinhardtii* has two phosphorylation sites whereas multicellular *G. pectorale* and *V. carteri* lack the

phosphorylation site. However, in the present analysis, phosphorylation sites were detected in three multicellular members (three in *T. socialis*, one in both *Y. unicocca*, and *Eudorina* sp.) (Figures 3.4, 3.6). These results suggested that the absence of the phosphorylation sites might not be important for transition to multicellularity in the volvocine lineage.

3.5 TABLES AND FIGURES

Table 3.1. Protein IDs, LXCXE motifs, and abbreviations of volvocine cyclin proteins used in this study.

Abbreviations are used in the alignment (Appendix 1) for the phylogenetic analyses (Figure 3.3).

Protein Name	Species Name	Protein IDs	LXCXE Motif	Abbreviation
CYCD1.1	*Chlamydomonas reinhardtii*	Cre11.g467772[a]	LICTE	CrCYCD1
	Tetrabaena socialis	scaffold_357[b]	LQCLE	TsCYCD1.1
	Gonium pectorale	GPECTOR_47g299[a]	N. D	GpCYCD1.1
	Volvox carteri	Vocar20010063m[a]	LTCTE	VcCYCD1.1
CYCD1.2	*T. socialis*	scaffold_357[b]	LQCLE	TsCYCD1.2
	G. pectorale	GPECTOR_47g300[a]	LLCDE	GpCYCD1.2
	V. carteri	Vocar20010067m[a]	N. D	VcCYCD1.2
CYCD1.3	*T. socialis*	scaffold_221[b]	N. D	TsCYCD1.3
	G. pectorale	GPECTOR_47g301[a]	N. D	GpCYCD1.3
	V. carteri	Vocar20010127m[a]	N. D	VcCYCD1.3
CYCD1.4	*G. pectorale*	GPECTOR_100g16[a]	LLCTE	GpCYCD1.4
	V. carteri	Vocar20013188m[a]	LLCTE	VcCYCD1.4
CYCD2	*C. reinhardtii*	Cre06.g289750[a]	LQCDE	CrCYCD2
	T. socialis	scaffold_137[b]	LACDE	TsCYCD2
	G. pectorale	GPECTOR_41g668[a]	LECEE	GpCYCD2
	V. carteri	Vocar20013437m[a]	LICEE	VcCYCD2
CYCD3	*C. reinhardtii*	Cre06.g298750[a]	LFCGE	CrCYCD3
	T. socialis	scaffold_137[b]	LACDE	TsCYCD3
	G. pectorale	GPECTOR_44g48[a]	LECED	GpCYCD3
	V. carteri	Vocar20007422m[a]	LHCED	VcCYCD3
CYCD4	*C. reinhardtii*	Cre06.g259500[a]	LDCTE	CrCYCD4
	T. socialis	scaffold357[b]	LGCTE	TsCYCD4
	V. carteri	Vocar20007145m[a]	LECSE	VcCYCD4
CYCD5	*G. pectorale*	GPECTOR_11g188[a]	N. D	GpCYCD5

CYCA1	*C. reinhardtii*	Cre03.g207900[a]	N. D	CrCYCA1
	V. carteri	Vocar20005704m[a]	N. D	VcCYCA1
CYCB1	*C. reinhardtii*	Cre08.g370401[a]	N. D	CrCYCB1
	V. carteri	Vocar20013188m[a]	N. D	VcCYCB1
CYCAB1	*C. reinhardtii*	Cre10.g466200[a]	N. D	CrCYCAB1
	V. carteri	Vocar20015027m[a]	N. D	VcCYCAB1

N. D.: Not detected.

[a]Based on Hanschen et al. (2016).

[b]Determined in this study.

Table 3.2. Primers used for amplifications and sequencing of *cyclin D* genes of *Tetrabaena socialis* (*TsCYCD1.3, TsCYCD2*, *TsCYCD3* and *TsCYCD4*).

Primer Designation	Sequences (5'-3')
TsCYCD1.3_F1	CATGTCCATTGCGGTCAAGTA
TsCYCD1.3_R2	AGCTGCTGCAGGCTGAGG
TsCYCD1.3_3'RACE_F1	CGACGTCCATCCTAGACCGCTTCAC
TsCYCD1.3_5'RACE_R1	ACCTCCTCGTACTTGACCGCAATGG
TsCYCD2_F1	GGATGGTGGAGGTGGTGACT
TsCYCD2R2	TGCTGTAGCCGTACGATAGGAA
TsCYCD2_3'RACE_F1	GTTGACTCGGACAACAACCCGCTCTACCTG
TsCYCD2_3'RACE_F2	AAGGGTCTCGTGTATGGTACAGCCCGTGAG
TsCYCD2_5'RACE_R1	GTACATGAGCGACAGCTCCGCCAGGAAGTT
TsCYCD2_5'RACE_R2	CAGTTCCAGGCTCGACTCATCCTCATCG
TsCYCD3_F1	CGTTCCTCGATCGCTTCCTA
TsCYCD3_R2	GAGTCCATGAGGGCAAGCTC
TsCYCD3_3'RACE_F1	GTCGCTTCTGCAGCTCCTGGCTCTAACCTG
TsCYCD3_3'RACE_F2	GACTCCGAGCTCACAGGCGTCAGCTACA
TsCYCD3_5'RACE_R1	TGCAGGAACATGGAGAGGAAGGTGTAGATGG
TsCYCD3_IC_F2	CGTCGCTTCTGCAGCTCCTGGCTCT
TsCYCD3_IC_R3	CGATGCGGTGCAGGAACATGGAGAG
TsCYCD4_F1	AGACTCTCTTCGCCGCCACTT
TsCYCD4_R3	AAGCGCTGCAGGAAGGTGAG

Table 3.3. Cyclin D1 (CYCD1) homologues from *Chlamydomonas* spp. by TBLASTN searches using *Chlamydomonas reinhardtii* CYCD1 as a query.

Species Name	Accession No.	*CYCD1* in Scaffold	E-value	LXCXE motif
C. debaryana	BDDB00000000[a]	Single in BDDB01000173.1	9E-49	LLCTE
C. sphaeroides	BDDC00000000[a]	Single in BDDC01001326.1	5E-50	LVCSE

[a]Hirashima et al. (2016).

Table 3.4. List of accession numbers of RB/MAT3 protein used in this study.

Species Name	Mating type/Sex	Accession No.
Chlamydomonas globosa		AY781411[a]
C. reinhardtii	Plus	AB771947[a]
C. reinhardtii	Minus	AB771948[a]
Tetrabaena socialis	Homothallic	LC279746[b]
Gonium pectorale	Plus	AB771928[a]
Yamagishiella unicocca	Plus	AB771932[a]
Eudorina sp.	Female	AB771936[a]
Pleodorina starrii	Female	AB771938[a]
Volvox carteri	Female	XM_002954427[c]
V. carteri	Male	GU784916[c]

[a]Hiraide et al. (2013).

[b]Determined in this study.

[c]Prochnik et al. (2010).

Table 3.5. Primers used for amplifications and sequencing of *RB/MAT3* gene of *Tetrabaena socialis* (*TsRB/MAT3*).

Primer Designation	Sequences (5'-3')
TsMAT3_F1	GACTGCGATGAGACTGTTTCTG
TsMAT3_F3	CGAGCAAGACGAAGACGTCAAG
TsMAT3_F5	GTAATGGGGTTGCTGGCAAAAA
TsMAT3_F8	CAGTGCAGCAGCTCAGTCGT
TsMAT3_F17	AATTGGGCAGCAAGTTGGTCGG
TsMAT3_R2	GGCACAATAGACATACGCAAAA
TsMAT3_R6	GTCGAAGGCCTTGATGTGAAGC
TsMAT3_R7	TGCTCAATGGCCTCGTAAACCT
TsMAT3_3'RACE_F1	CAGCCGCAGTCACAGCAATCCATTT
TsMAT3_3'RACE_F2	AGCACAGGCATATCCCCCTTGAGAC
TsMAT3_3'RACE_F3	ACAGCCAGCAGAGTGCAGACAACGAAGAAG
TsMAT3_5'RACE_R1	TTTTGCCAGCAACCCCATTACCACCAC
TsMAT3_5'RACE_R2	TACGACGTTGGCCTCGCGAAAGAAGTC

Table 3.6. The length of linker (L1) region of volvocalean RB/MAT3 proteins.

Species Name	Matingtype /Sex	Length of L1 region (aa)	Vegetative Form
Chlamydomonas globosa[a]		201	Unicellular
C. reinhardtii[a]	Plus/Minus	197	Unicellular
Tetrabaena socialis[b]	Homothallic	144	Multicellular
Gonium pectorale[a]	Plus/Minus	104	Multicellular
Yamagishiella unicocca[a]	Plus/Minus	174	Multicellular
Eudorina sp.[a]	Female/Male	162	Multicellular
Pleodorina starri[a]	Female/Male	163	Multicellular
Volvox carteri[c]	Female	106	Multicellular
V. carteri[c]	Male	149	Multicellular

[a]Hiraide et al. 2013.

[b]Determined in this study.

[c]Prochnik et al. 2010.

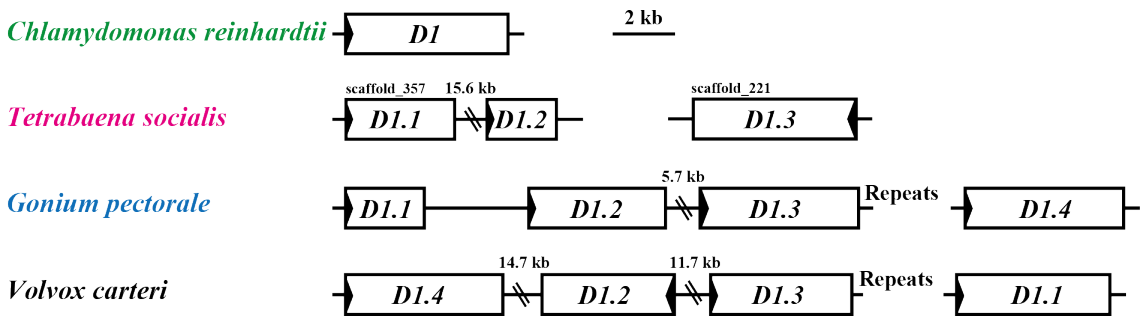

Figure 3.1. Syntenic relationships of duplicated *cyclin D1* (*CYCD1*) genes of multicellular volvocine algae.

Diagrams of *Chlamydomonas reinhardtii*, *Gonium pectorale* and *Volvox carteri* are based on Hanschen et al. (2016).

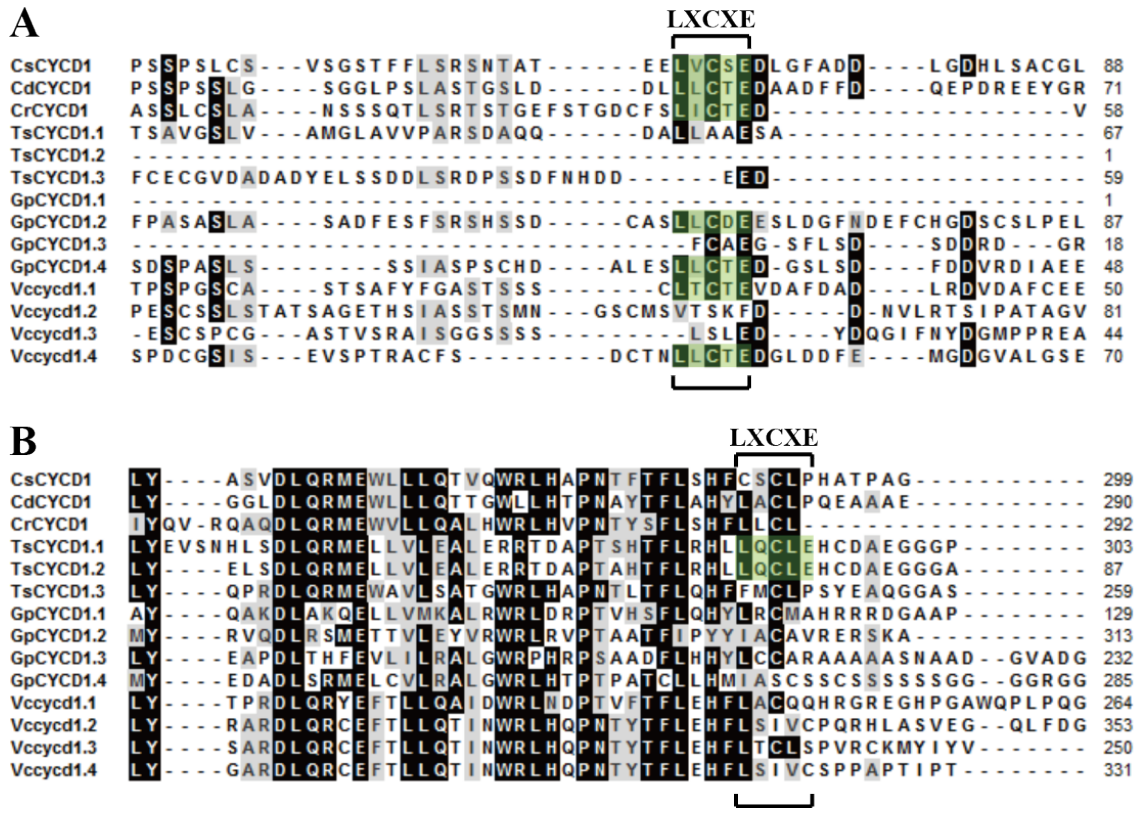

Figure 3.2. LXCXE motifs in volvocalean cyclin D1 (CYCD1) proteins.

Parts of alignment of volvocalean CYCD1 proteins. LXCXE motifs in CYCD1 protein of *Chlamydomonas sphaeroides* (CsCYCD1), *C. debaryana* (CdCYCD1), and *C. reinhardtii* (CrCYCD1), *Gonium pectorale* (GpCYCD1.2 and GpCYCD1.4), and *Volvox carteri* (Vccycd1.1 and Vccyc1.4) are indicated by light green background color (A). LXCXE motifs of *Tetrabaena socialis* (TsCYCD1.1 and TsCYCD1.2) are indicated by light green background color (B) (Table 3.1).

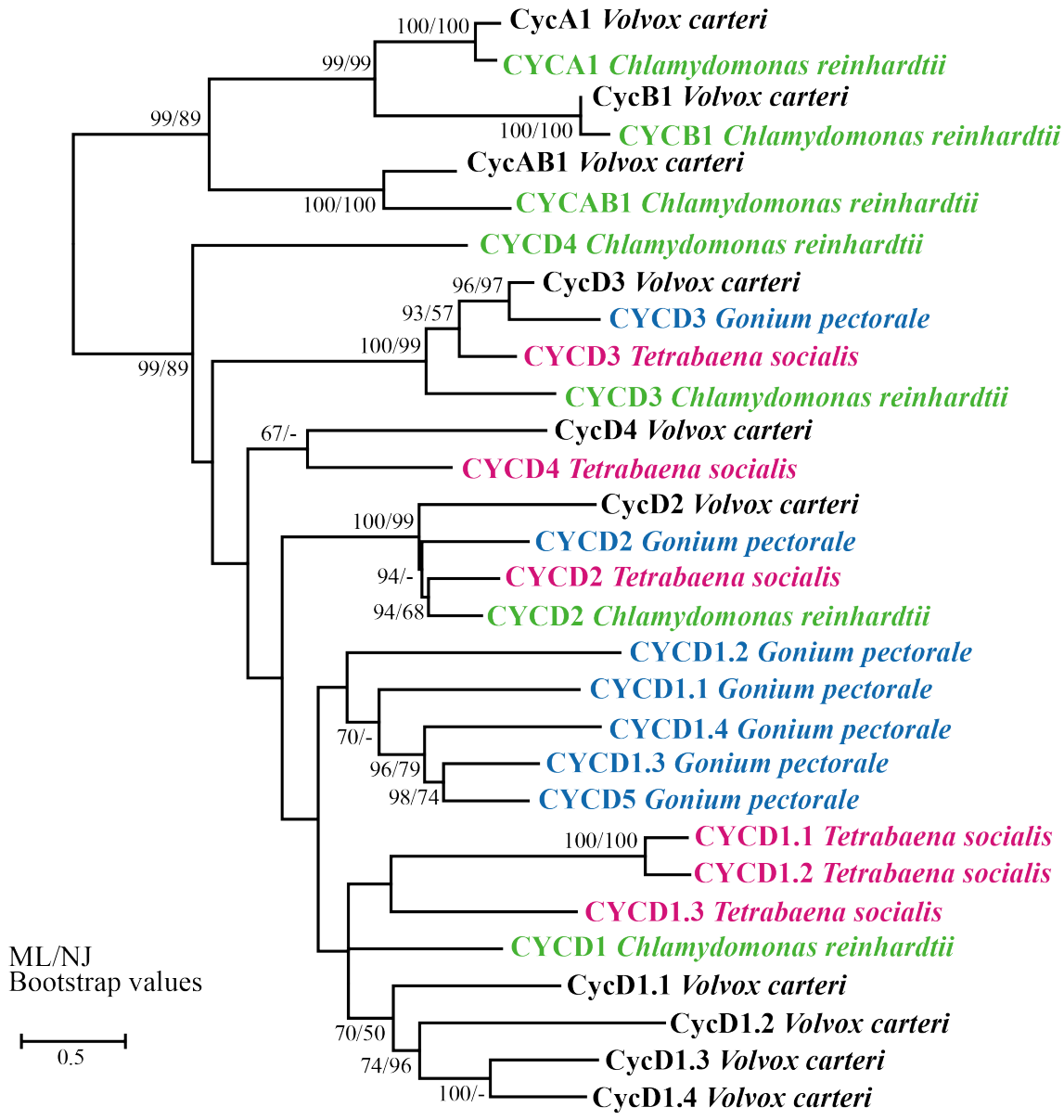

Figure 3.3. Maximum-likelihood (ML) tree of cyclin D (CYCD) family of multicellular volvocine algae.

Bootstrap values (≥50%) for the ML and neighbor-joining (NJ) analyses are indicated left and right side, respectively. The scale bar corresponds to 0.5 amino acid substitutions per position. Protein IDs and an alignment for the phylogenetic analyses are shown in Table 3.1 and Appendix 1, respectively.

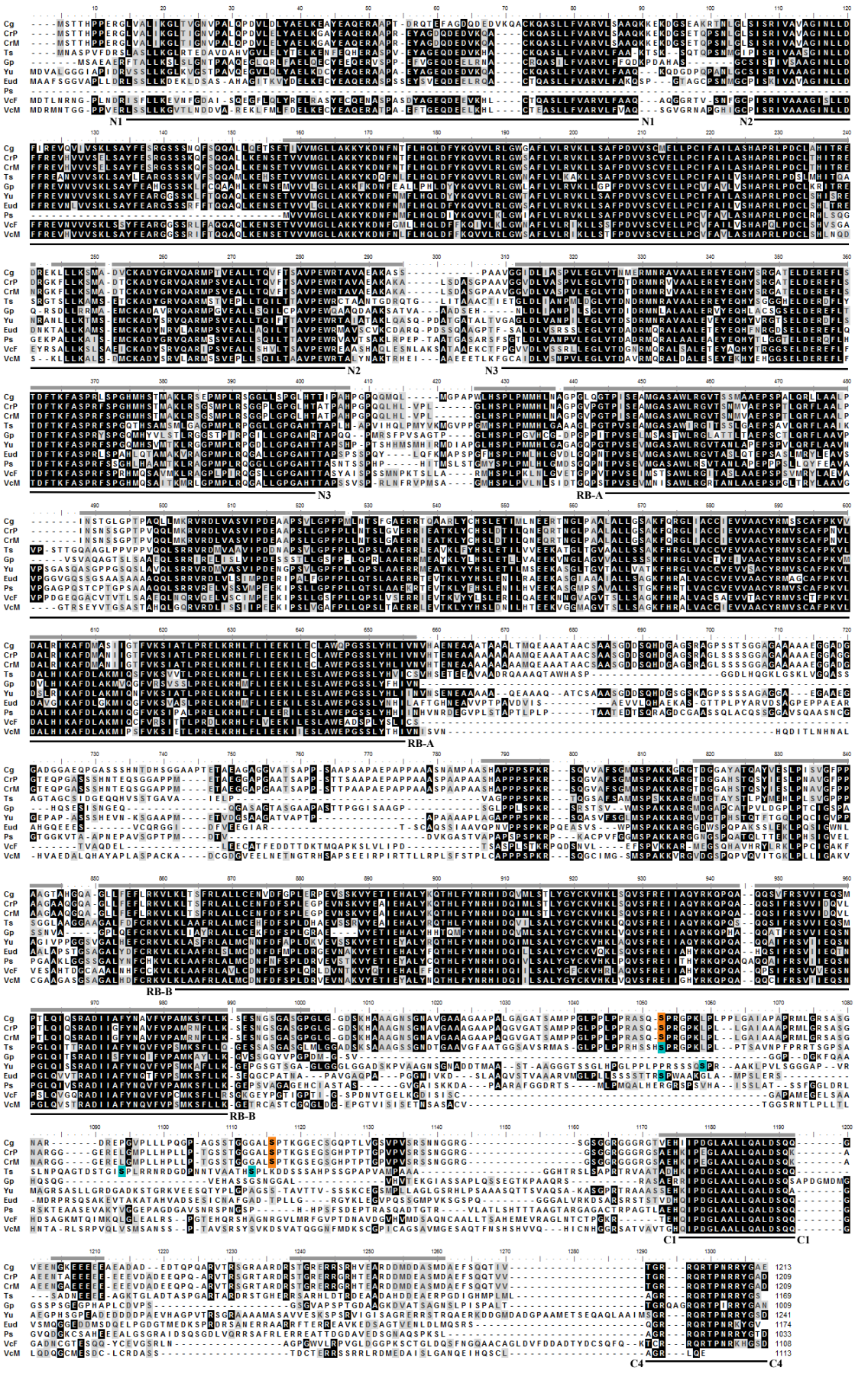
Cg
CrP
CrM
Ts
Gp
Yu
Eud
Ps
VcF
VcM
N1
N2
N3
RB-A
RB-B
C1
C4

Figure 3.4. Alignment of RB/MAT3 of volvocine algae.

RB/MAT3 amino acid sequences of *Chlamydomonas globosa* (Cg), *C. reinhardtii* mating type plus (CrP), *C. reinhardtii* mating type minus (CrM), *Tetrabaena socialis* (Ts), *Gonium pectorale* (Gp), *Yamagisiella unicocca* (Yu), *Eudorina* sp. (Eud), *Pleodorina starii* (Ps), *Volvox carteri* female (VcF), and *V. carteri* male (VcM) were aligned based on Hanschen et al. (2016). Domains are indicated under the alignment. Linker (L1) region is the sequence between RB-A domain and RB-B domain. Phosphorylation sites between RB-B domain and C-domain are indicated with orange background in unicellular, and blue background in multicellular. Positions 158-241, 244-251, 253-295, 312-407, 426-437, 439-480, 488-526, 528-657, 787-796, 818-845, 851-944, 947-989, 991-1001, and 1173-1192 (gray bars) were used for phylogenetic analyses (Figure 3.5）.

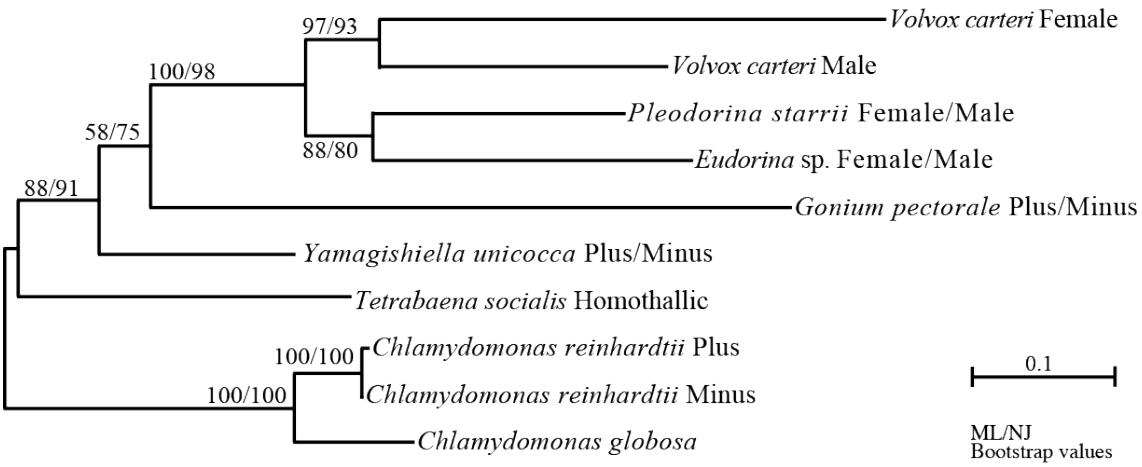

Figure 3.5. Maximum-likelihood (ML) tree of RB/MAT3 of volvocalean algae. Bootstrap values (≥50%) for the ML and neighbor-joining (NJ) analyses are indicated left and right side, respectively. The scale bar corresponds to 0.1 amino acid substitutions per position. Accession numbers of the amino acid sequences and an alignment for the phylogenetic analyses are shown in Table 3.4 and Figure 3.4, respectively.

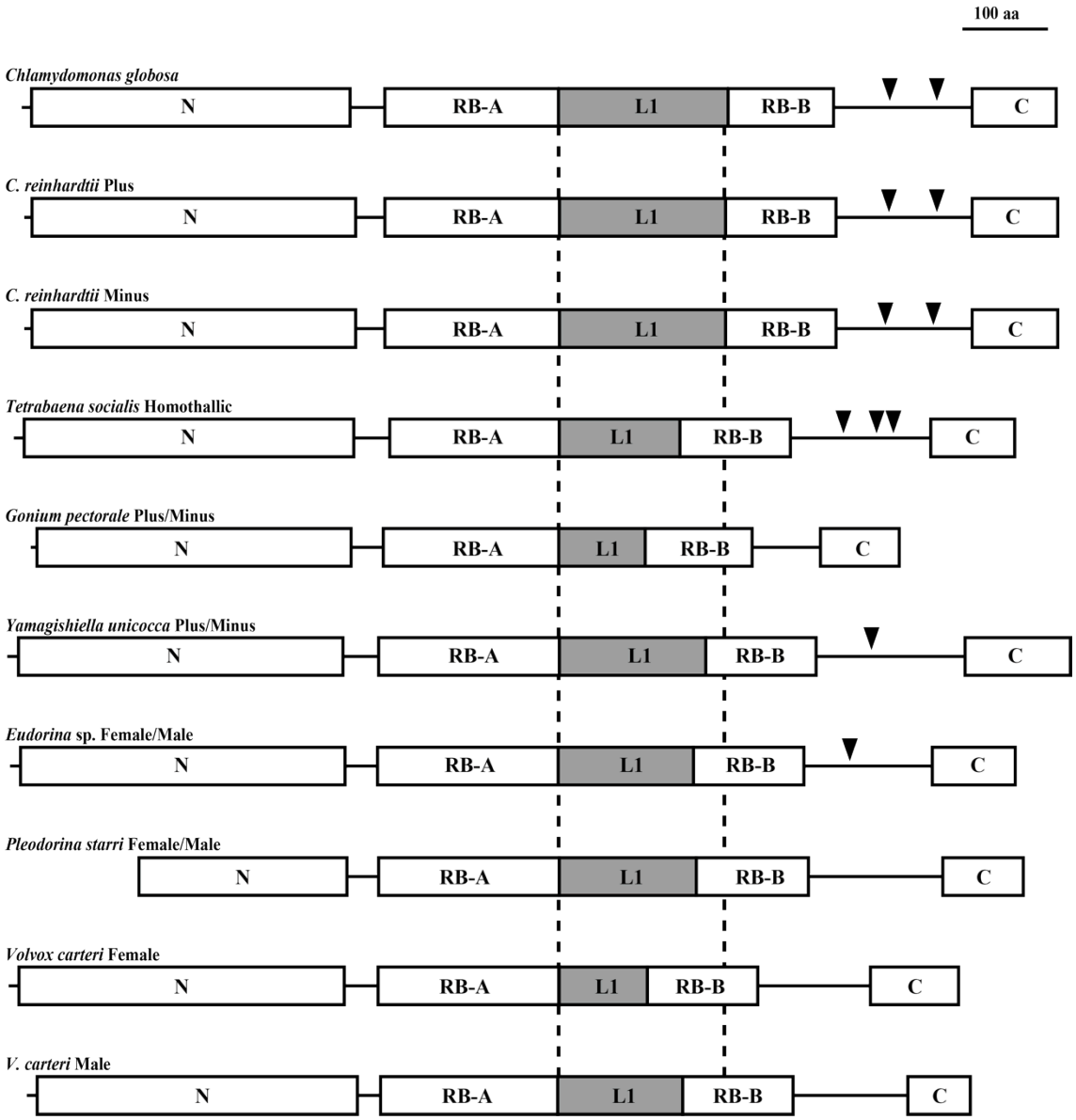

Figure 3.6. Comparison of volvocalean RB/MAT3 structures.

Length of linker (L1) region of *Chlamydomonas reinhardtii* (Plus) is indicated by dotted lines. L1 regions of multicellular species tend to be short. Arrowheads indicate the phosphorylation sites between RB-B domain and C domain, predicted in this study by using PlantPhos (Lee et al. 2011) server (http://csb.cse.yzu.edu.tw/PlantPhos/). Several phosphorylation sites were predicted in multicellular *Tetrabaena socialis*, *Yamagishiella unicocca*, and *Eudorina* sp. Accession numbers of the amino acid sequences for this comparison are shown in Table 3.4.

Chapter 4.

Comparative cell biological analyses of the cytokinesis-related protein DRP1

4.1 INTRODUCTION

In Chapter 3, I demonstrated the modifications of the cell cycle-related molecules (*CYCD1* genes and RB/MAT3 protein) in the simplest multicellular species *Tetrabaena socialis* (see Chapter 2), based on the newly constructed draft genome. Thus, the relationship between the modifications of cell cycle-related genes and evolution of multicellularity previously suggested by whole genome analyses of *Gonium pectorale* (Hanschen et al. 2016) could be considered in the four-celled common ancestor of the colonial or multicellular volvocine green algae (TGV- clade) (Chapter 2). However, there is little information about more downstream genes that actually participate in the formation of the integrated multicellular individuals during embryogenesis.

During asexual life cycles of unicellular and multicellular volvocine algae, reproductive cells perform successive divisions (rapid S/M phase alternating without G2 phase) known as multiple fission (e.g. Kirk 1998). The unicellular species *C. reinhardtii* forms 2^n daughter cells depending on the mother cell size (Umen and Goodenough 2001), whereas in multicellular volvocine members, genetic modulations of daughter cell number are additionally present in the multiple fission and daughter protoplasts are arranged in the species-specific shape of embryos or daughter colonies (Kirk 2005). These daughter protoplasts are connected to one another by cytoplasmic bridges (CBs), which are formed by incomplete cytokinesis. CBs were observed in multicellular species such as four-celled *T. socialis* (Chapter 2), flattened 16-celled *G. pectorale* (Iida et al. 2013), and spheroidal >500-celled *V. carteri* (Green et al. 1981). Considering that both of these two multicellular member-specific traits (modulation of daughter cell number and incomplete cytokinesis) are recognized in the most ancestral species *T. socialis*, comparative molecular analyses of multiple fission between unicellular and multicellular forms are fruitful for further understanding the initial transition to multicellularity in this lineage. Moreover, the incomplete cytokinesis might be essential

for the initial evolution of multicellularity prior to increasing of cell numbers and cell differentiation, therefore I focused on cytokinesis-related genes in this chapter.

Various cytokinesis-related genes have been characterized in animals (Eggert et al. 2006) and land plants (Jürgens 2005). Modes of cytokinesis are various; mother cells divide into two daughter cells by fission in metazoans, whereas two daughter cells are produced by a cell plate newly formed in land plant mother cells (Field et al. 1999). However, there are some common molecules associated with cytokinesis in metazoans and land plants (Jürgens 2005; Eggert et al. 2006) such as dynamin-related proteins (DRP). Dynamin was originally described as a microtubule-binding protein that was isolated from bovine brain extracts (Shpetner and Vallee, 1989). Dynamin orthologues are often categorized as classical or conventional dynamins, which have five distinct domains: GTPase domain, middle domain, pleckstrin-homology domain, GTPase effecter domain (GED), and prolin-rich domain (Praefcke and McMahon 2004; Konopka et al. 2006). However, dynamin superfamily contains members that lack pleckstrin-homology domain and/or prolin-rich domain, or have additional domains that are not present in classical dynamins, and these members are defined as DRPs (Konopka et al. 2006). In metazoans and land plants, several dynamins and DRPs play important roles in cytokinesis (Praefcke and McMahon 2004; Konopka et al. 2006). For example, in *Arabidopsis thaliana*, double mutant line *drp1a/drp1e* is unable to accomplish the embryogenesis because of the defects in cell wall formation (Kang et al. 2003), DRP1A and DRP1E are localized in the cell plate (Kang et al. 2003), DRP2B are co-localized with DRP1A in the cell plate during cytokinesis and function in vesicle formation (Fujimoto et al. 2010), and DRP5A are localized in the cell plate at the end of cell division (Miyagishima et al. 2008).

In this chapter, I focused on the DRP1 homologues in the volvocine lineage to examine the contribution of cytokinesis-related genes to the initial stage of multicellularity. I determined CDS of the *DRP1* homologue of the simplest

multicellular species *T. socialis* (*TsDRP1*), and performed immunofluorescence microscopy with a newly raised anti-TsDRP1 antibody in unicellular *C. reinhardtii* and ancestral multicellular *T. socialis* and *G. pectorale*.

4.2 MATERIALS AND METHODS

4.2.1 Cultures

Three algal strains were used in this chapter: *C. reinhardtii* strain cw92, *T. socialis* strain NIES-571, and *G. pectorale* strain 2014-0520-F-4. *C. reinhardtii* and *T. socialis* were cultured synchronously as described in Chapter 2 (2.2.1 Cultures). To establish synchronous culture of *G. pectorale*, approximately 10 mL culture in SVM (Kirk and Kirk 1983) was inoculated into a silicon-capped 500 mL flask containing 300 mL SVM with aeration at 25°C, on a light: dark cycle 12 h: 12 h under cool-white fluorescent lamps at an intensity of 130–180 μmol·m^{-2}·s^{-1}. To evaluate the synchrony, I counted ratios of dividing cells in cultures at several times during 24 h (Figure 4.3).

4.2.2 Sequencing of dynamin-related gene homologues

To determine the complete CDS of *TsDRP1*, partial sequence was obtained from *T. socialis* strain NIES-571 genome assembly (see Chapter3) by TBLASTN search using *C. reinhardtii* DRP1 (CrDRP1) as the query and designed *TsDRP1* specific primers (Table 4.1). cDNA was synthesized and sequenced as described in Chapter 3 (3.2.3 Sequencing). Domains of DRP1 proteins were searched by using the Pfam program (http://pfam.xfam.org) (Finn et al. 2016).

4.2.3 Phylogenetic analyses

The amino acid sequences of DRP1 and DRP2 from six streptophytes (land plants and *Klebsormidium flaccidum*) and six chlorophytes (Table 4.2) were collected from the genome databases in Phytozome version 10 and NCBI by TBLASTN searches using CrDRP1 and *A. thaliana* DRP2A as the queries, and they were aligned with the newly determined TsDRP1 by MAFFT version 7. Phylogenetic analyses were performed using

the ML and the NJ methods with PhyML program and MEGA 5.2.2 program, respectively. The LG+I+G+F model, selected by ProtTest3 optimized using Akaike information criteria. The bootstrap analyses were performed with 1000 replicates. The constructed phylogenetic tree was rooted between DRP1 and DRP2.

4.2.4 Preparation of an anti-TsDRP1 antibody

The antibody against TsDRP1 was raised in rabbits using the recombinant polypeptide. The cDNA sequence encoding the protein was amplified by PCR using the newly designed primers (Table 4.1). The PCR product (indicated in Figure 4.1) was cloned into a pET100 expression vector (Life Technologies) and 6xHis fusion polypeptide was expressed in Rosetta (DE3) *Escherichia coli* cells, purified using a HisTrap HP column (GE healthcare) . The purified polypeptide was subjected to SDS-PAGE, and gel slices containing the recombinant polypeptide were injected into rabbits for antibody production (Kiwa Laboratory Animals. Co., Ltd., Wakayama, Japan). Antibodies were affinity-purified from the antisera by using the recombinant polypeptide coupled to a HiTrap NHS-activated HP column (GE Healthcare).

4.2.5 Western blot analyses of DRP1

To evaluate the specificity of the anti-TsDRP1 antibody, SDS-PAGE and WB analyses were performed as described in Chapter 2 (2.2.2 Indirect immunofluorescence microscopy) except for antibodies. Both the anti-TsDRP1 antibody and an anti-IgG antibody conjugated to horseradish peroxidase (Jackson ImmunoReserch) were diluted 1: 2000 for WB. Molecular weight (69 kDa) of TsDRP1 was calculated based on the deduced amino acid sequence by Compute pl/Mw tool (http://web.expasy.org/compute_pi/) of Swiss Institute of Bioinformatics (Bjellqvist et al. 1993; Bjellqvist et al. 1994; Gasteiger et al. 2005).

To examine the expression of DRP1 at the protein level, following five time-course samples were obtained from each synchronous culture of *C. reinhardtii*, *T. socialis*, and *G. pectorale*: a sample with the greatest number of dividing cells during 24 hours (0 point), three hours before the 0 point (-3 point), six hours before the 0 point (-6 point), three hours after the 0 point (+3 point), and six hours after the 0 point (+6 point). The time-course samples were analyzed by SDS-PAGE and western blot as described above. For Coomassie brilliant blue staining as loading control, each duplicated SDS-PAGE gel was stained by EzStain AQua (ATTO, Tokyo, Japan).

4.2.6 Indirect immunofluorescence microscopy

Immunostaining of *C. reinhardtii* was performed using a modified method of Lechtreck et al. (2009). *C. reinhardtii* cells were attached to PEI coated coverslips and fixed in –20°C methanol for 5 minutes, transferred to fresh –20°C methanol for 5 minutes and air-dried. The dried cells were incubated in phosphate-buffered saline for 10 minutes. Subsequent blocking and antibody reactions were performed as described in Chapter 2 (2.2.2 Indirect immunofluorescence microscopy).

Immunostainings of *T. socialis* and *G. pectorale* were performed as described in Chapter 2 (2.2.2 Indirect immunofluorescence microscopy) except for antibodies used. The anti-TsDRP1 antibody and monoclonal anti-tubulin alpha antibody (Bio-Rad, Hercules, CA, USA), used as primary antibodies were diluted 1: 500 with the blocking buffer (see Chapter 2). Alexa Fluor 488 goat anti-rabbit IgG (H＋L) (# A11008, Invitrogen, Carlsbad, CA, USA) and Alexa Fluor 568 goat anti-rat IgG (H＋L) (# A11077, Invitrogen) were also diluted 1: 500 with the blocking buffer (see Chapter 2). Confocal and differential interference contrast (DIC) images were obtained with an FV-1200 (Olympus) and three serial images were merged by using Adobe Photoshop CS6 software (Adobe Systems Inc., San Jose, CA, USA).

4.3 RESULTS

4.3.1 Identification and characterization of *TsDRP1*

The full-length CDS of *TsDRP1* gene (1890 bp) was determined and the deduced amino acid sequence of TsDRP1 (629 amino acids) was aligned with DRP1 homologues of *A. thaliana* (AtDRP1A), *C. reinhardtii* (CrDRP1), *G. pectorale* (GpDRP1), and *V. carteri* (VcDRP1) (Figure 4.1). The DRP1 sequences were highly conserved within the volvocine algae: the identity of TsDRP1 with CrDRP1, GpDRP1, and VcDRP1 was 92%, 92%, and 91%, respectively. The GC contents of the volvocine *DRP1* CDS were apparently higher (*CrDRP1*: 64.18%, *TsDRP1*: 65.12%, *GpDRP1*: 62.22%, and *VcDRP1*: 57.55%) than that of *AtDRP1A* (46.78%), which is consistent with their GC-rich genome compositions (Merchant et al. 2007; Prochnik et al. 2010; Hanschen et al. 2016; Chapter3). Three domains that characterize DRP1, GTPase domain, middle domain, and GED (Konopka et al. 2006), were found in all DRP1 sequences of volvocine algae as well as AtDRP1A. The motifs for interactions to GTP (G1-4) (Praefcke and McMahon 2004) were conserved in AtDRP1A and volvocine DRP1 sequences (Figure 4.1).

To confirm that DRP1 sequences of volvocine algae are orthologous to the DRP1 proteins of land plants, phylogenetic analyses were performed. All five land plants possessed several paralogues of *DRP1* genes, whereas each of the green algae (six chlorophytes and charophycean *K. flaccidum*) possessed a single *DRP1* gene in the nuclear genome. Phylogenetic analyses resolved two large robust monophyletic groups, DRP1 clade and DRP2 clades. DRP1 clade was composed of all DRP1 sequences analyzed here and separated from DRP2 clade with 100% bootstrap support (Figure 4.2). The DRP1 clade was subdivided into two monophyletic groups corresponding to streptophytes and chlorophytes (Figure 4.2). The chlorophytes were composed of two robust clades, Chlorophyceae and Mamiellophyceae (*Micromonas pusilla* and

Micromonas sp.), with 99-100% bootstrap values. Within the Chlorophyceae, four volvocine DRP1 sequences formed a robust monophyletic group with 100% bootstrap values. These results were consistent with the phylogeny using multiple chloroplast genes (Smith et al. 2009; Leliaert et al. 2012; Ruhfel et al. 2014), and indicate that *DRP1* genes of volvocine algae are orthologues of *DRP1* of streptophytes.

4.3.2 Expression patterns of DRP1

To examine the relationship between volvocine DRP1 and cytokinesis at a protein expression level, I performed WB analyses using the anti-TsDRP1 antibody. The CrDRP1, TsDRP1, and GpDRP1 signals were detected as major bands at ~75 kDa with the anti-TsDRP1 antibody (Figure 4.3). DRP1 signals were detected from all time-course samples of the three species (Figure 4.3).

4.3.3 Subcellular localization patterns of DRP1

To verify the subcellular localization of DRP1, immunofluorescence microscopy was carried out using the anti-TsDRP1 and an anti-tubulin alpha antibodies. Immunofluorescences of tubulin were used as the division plane marker, because microtubule structures (phycoplast) are observed in division planes of volvocine algae (Doonan et al. 1987; Kirk et al. 1991; Dymek et al. 2006). In vegetative cells of *C. reinhardtii*, *T. socialis* and *G. pectorale*, DRP1 signals were observed as many speckles in their cytoplasm (Figure 4.4A-D, 4.5A-D, 4.6A-D). In two-celled stage, microtubules were observed in the cleavage furrows and DRP1 signals were localized near the furrows of *C. reinhardtii* (white arrowheads in Figure 4.4E-H), *T. socialis* (white arrowheads in Figure 4.5 E-H) and *G. pectorale* (white arrowheads in Figure 4.6E-H). DRP1 was localized in the vicinity of the division plane, while apparent co-localization of DRP1 and tubulin were not observed in two-celled stages of the three volvocine species (Figure 4.4H, 4.5H, 4.6H). The DRP1 fluorescence in cytoplasm at this stage

was less than that of vegetative cell (Figure 4.4F, 4.5F, 4.6F).

DRP1 localizations of the four-celled stage were different between the unicellular and multicellular species examined. In the four-celled stage of *C. reinhardtii*, DRP1 was mainly localized in second division planes (Figure 4.4I-L). In contrast, DRP1 in four-celled embryos of *T. socialis* and *G. pectorale* were observed clearly in both first and second division planes (Figure 4.5I-L, 4.6I-L). Eight-celled embryo of *G. pectorale* also exhibited clear DRP1 localization in the first, second and third division planes (Figure 4.6M-P).

4.4 DISCUSSION

The volvocine DRP1 homologues had three conserved domains (GTPase domain, dynamin middle domain, and GED) as in land plants (Konopka et al. 2006) (Figure 4.1), and the present phylogenetic analyses clearly demonstrated that DRP1 proteins of chlorophytes (including volvocine algae) and streptophytes formed a robust monophyletic group with 100% bootstrap values (Figure 4.2). Within chlorophytes, each species had a single DRP1 homologue and the phylogenetic relationships of DRP1 proteins were consistent with the species phylogeny (Smith et al. 2009; Leliaert et al. 2012; Ruhfel et al. 2014). Thus, the volvocine DRP1 proteins are orthologous to DRP1 of land plants.

In *C. reinhardtii*, *T. socialis* and *G. pectorale*, DRP1 signals were mainly observed in their cytoplasm during the vegetative phase (Figures 4.4B, 4.5B, 4.6B), but in the division plane during multiple fission (Figures 4.4F, J, 4.5F, J, 4.6 F, J, N). DRP1 expression was almost constitutive in the three species (Figure 4.3). Thus, volvocine DRP1 might change localization during cell cycle. The volvocine DRP1 localizations in the division plane were similar to those of some DRP1 proteins of land plants: DRP1A (ADL1) in *A. thaliana* (Kang et al. 2003) and tobacco BY-2 cells (Hong et al. 2003), DRP1C in tobacco BY-2 cells (Hong et al. 2003). Therefore, DRP1 proteins of volvocine algae may act as cytokinesis-related molecules.

In the second division of multiple fission (4-celled stage), DRP1 of *C. reinhardtii* was mainly localized in the second division plane (Figure 4.4J), while DRP1 signals of *T. socialis* (Figure 4.5J) and *G. pectorale* (Figure 4.6J) were clearly observed in the both division planes, which were formed by the first and second divisions. Moreover, in the third division of *G. pectorale* (8-celled stage), DRP1 signals were observed in all division planes (Figure 4.6N). Thus, DRP1 may have a role mainly in the last division plane of unicellular *C. reinhardtii* (Figures 4.4F, J), whereas DRP1

may equally work in all division planes of multicellular *T. socialis* and *G. pectorale* (Figures 4.5F, J, 4.6F, J, N, 4.7).

Each cell division during multiple fission of multicellular *T. socialis* (Chapter 2), *G. pectorale* (Iida et al. 2013), and other multicellular volvocine algae (e.g. Green et al. 1981) proceeds through incomplete cytokinesis and the resulting daughter protoplasts are connected to one another by CBs, whereas daughter protoplasts of *C. reinhardtii* are completely separated from one another by means of complete cytokinesis (Kirk 2005; Harris 2009). The division planes of multicellular volvocine species are therefore different from those of unicellular *C. reinhardtii*. Given the possibility that DRP1 functions in the volvocine cytokinesis, the different DRP1 localization patterns between unicellular *C. reinhardtii* and multicellular *T. socialis* and *G. pectorale* (Figure 4.7) may indicate the differences in multiple fission between unicellular forms and multicellular forms.

Dynamins and DRPs are involved in various membrane remodeling events such as budding and trafficking of vesicles, fission or fusion of organelles, and cytokinesis (Miyagishima et al. 2008; Antonny et al. 2016). Particularly in cytokinesis, dynamins are localized in newly formed membranes of metazoans such as *Caenorhabditis elegans* (Thompson et al. 2002) and zebrafish (Feng et al. 2002). In *Dictyostelium discoideum*, the relationships between cytokinesis and dynamin A (Wienke et al. 1999), dynamin-like protein (Dlp) A, DlpB and DlpC (Miyagishima et al. 2008) were reported. In *A. thaliana*, DRP1A (Kang et al. 2003), DRP1E (Kang et al. 2003), DRP2B (Fujimoto et al. 2010), and DRP5A (Miyagishima et al. 2008) are localized in the division plane, and function in cytokinesis. Those dynamins and DRPs play important roles for cytokinesis such as membrane fission and vesicle formation for cytokinesis. Therefore, volvocine DRP1 proteins might be related to membrane remodeling during the multiple fission. Hence, the few DRP1 signals in the first division plane of *C. reinhardtii* 4-celled stage (Figure 4.4J) may indicate that membrane

fission/formation mediated by DRP1 has been finished in this plane after the first division (white arrowheads in Figure 4.4J), but has been occurring at the second division plane (black arrowheads in Figure 4.4J). The presence of DRP1 signals in all division planes of *T. socialis* (Figures 4.5F, J) and *G. pectorale* (Figures 4.6F, J, N) may be due to the continuous membrane remodeling during the incomplete cytokinesis in these two multicellular species.

4.5 TABLES AND FIGURES

Table 4.1. Primers used for amplifications and sequencing of *dynamin-related protein 1* gene of *Tetrabaena socialis* (*TsDRP1*).

Primer Designation	Sequences (5'-3')
CrDRP1_R3	GTCCATAATGTCCACCTTGGTC
CrDRP1_R9	GATCTCCTCGCTCTCGTTGAT
TsDRP1_F1	GTGATCGGACTCGTCAACAA
TsDRP1_F3	AAGTCGTCGGTGCTGGAG
TsDRP1_F4	GCAGTACATCAAGAGCGACAAC
TsDRP1_F12	CGAGTTCTTCCAGAGCAAGC
TsDRP1_R2	GTGCGCGAACTCCCCATAGT
TsDRP1_R14	ACACGTCCAGGATCTTCTCG
TsDRP1_3'UTR_F1	TCAACGGCGAGAACCTGTTCGAGAAGC
TsDRP1_3'UTR_F2	CTGCTGACGGACCTGCAGGAGGAGAC
TsDRP1_5'UTR_R1	GGAGCTCTGTCCACCGACAACGACGAT
TsDRP1_5'UTR_R2	ATGGTTGGGAGCTTGCTCCACAGGATG
TsDRP1_antigen_F1[a]	CACCCTGCAGCAAATTTGCACGTCGCTC
TsDRP1_antigen_R2[a]	TTAGAGGCGCCGCAGCTGCGGCTCCTC

[a]Primers for antigen.

Table 4.2. List of Phytozome locus names/Genbank accession numbers accession numbers of dynamin-related protein 1 (DRP1) and dynamin-related protein 2 (DRP2) used in phylogenetic analyses and the abbreviations used in the alignment for the phylogenetic analyses (Appendix 2).

Species	Protein Name	Locus Name/Accession Number	Abbreviations used in Alignment (Appendix 2)
Chlamydomonas reinhardtii	DRP1	Cre05.g245950.t1.1[b]	CrDRP1
Tetrabaena socialis	DRP1	LC279615 [a]	TsDRP1
Gonium pectorale	DRP1	KXZ46173[c]	GpDRP1
Volvox carteri	DRP1	Vocar.0026s0065[b]	VcDRP1
Coccomyxa subellipsoidea	Dynamin family	estExt_fgenesh1_pm.C_190089[b]	CsDynamin family
Micromonas pusilla	DYNAMIN	e_gw1.14.510.1[b]	MpDINAMIN
Micromonas sp.	Dynamin family	EuGene.1500010100[b]	Msp.Dynamin family
Arabidopsis thaliana	DRP1A[a]	AT5G42080[b]	AtaDRP1A
	DRP1B[a]	AT3G61760[b]	AtaDRP1B
	DRP1C[a]	AT1G14830[b]	AtaDRP1C
	DRP1D[a]	AT2G44590[b]	AtaDRP1D
	DRP1E[a]	AT3G60190[b]	AtaDRP1E
	DRP2A[a]	AT1G10290[b]	AtaDRP2A
	DRP2B[a]	AT1G59610[b]	AtaDRP2B

Oryza sativa	Os02 g50550[a]	LOC_Os02g50550[b]	Os02
	Os03 g50520[a]	LOC_Os03g50520[b]	Os03
	Os05 g48240[a]	LOC_Os05g48240[b]	Os05
	Os06 g13820[a]	LOC_Os06g13820[b]	Os06
	Os08 g32920[a]	LOC_Os08g32920[b]	Os08
	Os09 g39960[a]	LOC_Os09g39960[b]	Os09
	Os10 g41820[a]	LOC_Os10g41820[b]	Os10
Amborella trichopoda	DRP1A	evm_27.TU.AmTr_v1.0_scaffold00021.256[b]	AtrDRP1A
	DRP1C	evm_27.TU.AmTr_v1.0_scaffold00176.26[b]	AtrDRP1C
	DYNAMIN	evm_27.TU.AmTr_v1.0_scaffold00002.113[b]	AtrDYNAMIN
	DRP2A	evm_27.TU.AmTr_v1.0_scaffold00080.49[b]	AtrDRP2A
Selaginella moellendorffii	DRP1C-1	183216[b]	SmDRP1C-1
	DRP1C-2	266589[b]	SmDRP1C-2
	DRP1C-3	90013[b]	SmDRP1C-3
	DRP2A-1	171046[b]	SmDRP2A-1
	DRP2A-2	77824[b]	SmDRP2A-2
Physcomitrella patens	DRP1C-1	Pp3c18_20531[b]	PpDRP1C-1
	DRP1C-2	Pp3c19_3590[b]	PpDRP1C-2
	DRP1C-3	Pp3c19_4870[b]	PpDRP1C-3

	DRP1C-4	Pp3c22_1100[b]	PpDRP1C-4
	DRP1C-5	Pp3c22_2500[b]	PpDRP1C-5
	DRP2A-1	Pp3c18_20600[b]	PpDRP2A-1
	DRP2A-2	Pp3c19_3640[b]	PpDRP2A-2
	DRP2A-3	Pp3c1_8440[b]	PpDRP2A-3
	DRP2A-4	Pp3c2_32060[b]	PpDRP2A-4
Klebsormidium flaccidum	DLP-1[c]	GAQ83701[b]	KfDLP-1
	DRP[c]	GAQ87226[b]	KfDRP

[a]Determined in this study.

[b]Obtained from Phytozome version 10 (http://www.phytozome.net/).

[c]Obtained from National Center for Biotechnology Information (NCBI) database (https://www.ncbi.nlm.nih.gov).

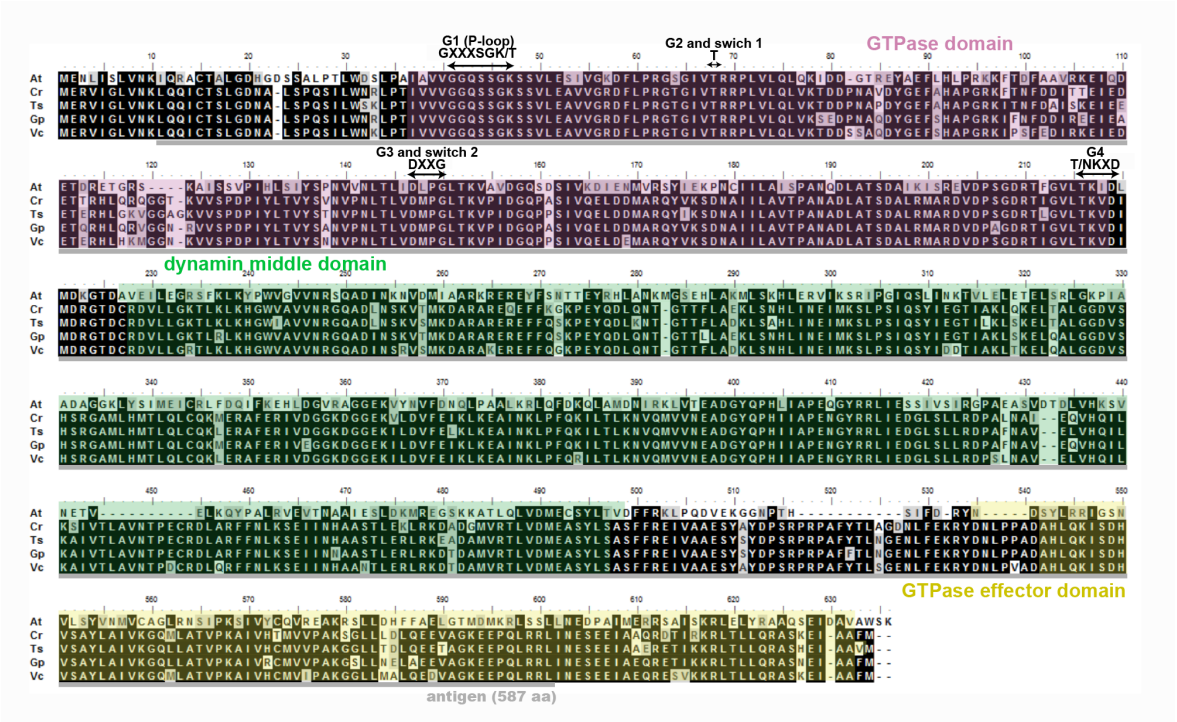

Figure 4.1. Alignment of deduced amino acid sequences of DRP1A from *Arabidopsis thaliana* (AtDRP1A) and DRP1 from *Chlamydomonas reinhardtii* (CrDRP1), *Tetrabaena socialis* (TsDRP1), *Gonium pectorale* (GpDRP1), and *Volvox carteri* (VcDRP1).

Black and gray background indicates identical and similar amino acid, respectively. Indicated three domains are based on AtDRP1A. GTPase domain, dynamin middle domain, and GTPase effector domain are indicated by pink, green, and yellow background color, respectively. The region corresponding to the antigen for an anti-TsDRP1 antibody is showed under the alignment (gray bar).

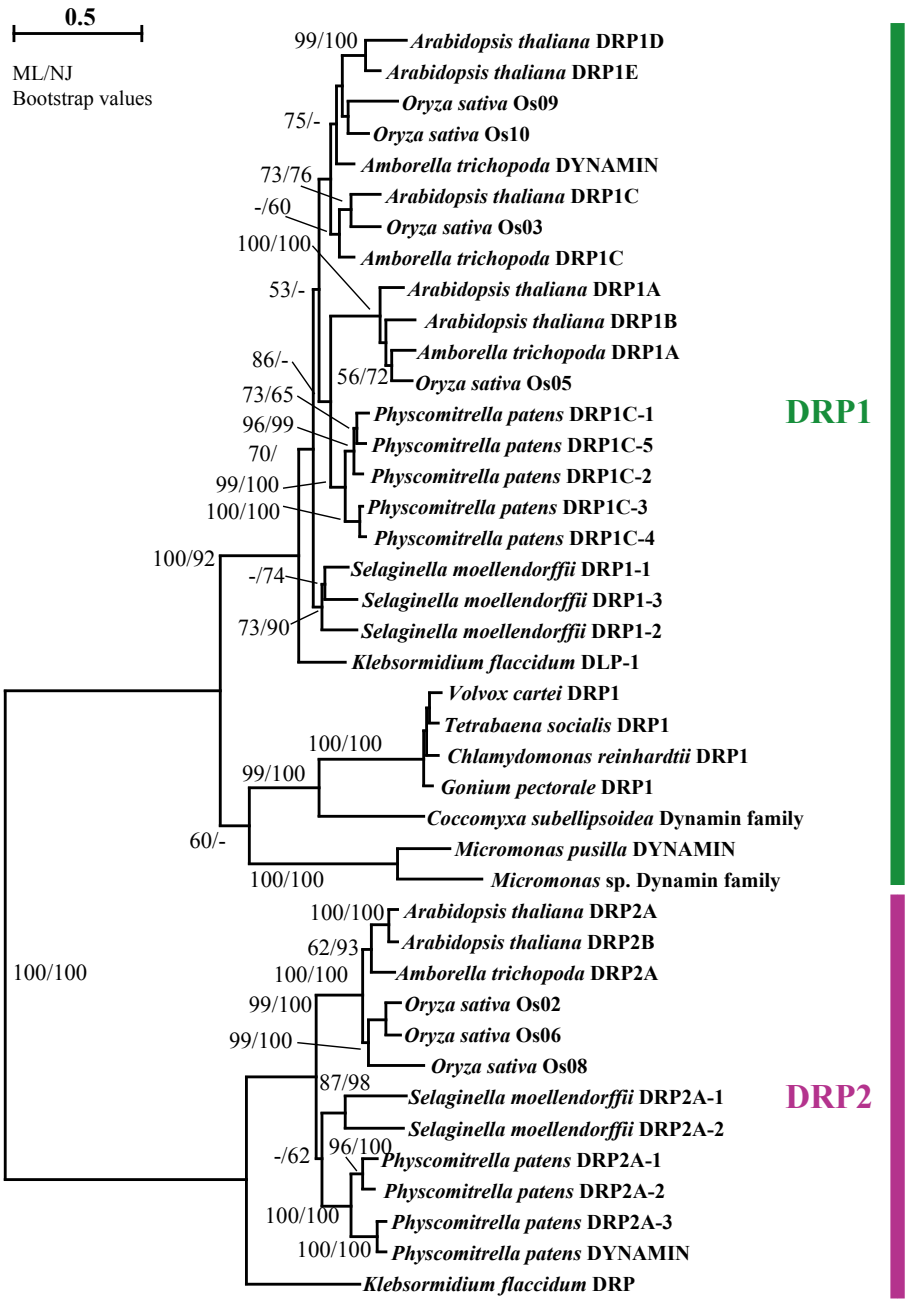

Figure 4.2. Maximum-likelihood (ML) tree of dynamin-related protein 1 (DRP1). Bootstrap values (≥50%) for the ML and neighbor-joining (NJ) analyses are indicated left and right side, respectively. DRP2 sequences were used as outgroup. The scale bar corresponds to 0.5 amino acid substitutions per position. Accession numbers of amino acid sequences and an alignment for the phylogenetic analyses are shown in Table 4.2 and Appendix 2, respectively.

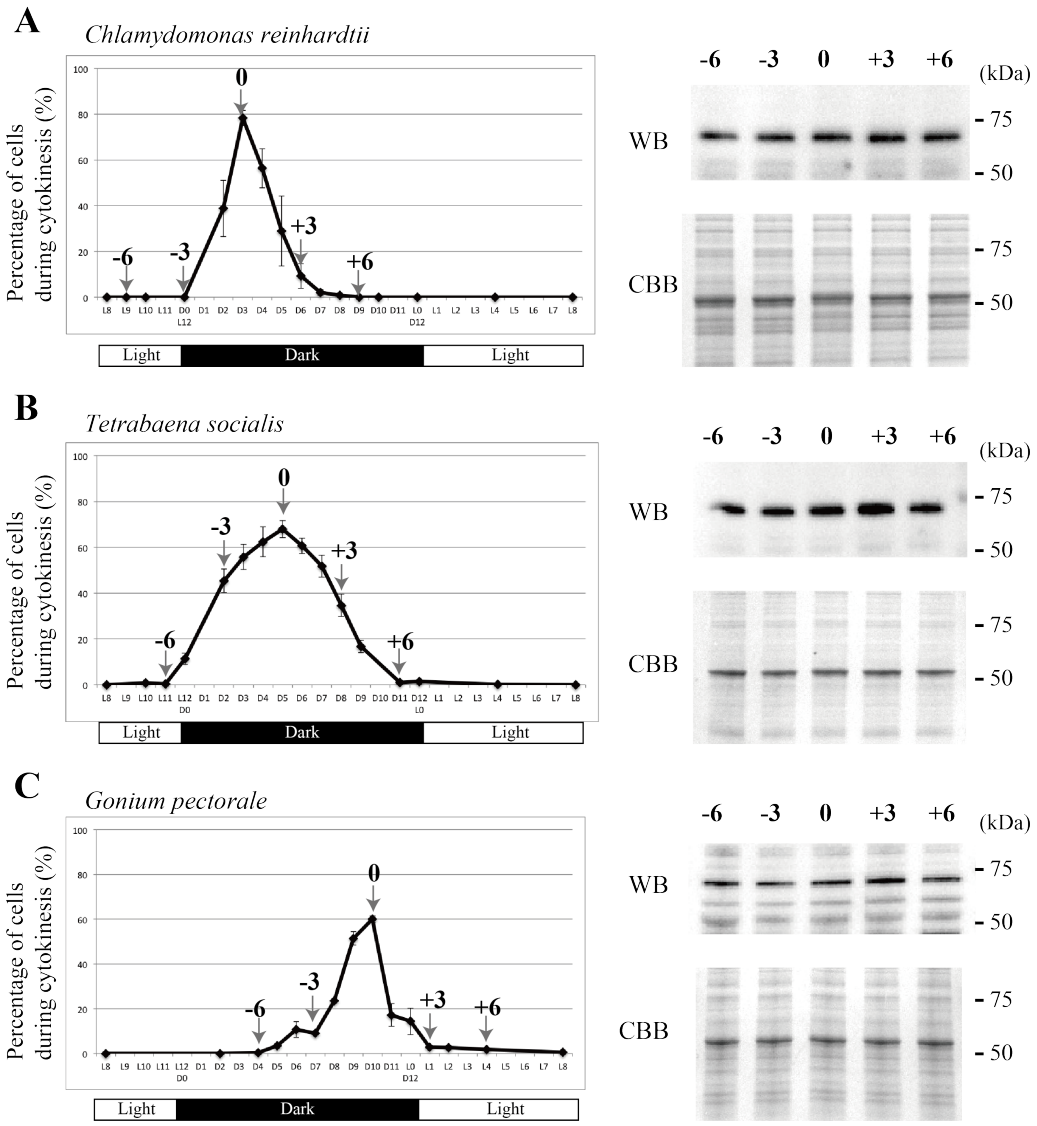

Figure 4.3. Western blot (WB) analyses of dynamin-related protein 1 (DRP1). DRP1 of *Chlamydomonas reinhardtii* (CrDRP1), *Tetrabaena socialis* (TsDRP1), and *Gonium pectorale* (GpDRP1) was detected by anti-TsDRP1 antibody. Time-course of synchronous culture and WB of *C. reinhardtii*, *T. socialis*, and *G. pectorale* are shown in A, B, and C, respectively. Time-course samples were obtained from five points (arrows in each line graph): the greatest number of dividing cells (0), three (-3) and six (-6) hours before 0 point, and three (+3) and six (+6) hours after 0 point. Coomassie brilliant blue (CBB) staining of a duplicate gel shows the equal protein loading in each lane.

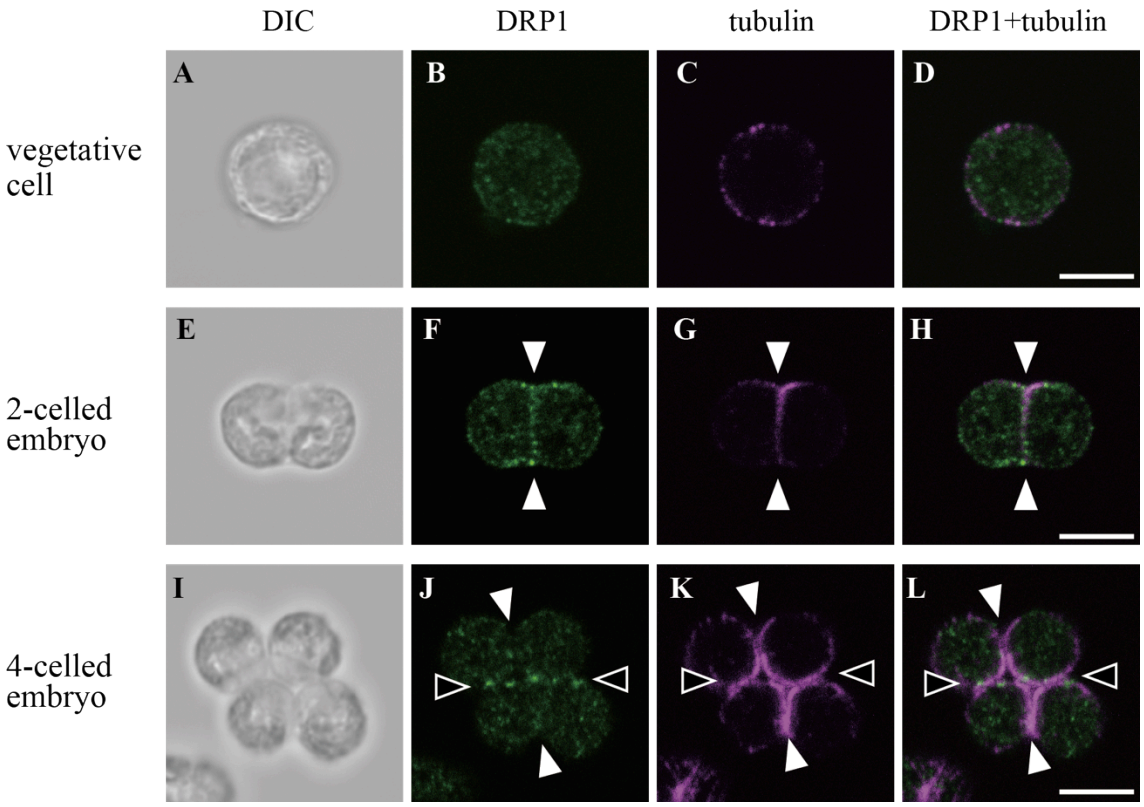

Figure 4.4. Immunofluorescence images of DRP1 localization in *Chlamydomonas reinhardtii*.

Differential interference contrast (DIC) images (A, E, I), immunofluorescence images labeled with an anti-TsDRP1 antibody (B, F, J), an anti-tubulin alpha antibody (C, G, K), and merged images of DRP1 and tubulin (D, H, L) are shown. In vegetative cells, DRP1 was localized in the cytoplasm (A-D). DRP1 was localized in a first division plane of two-celled embryo (white arrowheads in F-H) and second division planes of four-celled embryo (black arrowheads in J-L) mainly. Note the less localization of DRP1 to the first division plane of four-celled embryo (J). The first and second division planes in the four-celled stage were estimated by relative positions of pyrenoids. Scale bars: 5 μm.

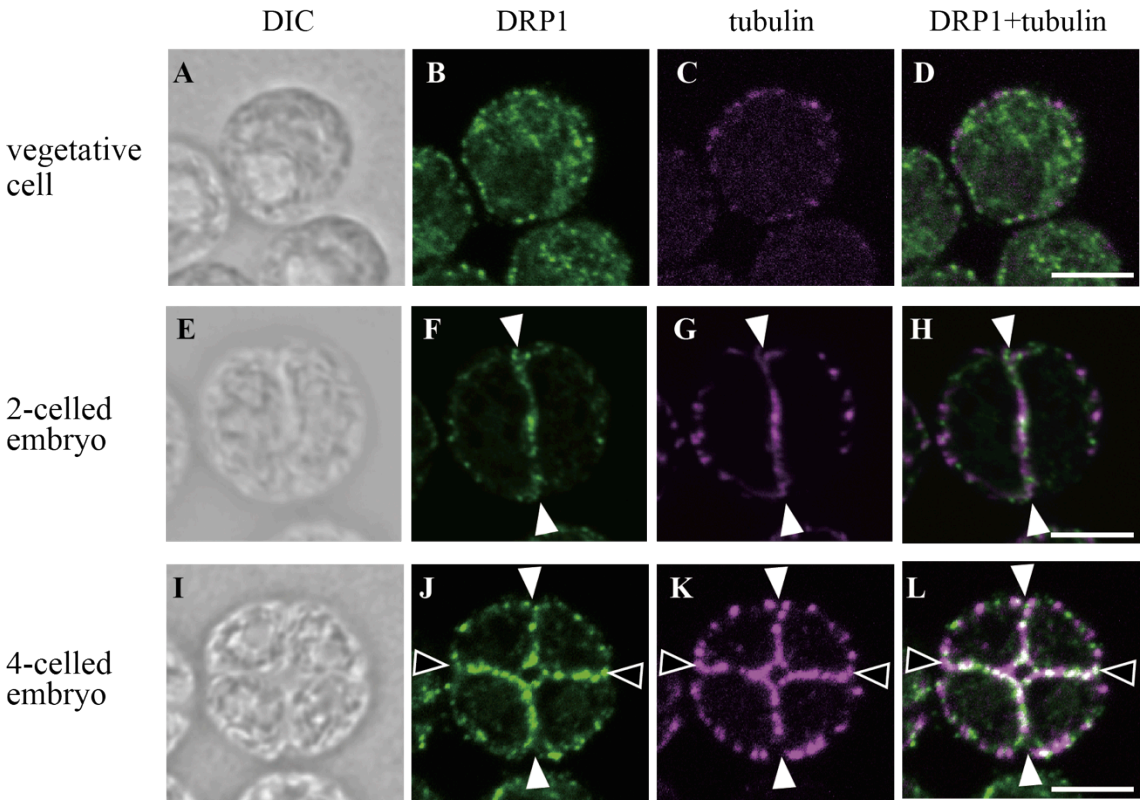

Figure 4.5. Immunofluorescence images of TsDRP1 localization in *Tetrabaena socialis.*

Differential interference contrast (DIC) images (A, E, I), immunofluorescence images labeled with an anti-TsDRP1 antibody (B, F, J), an anti-tubulin alpha antibody (C, G, K), and merged images of DRP1 and tubulin (D, H, L) are shown. In vegetative cells, TsDRP1 was localized in the cytoplasm (A-D). DRP1 was localized in a first division plane (white arrowheads in F-H) of two-celled embryo and both first (white arrowheads) and second (black arrowheads) division planes of four-celled embryo (J-L). DRP1 apparently localized to first division planes of four-celled embryo, and this pattern was different from *Chlamydomonas reinhardtii* (Figure 4.4). The first and second division planes in the four-celled stage were estimated by directions of the planes within the parental colony. Scale bars: 10 μm.

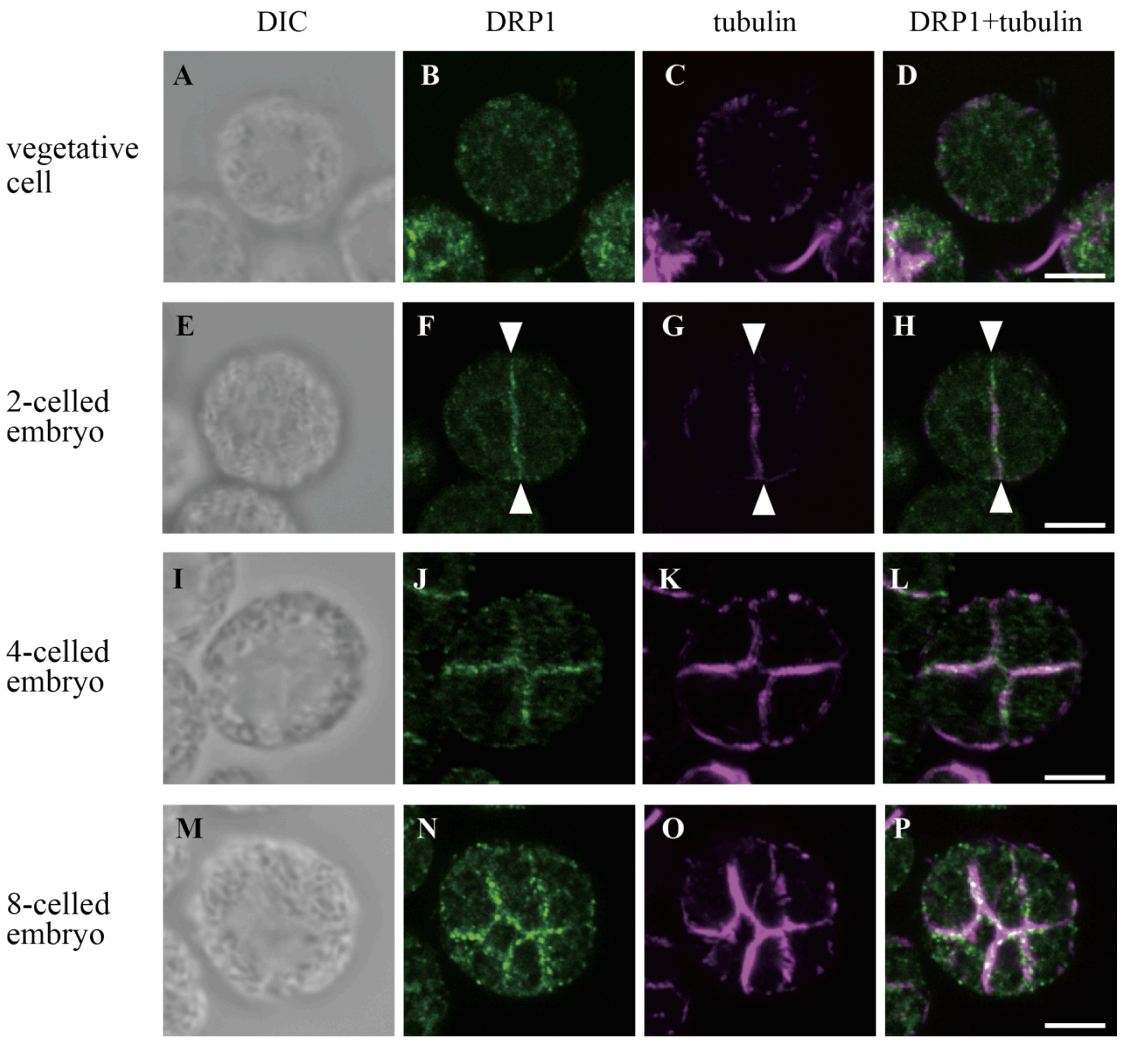

Figure 4.6. Immunofluorescence images of DRP1 localization in *Gonium pectorale*. Differential interference contrast (DIC) images (A, E, I, M), immunofluorescence images labeled with an anti-TsDRP1 antibody (B, F, J, N), an anti-tubulin alpha antibody (C, G, K, O), and merged images of DRP1 and tubulin (D, H, L, P) are shown. In vegetative cells, DRP1 was localized in the cytoplasm (A-D). DRP1 was localized in a first division plane of two-celled embryo (arrowheads in E-H), both first and second division planes of four-celled embryo (I-L), and first, second, and third division planes of eight-celled embryo (M-P). DRP1 apparently localized to all division planes of four-celled and eight-celled embryo and the pattern is different from *Chlamydomonas reinhardtii* (Figure 4.4) as well as *Tetrabaena socialis* (Figure 4.5). Scale bars: 10 μm.

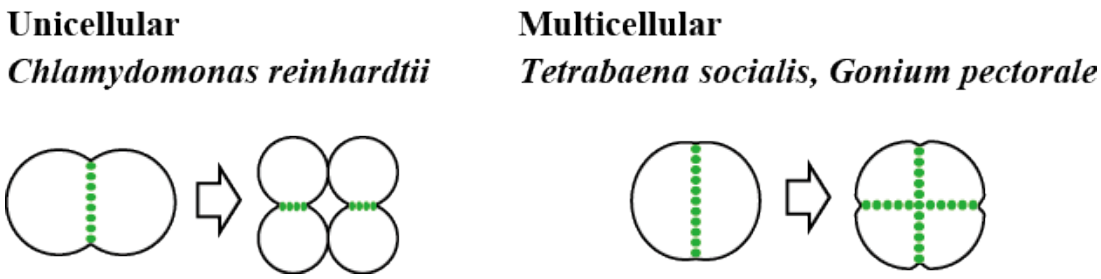

Figure 4.7. Schematic diagram of DRP1 localization patterns in unicellular *Chlamydomonas reinhardtii* and ancestral multicellular *Tetrabaena socialis* and *Gonium pectorale*.

Chapter 5.

General discussion

The simplest multicellular organism *Tetrabaena socialis*

The traditional hypothesis of "volvocine lineage" describes a directional, phylogenetically stepwise increase in individual complexity from a simple, undifferentiated colonial form such as *Gonium* to differentiated multicellular forms such as *Volvox* (e.g. Pickett-Heaps 1975, Kirk 1998). Bell (1985) remarked that volvocine green algae are a fascinating model group for exploring the evolution of multicellularity. Based on the morphological observations of cell ultrastructure (e.g. Lang 1963) and a physiological study of ECM (Matsuda et al. 1987), the volvocine algae were thought to have evolved from a *Chlamydomonas reinhardtii*-like ancestor. Larson et al. (1992) performed a phylogenetic analysis using ribosomal RNA sequences. Although statistical support for branches in their phylogenetic tree was not shown, the tree topology showed monophyly of colonial/multicellular volvocine members and phylogenetic relationships that were inconsistent with the traditional volvocine hypothesis (Larson et al. 1992). However, based on a cladistic analysis of the morphological data of vegetative cells and sexual reproduction characteristics, Nozaki and Ito (1994) demonstrated a strict consensus tree that shows phylogenetic relationships that support the traditional volvocine lineage hypothesis. Their results also called for the separation of the four-celled species *Gonium sociale* from all other colonial/multicellular volvocine species analyzed. They transferred *G. sociale* to the genus *Tetrabaena* and proposed a new family, Tetrabaenaceae. Subsequent chloroplast multigene phylogenetic analyses resolved robust phylogenetic relationships of the volvocine algae: all of the colonial/multicellular volvocine members (Tetrabaenaceae, Goniaceae and Volvocaceae) form a robust monophyletic group (TGV-clade) in which Tetrabaenaceae represents the most ancestral group (Nozaki et al. 2000). Moreover, results of the chloroplast multigene phylogenetic analyses are consistent with the traditional volvocine lineage hypothesis in that colonial volvocine algae evolved from a *Chlamydomonas*-like ancestor and show a gradual progression in colonial or individual complexity (Nozaki et al. 2000; Nozaki

2003). On the basis of the revised chloroplast multigene phylogeny (Nozaki 2003), Kirk (2005) proposed twelve evolutionary steps from a *Chlamydomonas*-like ancestor to differentiated *V. carteri*. However, he did not discuss the twelve steps in the origin of the most ancestral colonial volvocine group Tetrabaenaceae. Herron et al. (2009) estimated that the divergence time of colonial/multicellular volvocine algae (TGV-clade) was 200 MYA, and assigned Kirk's twelve steps to their phylogenetic tree (summarized in Figure2.1). According to the results in Herron et al. (2009), the Tetrabaenaceae might have experienced only two of Kirk's twelve evolutionary steps. Whereas some of Kirk's twelve steps might have been necessary for the evolution of integrated multicellular organisms such as rotation of BBs and incomplete cytokinesis, they might have not been attained in the tetrabaenacean lineage.

In Chapter 2, I examined two morphological features (rotation of BBs and incomplete cytokinesis) using *Tetrabaena socialis*, and clearly demonstrated that *T. socialis* possessed these two morphological traits. Therefore, *T. socialis* is one of the simplest integrated multicellular organisms in which four identical cells constitute the individual. Because the Tetrabaenaceae is sister to other multicellular volvocine algae (Goniaceae and Volvocaceae) including the complex organism *Volvox*, four of Kirk's twelve evolutionary steps (Kirk 2005) (incomplete cytokinesis, rotation of BBs, transformation of cell walls into an ECM, and genetic modulation of cell number) might have been attained in the common ancestor of TGV-clade. Thus, these four morphological characteristics are considered to be important for the initial evolution of volvocine multicellularity.

The initial evolution of cell cycle-related molecules and cytokinesis-related protein DRP1 in volvocine lineage

To investigate the genetic changes that are related to the evolution from a unicellular *Chlamydomonas*-like ancestor to >500-celled, differentiated *Volvox*, the whole genome

of *V. carteri* was sequenced and compared with the *C. reinhardtii* genome (Prochnik et al. 2010). Surprisingly, in spite of fundamental differences in their organismal structure, the genome of *V. carteri* encodes almost the same number of genes as the *C. reinhardtii* genome (Merchant et al. 2007). However, both volvocine genomes exhibit three exceptional protein families (Prochnik et al. 2010): two ECM-related protein families (pherophorins and gametolysin/*Volvox* matrix metalloprotease) and one cell cycle-related protein family (CYCD1). These three families are expanded in multicellular *V. carteri*, but not in *C. reinhardtii*, raising the possibility that the gene expansions found in three protein families are related to the multicellularity of *V. carteri* (Prochnik et al. 2010). Subsequently, Hanschen et al. (2016) analyzed the 16-celled, undifferentiated *G. pectorale* genome, and found apparent gene expansion in only CYD1 among the three families of *G. pectorale*. They argued that the change of cell cycle-regulation with expansion of CYCD1 proteins is critical for the evolution of undifferentiated multicellular species such as *G. pectorale*.

In Chapter 3, I demonstrated that four-celled, undifferentiated *T. socialis* had three *CYCD1* genes (Figures 3.1, 3.2) and a RB/MAT3 protein with a short L1 region (Figures 3.5, 3.7), as in more advanced multicellular species such as *G. pectorale* and *Volvox carteri*. Therefore, the modification of cell cycle-related molecules (expansion of *CYCD1* genes and structural change of RB/MAT3 protein) can be traced back to the common ancestor of the TGV-clade and might have contributed to the evolution of volvocine multicellularity. Gene expansion or duplication has been pointed out as a major basis for the evolution of genes since the 1950s (e.g. Stephens 1951; Ohno 1970), and duplicated genes are believed to have evolutionary potential for subfunctionalization and neofunctionalization (e.g. Zhang et al. 2003). The duplicated *CYCD1* genes of multicellular volvocine algae are thought to be important for RB regulation and may be co-opted from unicellular ancestor (Hanschen et al. 2016), because the evolution of eukaryotic multicellularity seems to rely on co-option of existing genes rather than *de*

novo gene evolution (Herron and Nedelcu 2015). Indeed, each of the four *CYCD* genes in *C. reinhardtii* (*CrCYCD1-4*) has a different expression profile during the cell cycle (Bisova et al. 2005; Zones et al. 2015) and the distinct expression patterns are considered to be associated with subfunctionalization of the four *CYCD* genes (Zones et al. 2015). Therefore, the duplicated *CYCD1* genes in multicellular volvocine algae *T. socialis* (*TsCYCD1.1-3*), *G. pectorale* (*GpCYCD1.1-4*), and *V. carteri* (*Vccycd1.1-4*) may play important roles in volvocine multicellularity by different regulation mechanisms.

In addition to the cell cycle-related genes, I demonstrated in Chapter 4 that the localization pattern of cytokinesis-related protein DRP1 in multicellular *T. socialis* and *G. pectorale* was different from that in unicellular *C. reinhardtii*. Together with the formation of CBs in multicellular species, these results suggest that cytokinesis during multiple fission in multicellular species is different from that of unicellular species at both the morphological and protein localization level. DRP1 was mainly localized in the last division plane of *C. reinhardtii* (Figure 4.4J), whereas DRP1 signals in *T. socialis* (Figure 4.5J) and *G. pectorale* (Figure 4.6J) were clearly observed in all division planes. As discussed in Chapter 4, volvocine DRP1 might be involved in membrane remodeling during cytokinesis, similar to some dynamins and DRPs (e.g. Praefcke and McMahon 2004; Konopka et al. 2006). Thus, the different localization patterns between *C. reinhardtii* and multicellular volvocine members may reflect different membrane remodeling manners during multiple fission. In multicellular volvocine algae, each cell division during multiple fission proceeds through incomplete cytokinesis and the resulting daughter protoplasts are connected to one another by CBs (e.g. Green et al. 1981; Iida et al. 2013; Chapter 2). Because the daughter protoplasts need to retain their CBs to form species-specific multicellular shapes during embryogenesis, the membrane reconstruction in multicellular volvocine species might be different from that of unicellular species. More detailed analyses such as localization of DRP1 by immunoelectron microscopy and comparative analyses of other cytokinesis-related

proteins are required to elucidate the direct relationships between incomplete cytokinesis and the evolution of volvocine multicellularity. In particular, to clarify the evolutionary events in the initial transition from unicellular ancestor to multicellular progeny, comparative studies of unicellular *C. reinhardtii* and the simplest volvocine alga *T. socialis* are necessary. Further detailed studies using *T. socialis* would shed light on the evolution of volvocine multicellularity.

Further prospects to understand the evolution of multicellularity

Volvocine lineage is a powerful model that can be used to investigate the evolution of eukaryotic multicellularity with modern biological approaches. The present comparative morphological and genomic analyses using the most ancestral multicellular volvocine alga *T. socialis* revealed that several morphological and molecular traits (rotation of BBs, incomplete cytokinesis, expansion of *CYCD1* genes, and change in subcellular localization pattern of DRP1) might have been obtained in the common ancestor of TGV-clade. Further studies using the volvocine algae are expected to elucidate the initial machinery responsible for evolution of multicellularity, which is difficult to explore in metazoans and land plants.

Acknowledgements

First of all, I would like to express my sincere gratitude to Dr. Hisayoshi Nozaki (University of Tokyo) for his encouragements, suggestions, critical proofreading of this manuscript and giving me the opportunity to study in his laboratory.

I am grateful to Dr. Hiroko Kawai-Toyooka (University of Tokyo) for technical guidance, discussions, and encouragements.

I also thank Drs. Tetsuya Higashiyama (Nagoya University), Yuki Hamamura (University of Hamburg), Kenji Kimura (National Institute of Genetics) for technical guidance for using confocal microscopies; Dr. Masafumi Hirono (Hosei University), Mr. Akira Noga (University of Tokyo), and Ms. Mishio Toh (University of Tokyo) for the provision of CrSAS-6 antibody, helpful suggestions, and technical guidance; Dr. Chieko Saito (Japan Science and Technology Agency) for the technical guidance of TEM; Mr. Jonathan Featherston (University of the Witwatersrand), Dr. Pierre M. Durand (University of the Witwatersrand), Mr. Erik R. Hanschen (University of Arizona), Dr. Patrick J. Ferris (University of Arizona), Dr. Richard E. Michod (University of Arizona), Dr. Bradley J. S. C. Olson (Kansas State University) for the technical guidance, sequencing and assembling of *Tetrabaena socialis* draft genome and transcriptome data; Dr. Masahiro Suzuki (Kobe University) for the DNA extraction for *T. socialis* draft genome; Dr. Kaoru Kawafune (Tokyo Institute of Technology) for the technical assistance of the analyses using the genome data and encouragements; Dr. Ryo Matsuzaki (National Institute for Environmental Studies) for technical guidance of the phylogenetic analyses; Dr. Takashi Hamaji (Kyoto University) for the helpful discussions; Dr. Shin-ya Miyagishima (National Institute of Genetics) for the technical guidance of preparing the anti-TsDRP1 antibody, DRP1 expression analyses, and helpful discussions and comments; Dr. Takayuki Fujiwara (National Institute of Genetics) for the technical guidance of DRP1 expression analyses; Ms. Sophia Chen (Johns Hopkins University) for helpful advice to write the manuscript; Drs. Naoki Irie, Ichiro Terashima, and Hirokazu Tsukaya (University of Tokyo) for helpful discussions and comments.

I am also grateful to all the current and former members of the Laboratory of Origin of Eukaryote Biodiversity (University of Tokyo) for their friendship, discussions, and encouragements.

Finally, I really thank to my family for their supports and encouragements.

A part of this study was supported by Grants-in-Aid for JSPS Fellows (No. 25-9234) from the Ministry of Education, Culture, Sports, Science and Technology (MEXT)/ Japan Society for the Promotion of Science (JSPS) KAKENHI, Japan Advanced Plant Science Network, and NIG-JOINT (2016-B).

A part of Chapter 2 was reproduced from Arakaki et al. (2013, *PLOS ONE* 8: e81641).

References

Adl SM, Simpson AGB, Farmer MA, Andersen RA, Anderson OR, Barta JR, Bowser SS, Brugerolle G, Fensome RA, Fredericq S, James TY, Karpov S, Kugrens P, Krug J, Lane CE, Lewis LA, Lodge J, Lynn DH, Mann DG, Mccourt RM, Mendoza L, Moestrup Ø, Mozley-Standridge SE, Nerad TA, Shearer CA, Smirnov AV, Spiegel EW, Taylor MFJR. 2005. The new higher level classification of eukaryotes with emphasis on the taxonomy of protists. *The Journal of Eukaryotic Microbiology*. 52: 399-451.

Altschul SF, Madden TL, Schäffer AA, Zhang J, Zhang Z, Miller W, Lipman DJ. 1997. Gapped BLAST and PSI-BLAST: a new generation of protein database search programs. *Nucleic Acids Research*. 25: 3389-3402.

Antonny B, Burd C, De Camilli P, Chen E, Daumke O, Faelber K, Ford M, Frolov VA, Frost A, Hinshaw JE, Kirchhausen T, Kozlov MM, Lenz M, Low HH, McMahon H, Merrifield C, Pollard TD, Robinson PJ, Roux A, Schmid S. 2016. Membrane fission by dynamin: what we know and what we need to know. *The EMBO Journal.* 35: 2270-2284.

Bankevich A, Nurk S, Antipov D, Gurevich AA, Dvorkin M, Kulikov AS, Lesin VM, Nikolenko SI, Pham S, Prjibelski AD, Pyshkin AV, Sirotkin AV, Vyahhi N, Tesler G, Alekseyev MA, Pevzner PA. 2012. SPAdes: A new genome assembly algorithm and its application to single-cell sequencing. *Journal of Computational Biology.* 19: 455-477.

Bell G. 1985. The origin and early evolution of germ cells as illustrated by the Volvocales, in: Halvorson HO, Monroy A. (Eds.). *The origin and evolution of sex.* pp. 221-256. Alan R. Liss, Inc., New York, NY, USA.

Beumer TL, Roepers-Gajadien HL, Gademan IS, Kal HB, de Rooij DG. 2000. Involvement of the D-type cyclins in germ cell proliferation and differentiation in the mouse. *Biology of Reproduction.* 63: 1893-1898.

Bisova K, Krylov DM, Umen JG. 2005. Genome-wide annotation and expression profiling of cell cycle regulatory genes in *Chlamydomonas reinhardtii*. *Plant Physiology*. 137: 457-491.

Bjellqvist B, Basse B, Olsen E, Celis JE. 1994. Reference points for comparisons of two-dimensional maps of proteins from different human cell types defined in a pH scale where isoelectric points correlate with polypeptide compositions. *Electrophoresis*. 15: 529-539.

Bjellqvist B, Hughes G.J, Pasquali Ch, Paquet N, Ravier F, Sanchez J-Ch, Frutiger S, Hochstrasser DF. 1993. The focusing positions of polypeptides in immobilized pH gradients can be predicted from their amino acid sequences. *Electrophoresis.* 14: 1023-1031.

Bowman JL, Sakakibara K, Furumizu C, Dierschke. 2016. Evolution in the cycles of life. *Annual Review of Genetics.* 50: 133-154.

Brown MW, Spiegel FW, Silberman JD. 2009. Phylogeny of the "forgotten" cellular slime mold, *Fonticula alba*, reveals a key evolutionary branch within Opistokonta. *Molecular Biology and Evolution*. 26: 2699-2709.

Brown MW, Kolisko M, Silberman JD, Roger AJ. 2012. Aggregative multicellularity evolved independently in the eukaryotic supergroup Rhizaria. *Current Biology.* 22: 1123-1127.

Brown MW, Silberman JD, Spiegel FW. 2011a. "Slime Molds" among the Tubulinea (Amoebozoa): Molecular systematics and taxonomy of *Copromyxa*. *Protist*. 162: 277-287.

Brown MW, Silberman JD, Spiegel FW. 2011b. A contemporary evaluation of the acrasids (Acrasidae, Heterolobosea, Excavata). *European Journal of Protistology*. 48: 103-123.

Cavalier-Smith T. 1974. Cell cycle and the sexual cycle of *Chlamydomonas reinhardtii*. *Journal of Cell Science*. 16: 529-556.

Chamnansinp A, Li Y, Lundholm N, Moestrup Ø . 2013. Global diversity of two widespread, colony-forming diatoms of the marine plankton, *Chaetoceros socialis* (syn *C. radians*) and *Chaetoceros gelidus* sp. nov. *Journal of Phycology*. 49: 1128-1141.

Chang Z, Li G, Liu J, Zhang Y, Ashby C, Liu D, Cramer CL, Huang X. 2015. Bridger: a new framework for *de novo* transcriptome assembly using RNA-seq data. *Genome Biology*. 16: 30.

Cock JM, Godfroy O, Strittmatter M, Scornet D, Uji T, Farnham G. Peters AF, Coelho SM. 2015. Emergence of *Ectocarpas* as a model system to study the evolution of complex multicellularity in the brown algae, in: Ruiz-Trillo I, Nedelcu AM. (Eds.). *Evolutionary transitions to multicellular life.* pp. 153-162. Springer Netherlands, Dordrecht, Netherland.

Dahiya A, Gavin MR, Luo RX, Dean DC. 2000. Role of the LXCXE binding site in Rb function. *Molecular and Cellular Biology*. 20: 6799-6805.

Dahl M, Meskiene I, Bögre L, Ha DTC, Swoboda I, Hubmann R, Hirt H, Heberle-Bors E. 1995. The D-type alfalfa cyclin gene *cycMs4* complements G_1 cyclin-deficient yeast and is induced in the G_1 phase of the cell cycle. *The Plant Cell*. 7: 1847-1857.

Darriba D, Taboada GL, Doallo R, Posada D. 2011. ProtTest 3: fast selection of best-fit models of protein evolution. *Bioinformatics*. 27: 1164-1165.

Dewitte W, Riou-Khamlichi C, Scofield S, Healy JMS, Jacqmard A, Kilby NJ, Murray AH. 2003, Altered cell cycle distribution, hyperplastida, and inhibited differentiation in *Arabidopsis* caused by the D-type cyclin CYCD3. *The Plant Cell.* 15: 79-92.

Dombrowski JE, Raikhel NV. 1995. Isolation of a cDNA encoding a novel GTP-binding protein of *Arabidopsis thaliana*. *Plant Molecular Biology*. 28: 1121-1126.

Doonan JH, Grief C. 1987. Microtubule cycle in *Chlamydomonas reinhardtii*: an immunofluorescence study. *Cell Motility and the Cytoskeleton*. 7: 381-392.

Dymek EE, Goduti D, Kramer T, Smith EF. 2006. A kinesin-like calmodulin-binding protein in *Chlamydomonas*: evidence for a role in cell division and flagellar functions. *Journal of Cell Science*. 119: 3107-3116.

Eggert US, Mitchison TJ, Field CM. 2006. Animal cytokinesis: from parts list to mechanisms. *Annual Review of Biochemistry.* 75: 543-566.

Fairclough SR, Chen Z, Kramer E, Zeng Q, Young S, Robertson HM, Begovic E, Richter DJ, Russ C, Westbrook MJ, Manning G, Lang BF, Haas B, Nusbaum C, King N. 2013 Premetazoan genome evolution and the regulation of cell differentiation in the choanoflagellate *Salpingoeca rosetta. Genome Biology.* 14: R15.

Feng B, Schwarz H, Jesuthasan S. 2002. Furrow-specific endocytosis during cytokinesis of zebrafish blastomeres. *Experimental Cell Research.* 279: 14-20.

Field C, Li R, Oegeme K. 1999. Cytokinesis in eukaryotes: a mechanistic comparison. *Current Opinion in Cell Biology.* 11: 68-80.

Finn RD, Coggill P, Eberhardt RY, Eddy SR, Mistry J, Mitchell AL, Potter SC, Punta M, Qureshi M, Sangrador-Vegas A, Salazar GA, Tate J, Bateman A. 2016. The Pfam protein families database: towards a more sustainable future. *Nucleic Acids Research.* 44: D279-D285.

FujimotoM, Arimura S, Ueda T, Takahashi H, Hayashi Y, Nakano A, Tsutsumi N. 2010. *Arabidopsis* dynamin-related proteins DRP2B and DRP1A participate together in clathrin-coated vesicle formation during endocytosis. *Proceedings of the National Academy of Sciences of the United States of America*. 107: 6094-6099.

Fulton AB. 1978. Colonial development in *Pandorina morum*. II. Colony morphogenesis and formation of the extracellular matrix. *Developmental Biology.* 64: 236-251.

Gasteiger E, Hoogland C, Gattiker A, Duvaud S, Wilkins MR, Appel RD, Bairoch A. 2005. Protein Identification and Analysis Tools on the ExPASy Server in:

Walker JM. (Ed): *The Proteomics Protocols Handbook*. Humana Press, New York City, US.

Gerisch G. 1959. Die Zelldifferenzierung bei *Pleodorina californica* Shaw and die Organisation der Phytomonadinenkolonien. *Archiv für Protistenkunde.* 104: 292–358.

Gnerre S, MacCallum I, Pryzbylski D, Ribeiro FJ, Burton JN, Walker BJ, Sharpe T, Hall G, Shea TP, Sykes S, Berlin AM, Aird D, Costello M, Daza R, Williams L, Nicol R, Gnirke A, Nusbaum C, Lander ES, Jaffe DB. 2011. High-quality draft assemblies of mammalian genomes from massively parallel sequence data. *Proceedings of the National Academy of Sciences of the United States of America*. 108: 1513-1518.

Guindon S, Dufayard JF, Lefort V, Anisimova M, Hordijk W, Gascuel O. 2010. New algorithms and methods to estimate maximum-likelihood phylogenies: assessing the performance of PhyML 3.0. *Systematic Biology*. 59: 307-321.

Gorman DS, Levine RP. 1965. Cytochrome *f* and plastocyanin: their sequence in the photosynthetic electron transport chain of *Chlamydomonas reinhardtii*. *Proceedings of the National Academy of Sciences of the United States of America*. 54: 1665-1669.

Green KJ, Viamontes GI, Kirk DL. 1981. Mechanism of formation, ultrastructure, and function of the cytoplasmic bridge system during morphogenesis in *Volvox. The Journal of Cell Biology.* 91: 756-769.

Greuel BT, Floyd GL. 1985. Development of the flagellar apparatus and flagellar orientation in the colonial green alga *Gonium pectorale* (Volvocales). *Journal of Phycology*. 21: 358-371.

Grosberg RK, Strathmann RR. 2007. The evolution of multicellularity: A minor major transition?. *Annual Review of Ecology, Evolution, and Systematics.* 38: 621-654.

Hanschen ER, Marriage TN, Ferris PJ, Hamaji T, Toyoda A, Fujiyama A, Neme R, Noguchi H, Minakuchi Y, Suzuki M, Kawai-Toyooka H, Smith DR, Sparks H, Anderson J, Bakaric R, Luria V, Karger A, Kirschner MW, Durand PM, Michod RE, Nozaki H, Olson BJSC. 2016. The *Gonium pectorale* genome demonstrates co-option of cell cycle regulation during the evolution of multicellularity. *Nature Communication*.7:11370.

Harris EH. 2009. *The Chlamydomonas Sourcebook, Second Edition: Introduction to Chlamydomonas and Its Laboratory Use.* Academic Press, Oxford, UK. pp. 444.

Herron MD, Hackett JD, Aylward FO, Michod RE. 2009. Triassic origin and early radiation of multicellular volvocine algae. *Proceedings of the National Academy of Sciences of the United States of America*.106: 3254-3258.

Herron MD, Nedelcu AM. 2015. Volvocine algae: from simple to complex multicellularity, in: Ruiz-Trillo I, Nedelcu AM. (Eds.). *Evolutionary transitions to multicellular life.* pp. 129-152. Springer Netherlands, Dordrecht, Netherland.

Hiraide R, Kawai-Toyooka H, Hamaji T, Matsuzaki R, Kawafune K, Abe J, Sekimoto H, Umen J, Nozaki H. 2013. The evolution of male-female sexual dimorphism predates the gender-based divergence of the mating locus gene *MAT3/RB*. *Molecular Biology and Evolution*. 30: 1038-1040.

Hirashima T, Tajima N, Sato N. 2016. Draft genome sequences of four species of *Chlamydomonas* containing phosphatidylcholine. *Genome Announcement*. 4: e01070-16.

Hong Z, Geisler-Lee CJ, Zhang Z, Verma DPS. 2003. Phragmoplastin dynamics: multiple forms, microtubule association and their roles in cell plate formation in plants. *Plant Molecular Biology.* 53: 297-312.

Hoops HJ. 1984. Somatic cell flagellar apparatuses in two species of *Volvox* (Chlorophyceae). *Journal of Phycology*. 20: 20-27.

Hoops HJ. 1993. Flagellar, cellular and organismal polarity in *Volvox carteri*. *Journal of Cell Science*. 104: 105-117.

Hoops HJ. 1997. Motility in the colonial and multicellular Volvocales: structure, function, and evolution. *Protoplasma*. 199: 99-112.

Hoops HJ, Floyd GL. 1982. Mitosis, cytokinesis and colony formation in the colonial green alga *Astrephomene gubernaculifera. British Phycological Journal.* 17: 297-310.

Hoops HJ, Floyd GL. 1983. Ultrastructure and development of the flagellar apparatus and flagellar motion in the colonial green alga *Astrephomene gubernaculifera*. *The Journal of Cell Biology.* 63: 21-41.

Iida H, Nishii I, Inouye I. 2011. Embryogenesis and cell positioning in *Platydorina caudata* (Volvocaceae, Chlorophyta). *Phycologia.* 50: 530-540.

Iida H, Ota S, Inouye I. 2013. Cleavage, incomplete inversion, and cytoplasmic bridges in *Gonium pectorale* (Volvocales, Chlorophyta). *Journal of Plant Research.* 126: 699-707.

Jones RF. 1970. Physiological and biochemical aspects of growth and gametogenesis in *Chlamydomoans reinhardtii*. *Annuals of the New York Academy of Sciences*. 175: 648-659.

Jürgens G. 2005. Plant cytokinesis: fission by fusion. *TRENDS in Cell Biology.* 15: 277-283.

Kang B-H, Busse JS, Bednarek SY. 2003. Members of the *Arabidopsis* dynamin-like gene family, ADL1, are essential for plant cytokinesis and polarized cell growth. *The Plant Cell*. 15: 899-913.

Kate JR, Jones RF. 1964. The control of gametic differentiation in liquid cultures of *Chlamydomonas*. *Journal of Cellular Physiology*. 63: 157-164.

Katoh K, Standley DM. 2013. MAFFT multiple sequence alignment software version 7: improvements in perforemance and usability. *Molecular Biology and Evolution.* 30: 772-780.

Kawafune K, Hongoh Y, Nozaki H. 2014. A rickettsial endosymbiont inhabiting the cytoplasm of *Volvox carteri* (Volvocales, Chlorophyceae). *Phycologia*. 53: 95-99.

Kawai-Toyooka H, Mori T, Hamaji T, Suzuki M, Olson BJSC, Uemura T, Ueda T, Nakano A, Toyoda A, Fujiyama A, Nozaki H. 2014. Sex-specific posttranslational regulation of the gamete fusogen GCS1 in the isogamous volvocine alga *Gonium pectorale. Eukaryotic Cell.* 13: 648-656.

Keller O, Kollmar M, Stanke M, Waack S. 2011. A novel hybrid gene prediction method employing protein multiple sequence alignments. *Bioinformatics*. 27: 757-763.

King N, Hittinger CT, Carroll SB. 2003. Evolution of key cell signaling and adhesion protein families predates animal origins. *Science*. 301: 361-363.

King N, Westbrook MJ, Young SL, Kuo A, Abedin M, Chapman J, Fairclough S, Hellsten U, Isogai Y, Letunic I, Marr M, Pincus D, Putnam N, Rokas A, Wright KJ, Zuzow R, Dirks W, Good M, Goodstein D, Lemons D, Li W, Lyons JB, Morris A, Nichols S, Richter DJ, Salamov A, JGI Sequencing, Bork P, Lim WA, Manning G, Miller WT, McGinnis W, Shapiro H, Tjian R, Grigoriev IV, Rokhsar D. 2008. The genome of the choanoflagellate *Monosiga brevicollis* and the origin of metazoans. *Nature.* 451: 783-788.

Kirk DL. 1998. *Volvox*: Molecular-Genetic Origins of Multicellularity and Cellular Differentiation. Cambridge University Press, Cambridge, UK, 381 pp.

Kirk DL. 2005. A twelve-step program for evolving multicellularity and a division of labor. *BioEssays*. 27: 299-310.

Kirk DL, Kaufman MR, Keeling RM, Stamer KA. 1991. Genetic and cytological control of the asymmetric divisions that pattern the *Volvox* embryo. *Development.* Supplement 1: 67-82.

Kirk DL, Kirk MM. 1983.Protein synthetic patterns during the asexual life cycle of *Volvox carteri*. *Developmental Biology*. 96: 493-506.

Knudsen ES, Wang JYJ. 1997. Dual mechanisms for the inhabitation of E2F binding to RB by cyclin-dependent kinase-mediated RB phosphorylation. *Molecular and Cellular Biology*. 17: 5771-5783.

Konopka CA, Bednarek SY. 2008. Comparison of the dynamics and functional redundancy of the *Arabidopsis* dynamin-related isoforms DRP1A and DRP1C during plant development. *Plant Physiology.* 147: 1590-1602.

Konopka CA, Schleede JB, Skop AR, Bednarek SY. 2006. Dynamin and cytokinesis. *Traffic.* 7: 239-247.

Lang NJ. 1963. Electron microscopy of the Volvocaceae and Astrephomenaceae. *American Journal of Botany.* 50: 280-300.

Lang BF, O'Kelly C, Nerad T, Gray MW, Burger G. 2002. The closest unicellular relatives of animals. *Current Biology.* 12: 1773-1778.

Larson A, Kirk MM, Kirk DL. 1992. Molecular phylogeny of the volvocine flagellates. *Molecular Biology and Evolution*. 9: 85-105.

Lasek-Nesselquist E, Katz LA. 2001. Phylogenetic position of *Sorogena stoianovitchae* and relationships within the class Colpodea (Ciliophora) based on SSU rDNA sequences. *The Journal of Eukaryotic Microbiology*. 48: 604-607.

Lechtreck K-F, Luro S, Awata J, Witman GB. 2009. HA-Tagging of putative flagellar proteins in *Chlamydomonas reinhardtii* identifies a novel protein of intraflagellar transport complex B. *Cell Motility and the Cytoskeleton*. 66: 469-482.

Lee T-Y, Bretana NA, Lu C-T. 2011. PlantPhos: using maximal dependence decomposition to identify plant phosphorylation sites with substrate site specificity.

BMC Bioinformatics. 12: 261.

Leliaert F, Smith DR, Moreau H, Herron MD, Verbruggen H, Delwiche CF, Clerck OD. 2012. Phylogeny and molecular evolution of green algae. *Critical Reviews in Plant Sciences*. 31: 1-46.

Marchant HJ. 1977. Colony formation and inversion in green alga *Eudorina elegans*. *Protoplasma*. 93: 325-339.

Matsuda Y, Musgrave A, van den Ende H, Roberts K. 1987. Cell walls of algae in the Volvocales: their sensitivity to a cell wall lytic enzyme and labeling with an anti-cell wall glycopeptide of *Chlamydomonas reinhardtii*. *The Botanical Magazine, Tokyo*. 100: 373-384.

Merchant SS, Prochnik SE, Vallon O, Harris EH, Karpowicz SJ, Witman GB, Terry A, Salamov A, Fritz-Laylin LK, Maréchal-Drouard, Marshall WF, Qu L-H, Nelson DR, Sanderfoot AA, Spalding MH, Kapitonov VV, Ren Q, Ferris P, Lindquist E, Shapiro H, Lucas SM, Grimwood J, Schmutz J, *Chlamydomonas* Annotation Team, JGI Annotation Team, Grigoriev IV, Rokhsar DS, Grossman AR. 2007. The *Chlamydomonas* genome reveals the evolution of key animal and plant functions. *Science*. 318: 245-251.

Michod RE. 2005. On the transfer of fitness from the cell to the multicellular organism. *Biology and Philosophy*. 20: 967-987.

Miller SM, Schmitt R, Kirk DL. 1993. *Jordan*, an active Volvox transposable element similar to higher plant transposons. *The Plant Cell*. 5: 1125-1138.

Miyagishima S, Kuwayama H, Urushihara H, Nakanishi H. 2008. Evolutionary linkage between eukaryotic cytokinesis and chloroplast division by dynamin proteins. *Proceedings of the National Academy of Sciences of the United States of America*. 105: 15202-15207.

Nakada T, Nozaki H. 2015. Flagellate green algae, in: Wehr JD, Sheath RG, Kociolek RP. (Eds.) *Freshwater algae of north America (Second Edition)*. pp. 265-313. Elsevier Inc., Amsterdam, Netherlands.

Nakada T, Nozaki H, Tomita M. 2010. Another origin of coloniality in volvocaleans: The phylogenetic position of *Pyrobotrys* Arnoldi (Spondylomoraceae, Volvocales). *The Journal of Eukaryotic Microbiology*. 57: 379-382.

Nakazawa Y, Hiraki M, Kamiya R, Hirono M. 2007. SAS-6 is a cartwheel protein that establishes the 9-fold symmetry of the centriole. *Current Biology.* 17:2169-2174.

Nishii I, Ogihara S, Kirk DL. 2003. A kinesin, InvA, plays an essential role in *Volvox* morphogenesis. *Cell*. 113: 743-753.

Nozaki H. 1986. Sexual reproduction in *Gonium sociale* (Chlorophyta, Volvocales). *Phycologia.* 25: 29-35.

Nozaki H. 1990. Ultrastructure of the extracellular matrix of *Gonium* (Volvocales, Chlorophyta). *Phycologia.* 29: 1-8.

Nozaki H. 2003. Origin and evolution of genera *Pleodorina* and *Volvox* (Volvocales). *Biologia.* 58: 425-431.

Nozaki H, Ito M. 1994. Phylogenetic relationships within the colonial Volvocales (Chlorophyta) inferred from cladistic analysis based on morphological data. *Journal of Phycology.* 30: 353-365.

Nozaki H, Ito M, Watanabe MM, Kuroiwa T. 1996. Ultrastructure of the vegetative colonies and systematic position of *Basichlamys* (Volvocales, Chlorophyta). *European Journal of Phycology.* 31: 67-72.

Nozaki H, Misawa K, Kajita T, Kato M, Nohara S, Watanabe MM. 2000. Origin and evolution of the colonial Volvocales (Chlorophyceae) as inferred from multiple, chloroplast gene sequences. *Molecular Phylogenetics and Evolution.* 17: 256-268.

Ohno S. 1970. Evolution by gene duplication. Springer Science + Business Media, New York, US, xv, 160 pp.

Olive LS, Blanton RL. 1980. Aerial sorocarp development by the aggregative ciliate, *Sorogena stoianovitchae*. *The Journal of Protozoology*. 27: 293-299.

Olson BJSC, Nedelcu AM. 2016. Co-option during the evolution of multicellular and developmental complexity in the volvocine green algae. *Current Opinion in Genetics & Development*. 39: 107-115.

Parfrey LW, Lahr DJG. 2013. Multicellularity arose several times in the evolution of eukaryotes. *Bioessays*. 35: 339-347.

Pickett-Heaps JD. 1975. Green Algae: Structure, Reproduction, and Evolution in Selected Genera. Sinauer Associates, Inc., Sunderland, MA, USA. 606 pp.

Piperno G, Fuller MT. 1985. Monoclonal antibodies specific for an acetylated form of a-tubulin recognize the antigen in cilia and flagella from a variety of organisms. *The Journal of Cell Biology.* 101: 2085-2094.

Praefcke GJK, McMahon HT. 2004. The dynamin superfamily: universal membrane tubulation and fission molecules?. *Nature reviews. Molecular cell biology*. 5: 133-147.

Preble AM, TH Giddings Jr., Dutcher SK. 2001. Extragenic bypass suppressors of mutations in the essential gene *BLD12* promote assembly of basal bodies with abnormal microtubules in *Chlamydomonas reinhardtii*. *Genetics*. 157: 163-181.

Prochnik SE, Umen J, Nedelcu AM, Hallmann A, Miller SM, Nishii I, Ferris P, Kuo A, Mitors T, Fritz-Laylin LK, Hellsten U, Chapman J, Simakov O, Rensing SA, Terry A, Pangilinan J, Kapitonov V, Jurka J, Salamov A, Shapiro H, Schmutz J, Grimwood J, Lindquist E, Lucas S, Grigoriev IV, Schmitt R, Kirk D, Rokhsar DS. 2010. Genome analysis of organismal complexity in the multicellular green alga *Volvox carteri*. *Science.* 329: 223-226.

Ringo DL. 1967. Flagellar motion and fine structure of the flagellar apparatus in

Chlamydomonas. The Journal of Cell Biology. 33: 543-571.

Ruhfel BR, Gitzendanner MA, Soltis PS, Soltis D, Burleigh JG. 2014. From algae to angiosperms-inferring the phylogeny of green plants (*Viridiplantae*) from 360 plastid genomes. *BMC Evolutionary Biology.* 14: 23.

Sachs JL. 2008. Resolving the first steps to multicellularity. *Trends in Ecolgy & Evolution.* 23:245-248.

Sharpe SC, Eme L, Brown MW, Roger AJ. 2015. Timing the origins of multicellular eukaryotes through phylogenomics and relaxed molecular clock analyses, in: Ruiz-Trillo I, Nedelcu AM. (Eds.). *Evolutionary transitions to multicellular life.* pp. 3-29. Springer Netherlands, Dordrecht, Netherland.

Shpetner HS, Vallee RB. 1989. Identification of dynamin, a novel mechanochemical enzyme that mediates interactions between microtubules. *Cell.* 59: 421-432.

Smith SA, Beaulieu JM, Donoghue MJ. 2009. Mega-phylogeny approach for comparative biology: an alternative to supertree and supermatrix approaches. *BMC Evolutionary Biology*. 9: 37.

Soni R, Carmichael JP, Shah ZH, Murray JAH. 1995. A family of cyclin D homologs from plants differentially controlled by growth regulators and containing the conserved retinoblastoma protein interaction motif. *The Plant Cell*. 7: 85-103.

Stein JR. 1959. The four-celled species of *Gonium*. *American Journal of Botany*. 46: 366-371.

Stephens SG. 1951. Possible significance of duplication in evolution. *Advanced in Genetics*. 4: 247-265.

Suga H, Ruiz-Trillo I. 2015. Filastereans and Ichthyosporeans: Models to Understand the Origin of Metazoan Multicellularity, in: Ruiz-Trillo I, Nedelcu AM. (Eds.). *Evolutionary transitions to multicellular life.* pp. 117-128. Springer Netherlands, Dordrecht, Netherland.

Tamura K, Peterson D, Peterson N, Stecher G, Nei M, Kumar S. 2011. MEGA5: Molecular evolutionary genetics analysis using maximum likelihood, evolutionary distance, and maximum parsimony methods. *Molecular Biology and Evolution*. 28: 2731-2739.

Taylor MG, Floyd GL, Hoops HJ. 1985. Development of the flagellar apparatus and flagellar position in the colonial green alga *Platydorina caudata* (Chlorophyceae). *Journal of Phycology*. 21: 533-546.

Thompson HM, Skop AR, Euteneuer U, Meyer BJ, McNiven MA. 2002. The large GTPase dynamin A associates with the spindle midzoe and is required for cytokinesis. *Current Biology.* 12: 2111-2117.

Tice AK, Silberman JD, Walthall AC, Le KN, Spiegel FW, Brown MW. 2016. *Sorodiplophrys stercorea*: Another novel lineage of sorocarpic multicellularity. *The Journal of Microbiology.* 63: 623-628.

Umen JG, Goodenough UW. 2001. Control of cell division by a retinoblastoma protein homolog in *Chlamydomonas*. *Genes & Development*. 15: 1652-1661.

Wienke DC, Knetsch MLW, Neuhaus EM, Reedy MC, Manstein DJ. 1999. Disruption of a dynamin homologue affects endocytosis, organelle morphology, and cytokinesis in *Dictyostelium discoideum. Molecular Biology of the Cell.* 10: 225-243.

Xie Q, Sanz-Burgos AP, Hannon GJ, Gutiérrez C. 1996. Plant cells contain a novel member of the retinoblastoma family of growth regulatory proteins. *The EMBO Journal*. 15: 4900-4908.

Yumoto K, Kasai F, Kawachi M. 2013. Taxonomic re-examination of *Chlamydomonas* strains maintained in the NIES-Collection. *Microbiology and culture collections*. 29: 1-12.

Zhang J. 2003. Evolution by gene duplication: an update. *Trends in Ecology & Evolution*. 18: 292-298.

Zones JM, Blaby IK, Merchant SS, Umen JG. 2015. High-resolution profiling of a synchronized diurnal transcriptome from *Chlamydomonas reinhardtii* reveals continuous cell and metabolic differentiation. *The Plant Cell*. 27: 2743-2769.

Appendices

Appendix 1. Alignment of cyclin D (CYCD), cyclin A1 (CYCA1), cyclin B1 (CYCB1), and cyclin AB1 (CYCAB1) proteins of *Chlamydomonas reinhardtii* (Cr), *Tetrabaena socialis* (Ts), *Gonium pectorale* (Gp), and *Volvox carteri* (Vc) for phylogenetic analyses.

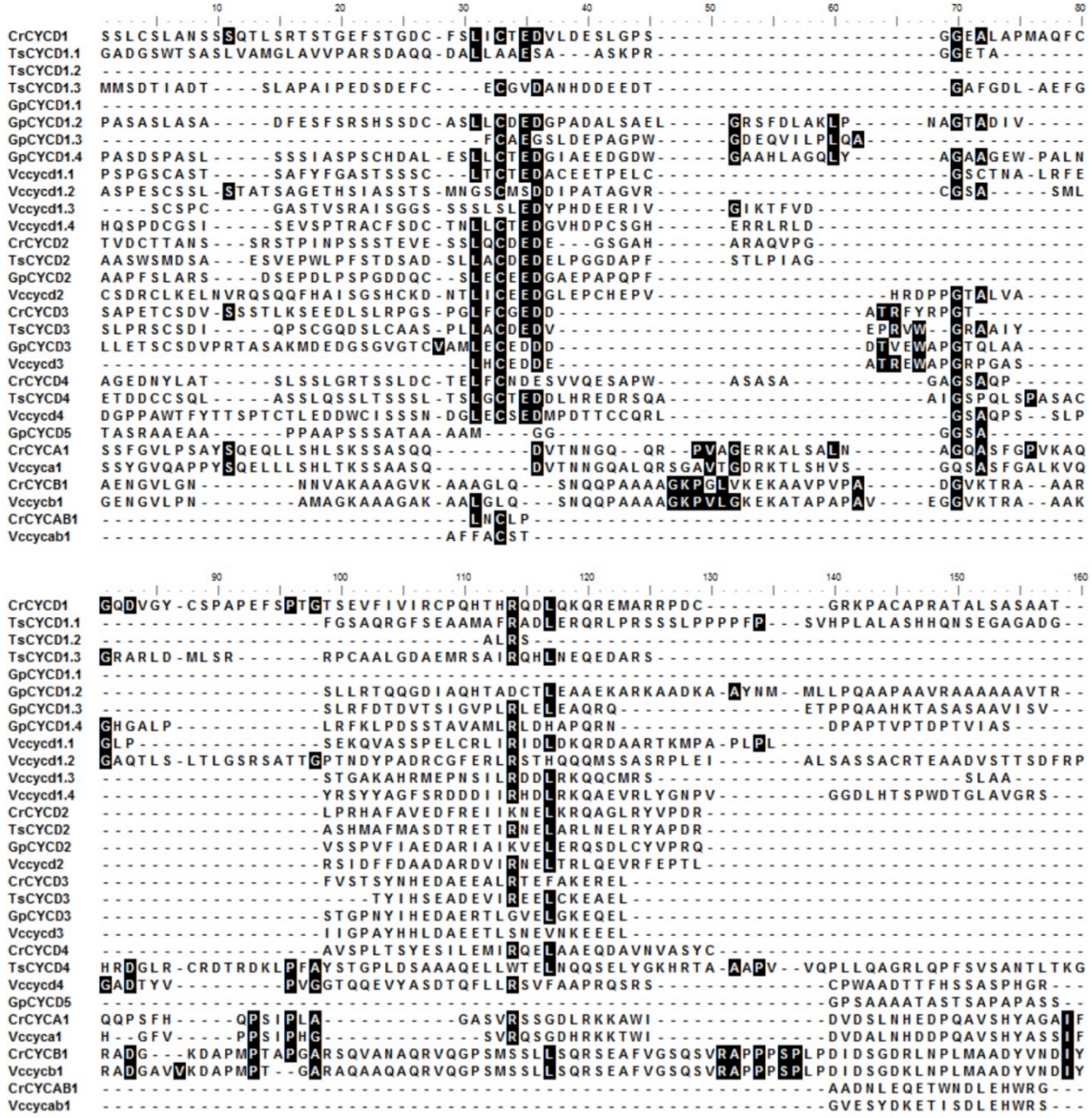

Appendix 1. (Continued)

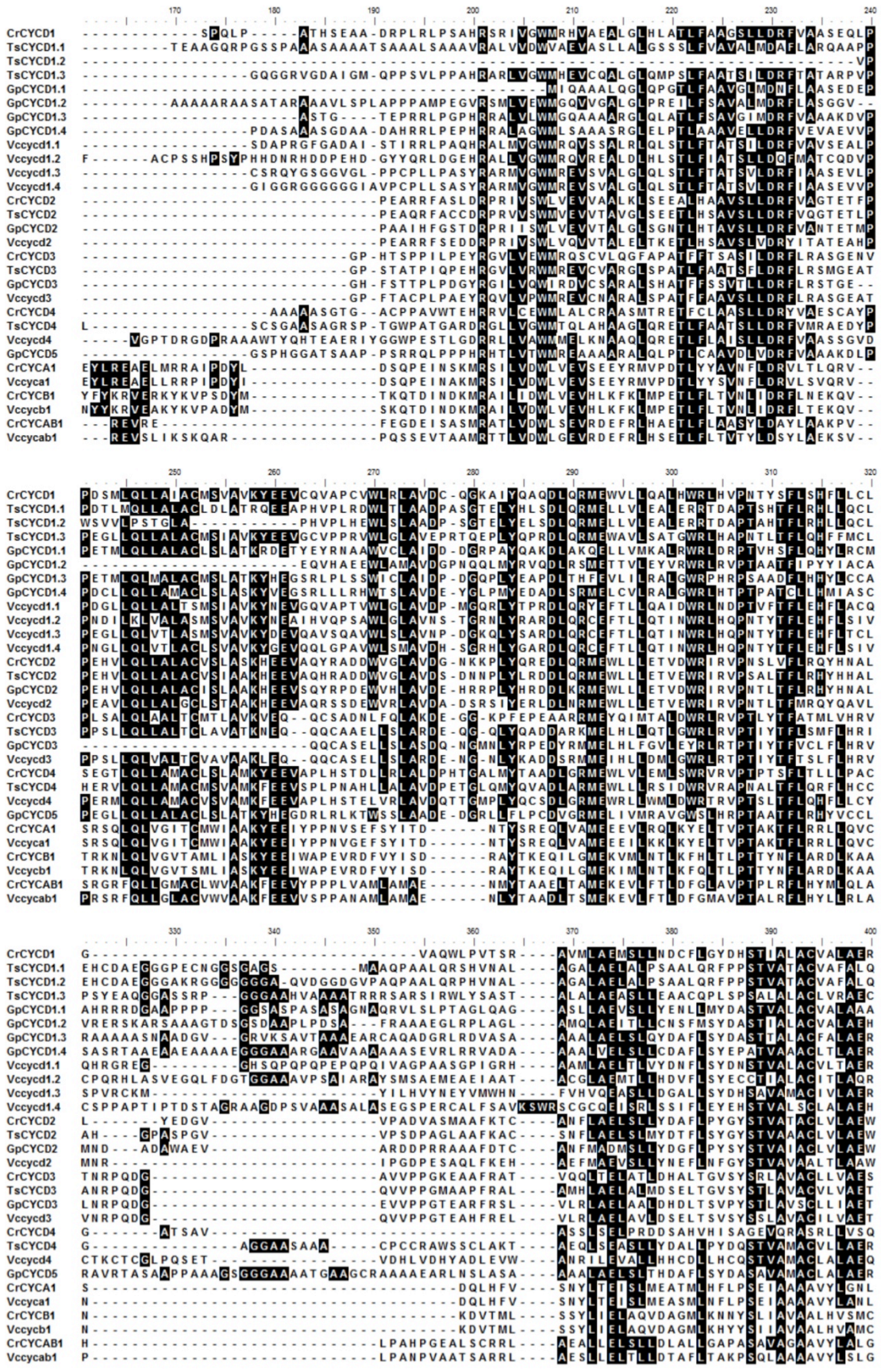

Appendix 1. (Continued)

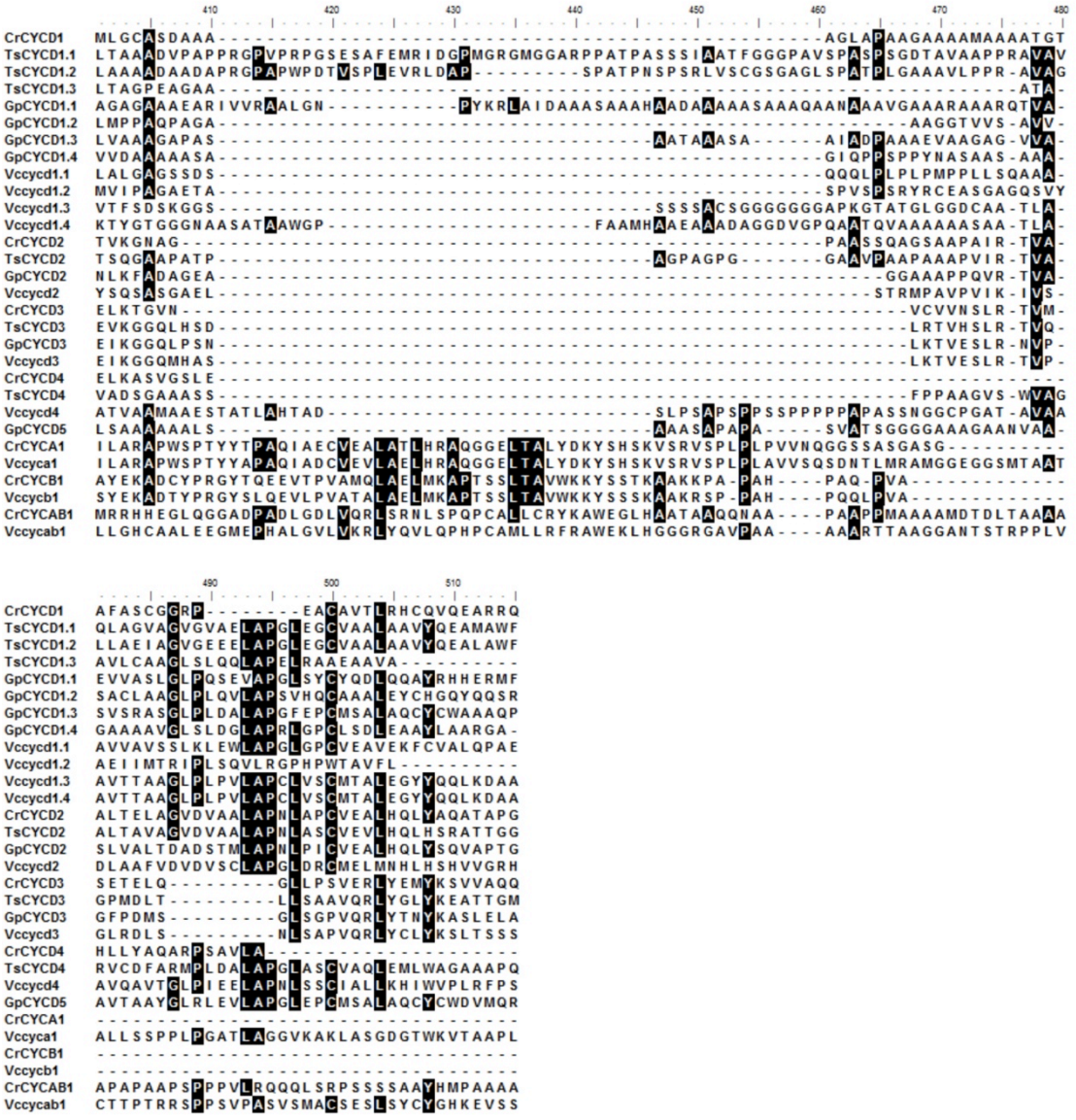

Appendix 2. Alignment of dynamin related protein 1 (DRP1) dynamin related protein 2 (DRP2) of viridiplantae for phylogenetic analyses (Figure 4.2).

Abbreviations are described in Table 4.2.

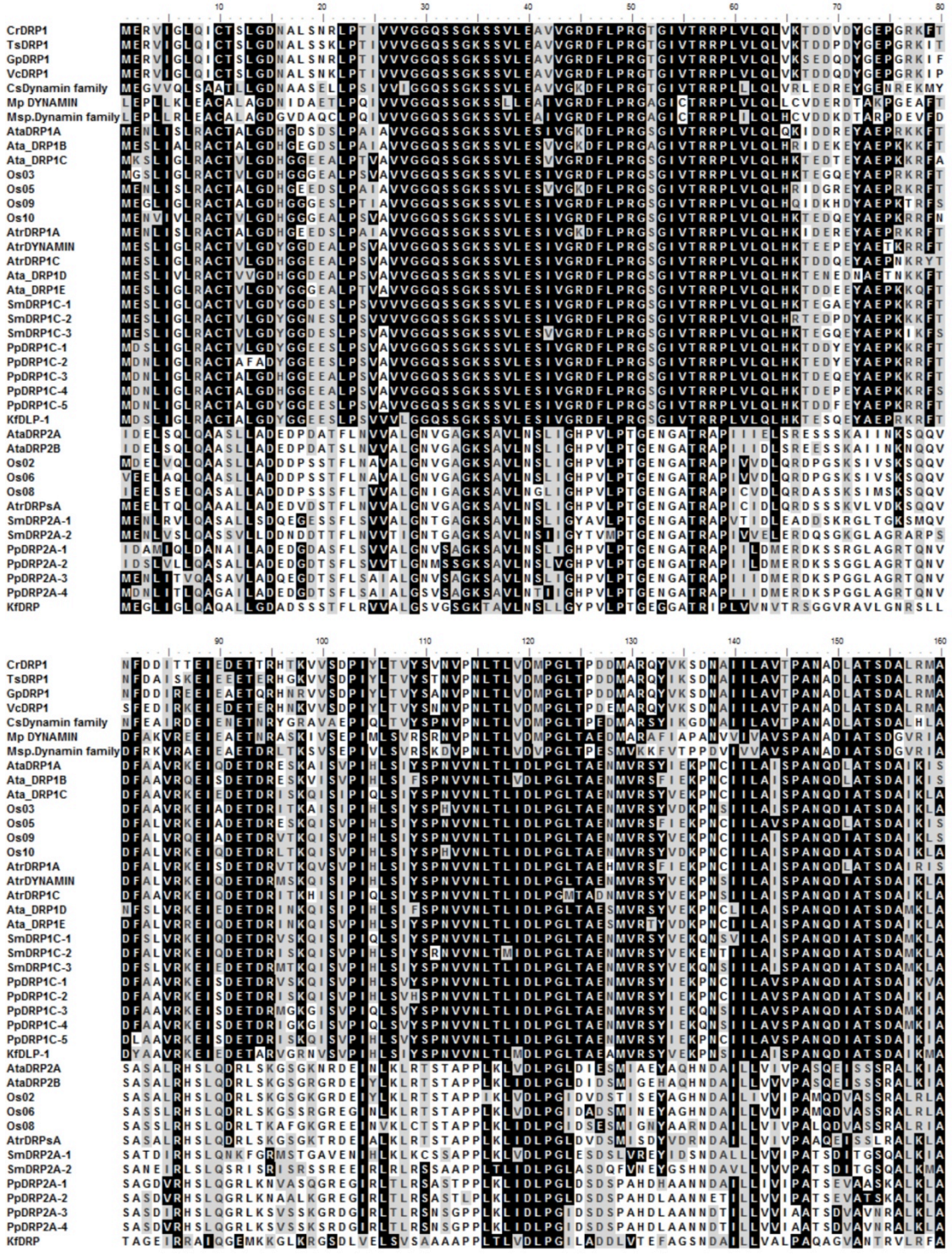

Appendix 2. (Continued)

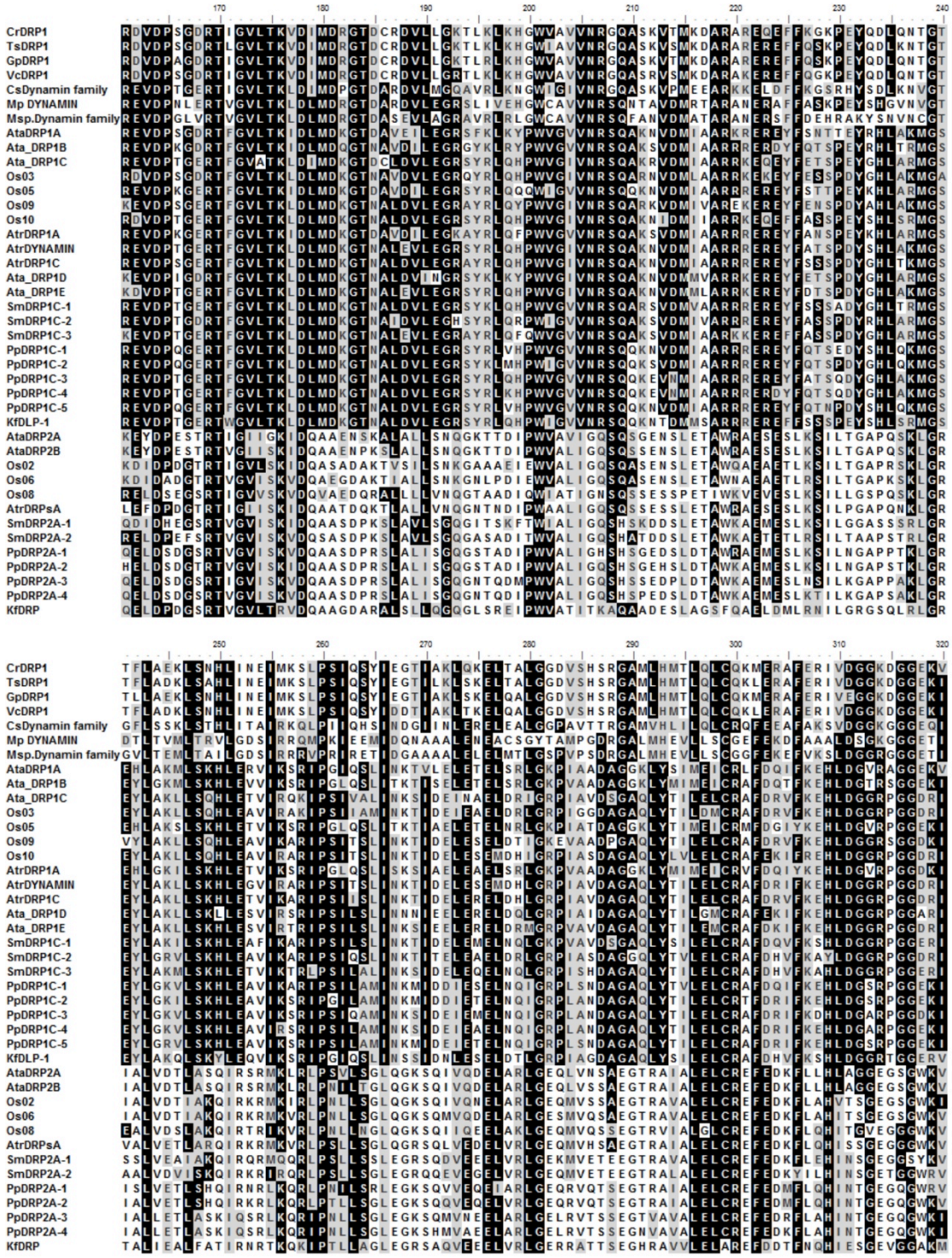

Appendix 2. (Continued)

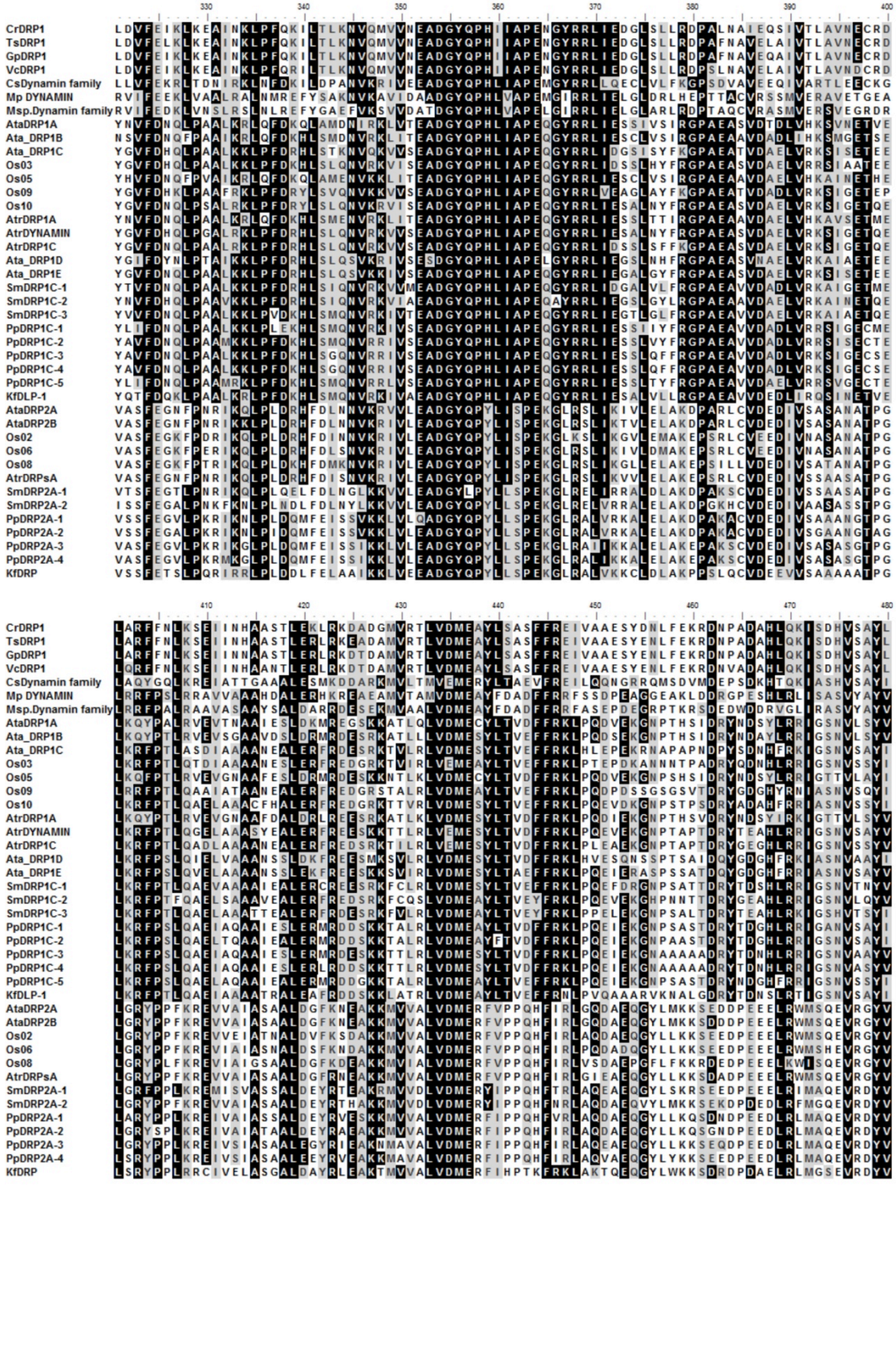

Appendix 2. (Continued)